



UNIVERSITA' DEGLI STUDI DI VERONA

DIPARTIMENTO DI

SCIENZE CHIRURGICHE, ODONTOSTOMATOLOGICHE E MATERNO-INFANTILI

SCUOLA DI DOTTORATO DI

SCIENZE DELLA VITA E DELLA SALUTE

DOTTORATO DI RICERCA IN

SCIENZE CARDIOVASCOLARI

Con il contributo di

UNIVERSITA' DEGLI STUDI DI VERONA

CICLO/ANNO XXXII/2016

TITOLO

VIDEO KINEMATIC EVALUATION OF THE HEART (VI.K.I.E.):
AN IDEA, A PROJECT, A REALITY

S.S.D. MED/23

Coordinatore: Prof. GIOVANNI BATTISTA LUCIANI

Firma _____

Tutor: Prof. GIOVANNI BATTISTA LUCIANI

Firma _____

Tutor: Prof. MICHELE MIRAGOLI




Firma _____

Dottorando: Dott. GIACOMO ROZZI

Firma _____

Quest'opera è stata rilasciata con licenza Creative Commons Attribuzione – non commerciale
Non opere derivate 3.0 Italia . Per leggere una copia della licenza visita il sito web:

<http://creativecommons.org/licenses/by-nc-nd/3.0/it/>

-  **Attribuzione** Devi riconoscere [una menzione di paternità adeguata](#), fornire un link alla licenza e [indicare se sono state effettuate delle modifiche](#). Puoi fare ciò in qualsiasi maniera ragionevole possibile, ma non con modalità tali da suggerire che il licenziante avalli te o il tuo utilizzo del materiale.
-  **Non Commerciale** Non puoi usare il materiale per [scopi commerciali](#).
-  **Non opere derivate** —Se [remixi, trasformi il materiale o ti basi su di esso](#), non puoi distribuire il materiale così modificato.

*VIDEO KINEMATIC EVALUATION OF THE HEART (V.I.K.I.E.):
AN IDEA, A PROJECT, A REALITY
Giacomo Rozzi
Tesi di Dottorato
Verona, 6/08/2020
ISBN: 9788869251627*

SOMMARIO

Introduzione:

Lo sviluppo tecnologico degli ultimi 20 anni ha impegnato tutti gli sforzi al fine di implementare modalità innovative di imaging non invasive per accelerare la translazionalità dalla ricerca di base alla clinica, specialmente in ambito cardiologico.

In questo lavoro è presentato e spiegato nel dettaglio, un innovativo approccio all'imaging cardiaco. Questo approccio è chiamato valutazione video cinematografica (Vi.Ki.E. da Video Kinematic Evaluation) ed è in grado di monitorare, con modalità non invasiva, la cinetica e la deformazione cardiaca *in-situ* durante la chirurgia. La cinetica cardiaca è stata approfonditamente valutata spaziando dall'animale sperimentale alle patologie cardiache negli umani che colpiscono entrambi i ventricoli, destro e sinistro.

Metodi:

La tecnologia Vi.Ki.E. può essere definita "tanto semplice quanto innovativa". Infatti, consiste semplicemente in una telecamera ad alta risoluzione temporale posizionata sopra un cuore battente *in-situ*, dopo esposizione tramite toracotomia e sospensione pericardica, che ne registra i cicli cardiaci. Successivamente un software di tracking è applicato al video precedentemente registrato per seguire i movimenti del tessuto epicardico. Questo tracker fornisce informazioni sulle traiettorie dell'epicardio e, grazie ad un algoritmo customizzato, la tecnologia recupera informazioni sulla meccanica cardiaca come forza di contrazione o fatica cardiaca, consumo energetico, velocità di contrazione, spostamento del marker e torsione epicardica.

Questa tecnica è stata testata su 21 ratti (9 sottoposti a protocollo di ischemia/riperfusione e/o per le validazioni, 12 per lo studio sulla differenza di genere) e 37 pazienti sottoposti a differenti operazioni tra il 2015 e il 2019. Nel dettaglio 10 pazienti sono stati sottoposti a Bypass aortocoronarico, 12 hanno effettuato una sostituzione della valvola polmonare dopo riparazione chirurgica di

Tetralogia di Fallot, 6 sono stati sottoposti ad un impianto di assistenza ventricolare sinistra (LVAD) (1 di questi è stato spostato nel capitolo case study), 6 pazienti con cuore ipoplasico sono stati sottoposti ad interventi di GLENN o FONTAN, 2 pazienti sono stati sottoposti a trapianto cardiaco ed infine 1 paziente ha ricevuto una doppia sostituzione valvolare (paziente spostato nel capitolo case study).

Risultati:

I risultati mostrano che in tutti i pazienti la tecnologia Vi.Ki.E. è stata in grado di discriminare in tempo reale, con potenza statistica, le differenze di cinetica cardiaca prima e dopo la chirurgia, suggerendo possibili implicazioni cliniche nel trattamento dei pazienti prima della chiusura del torace e/o in terapia intensiva. Per quanto riguarda gli animali sperimentali i risultati ottenuti sono alla base delle validazioni della tecnologia. Alcuni di essi sono stati usati come modello in comparazione coi risultati Vi.Ki.E. ottenuti da pazienti.

Conclusioni:

In conclusione, questo studio ha dimostrato che la tecnologia di valutazione video cinematica è sicura e non invasiva con una possibile e promettente applicazione clinica. La facilità della valutazione e l'approccio basato sull'algoritmo rendono il Vi.Ki.E. una tecnologia ad ampio spettro, in grado di acquisire dati dalle cellule battenti in vitro fino alla clinica, passando per la valutazione preclinica e possibilmente anche in quella *ex-vivo* come l'approccio nel cuore isolato di Langerdorff.

ABSTRACT

Introduction:

The technological development of the last 20 years pledges the intensity of efforts for implementing novel imaging contactless modalities that accelerate the translation from the research bench to the patient bedside, especially in the cardiac field. In this work, a novel intraoperative cardiac imaging approach, named Video Kinematic Evaluation (Vi.Ki.E.), is presented and explained in detail. This technology is able to monitor, contactless, the cardiac mechanics and deformation *in-situ* during heart surgery. Cardiac kinematics have been deeply evaluated ranging from the experimental animal approach to the human myocardial pathologies in both left and right ventricles.

Methods:

Vi.Ki.E. can be defined “as simple as innovative”. It only consists of a high-speed camera placed upon an exposed beating heart *in-situ* to record cardiac cycles. Afterwards a tracker software is used on the recorded video to follow the epicardial tissue movements. This tracker provides information about trajectories of the epicardium and, thanks to a custom-made algorithm, the technology supplies heart mechanical information such as: Force of contraction or cardiac fatigue, Energy expenditure, Contraction velocity, displacement of the marker and epicardial torsion.

This approach has been tested on 21 rats (9 ischemia/reperfusion and/or for validation, 12 for the gender difference study) and on 37 patients who underwent different surgery between 2015 and 2019. In detail 10 patients underwent Coronary Artery Bypass Grafting, 12 underwent Valve Replacement after Tetralogy of Fallot correction surgery, 6 implanted a Left Ventricular Assist Device (1 is moved in the case study section), 6 patients with Hypoplastic Heart Syndrome underwent GLENN or FONTAN surgery, 2 patients underwent Heart Transplantation and finally 1 patient underwent double valve replacement (this patient is moved into case study section).

Results:

The patients' results demonstrated that the Vi.Ki.E. technology was able to discriminate, with statistic potency, the kinematic differences before and after the surgery in real-time, suggesting possible clinical implications in the treatment of the patients before the chest closure and/or in the intensive care unit. As it concerns the experimental animals, the results are the basics of the validation technology. Some of them were used as accepted model in comparison with the Vi.Ki.E. results on patients.

Conclusions:

In conclusion, this study has shown that Vi.Ki.E. is a safe and contactless technology with promising possible clinical application. The ease in the evaluation and the algorithm-based approach makes Video Kinematic Evaluation a widespread technique from cellular level to human cases covering the entire experimental field with *in-vivo* evaluation and possibly Langendorff/Working Heart approaches.

INDEX

1. INTRODUCTION.....	page 14
1.1. Cardiac Imaging.....	page 14
1.1.1 Echocardiography (ECHO).....	page 15
- 2D imaging.....	page 16
- M-mode.....	page 16
- Doppler Imaging.....	page 17
- CW Doppler.....	page 17
- PW Doppler.....	page 17
- Color-flow mapping or Color Doppler.....	page 18
- 3D echocardiography.....	page 19
- Multi-beat.....	page 20
- Real-time.....	page 20
1.1.2 Nuclear Cardiology.....	page 21
- Myocardial perfusion scintigraphy (MPS or SPECT).....	page 21
- Evaluation of Cardiac Function with Radionuclide Ventriculography (RNV).....	page 22
- Assessment of Myocardial Injury, Infarction and Infection.....	page 22
- Imaging of the Nervous System of the Heart.....	page 22
- Positron Emission Tomography (PET).....	page 23
1.1.3 Cardiac Computer Tomography.....	page 24
- Calcium Scoring.....	page 24
- Coronary CT angiography.....	page 25
- Retrospectively ECG-gated cCTA protocols.....	page 26
- Prospectively ECG-gated cCTA protocols.....	page 26
- Ventricles Function.....	page 27
1.1.4 Magnetic Resonance.....	page 29
- Spin-Echo sequence.....	page 30
- Gradient-Echo (GRE) sequence.....	page 30
- Cine MRI.....	page 31

- Perfusion MRI.....	page 31
- Myocardial T1 mapping.....	page 32
- Myocardial T2 mapping.....	page 32
1.2. Video Kinematic Evaluation (Vi.Ki.E.).....	page 33
1.2.1. Introduction.....	page 33
1.2.2. Vi.Ki.E. functioning.....	page 34
1.2.3. Camera speed selection.....	page 35
1.2.4. Trajectories and Video cardiograms:	
a qualitative point of view.....	page 37
1.2.5. Mechanical parameters explanation and	
physiological meaning.....	page 39
- Energy.....	page 40
- Force.....	page 40
1.3. Particle Image Velocimetry (PIV).....	page 41
1.4. The Vi.Ki.E. competitive advantage.....	page 42
Echography.....	page 42
- Transthoracic Echocardiography.....	page 42
- Pros.....	page 42
- Cons.....	page 42
- Transesophageal Echocardiography.....	page 42
- Pros.....	page 42
- Cons.....	page 42
Nuclear Cardiology.....	page 43
- Pros.....	page 43
- Cons.....	page 43
Cardiac Computer Tomography.....	page 43
- Pros.....	page 43
- Cons.....	page 43
Magnetic Resonance.....	page 43
- Pros.....	page 43
- Cons.....	page 44

Video Kinematic Evaluation.....	page 44
- Pros.....	page 44
- Cons.....	page 44
2. METHODS.....	page 46
2.1. Instrumentation.....	page 46
- Vi.Ki.E. clinical instrumentation.....	page 46
- Vi.Ki.E. Experimental instrumentation.....	page 46
2.2. Settings and placement of the marker.....	page 47
2.3. Vi.Ki.E. Validation.....	page 51
2.3.1. Kinetic Energy validation.....	page 51
2.3.2. Force validation.....	page 52
2.3.3. Validation of data during time.....	page 53
2.3.4. Validation in computer model.....	page 54
2.4. Conversion curve from pixels to millimeters.....	page 57
2.5. Protocols.....	page 58
- Human Surgical Protocols.....	page 58
- Vi.Ki.E. clinical protocols.....	page 58
- Animal surgical protocols.....	page 60
- Vi.Ki.E. experimental protocols.....	page 60
- Measurement of contraction Force.....	page 60
- Reproducibility of the data acquired.....	page 60
- Ischemia/Reperfusion.....	page 61
- Induced AV block.....	page 61
- Atrial Stimulation.....	page 61
3. RESULTS.....	page 63
3.1. Cardiac Kinematic parameters computed from video of	
<i>in situ</i> beating heart.....	page 63
3.1.1. Abstract.....	page 63
3.1.2. Introduction.....	page 64
3.1.3. Results.....	page 66
- Validation of the measured parameters in rat hearts.....	page 67
- Temporal and spatial resolution.....	page 68

- Reproducibility of the acquired data.....	page 68
- Kinetic energy acquisition in a controlled and simple system.....	page 69
- Measurement of the contraction force.....	page 69
- Simulation of kinematic parameter measurement in ischemic contractile hearts.....	page 71
- Video kinematic parameters in ischemic and reperfused rat hearts.....	page 73
- Video kinematic parameters in patients underwent CABG.....	page 76
- Improved kinetic energy following atrioventricular block in rat and human hearts: the Frank-Starling effect.....	page 78
3.1.4. Discussion.....	page 79
3.1.5. Limitations.....	page 81
3.1.6. Methods.....	page 82
- Experimental animals.....	page 82
- Human patients.....	page 82
- Functional imaging.....	page 83
- Low-speed video camera.....	page 83
- High-speed video camera.....	page 83
- Video acquisition.....	page 84
- Video kinematic evaluation in rats.....	page 84
- Video kinematic evaluation during CABG in human Patients.....	page 85
- Quantitative analysis.....	page 85
- Kinematics.....	page 85
- Particle Image Velocimetry.....	page 85
- Mathematical models.....	page 86
- Numerical simulations.....	page 86
- Numerical methods.....	page 87
- General statistics.....	page 88
3.1.7. Supplementary information.....	page 88

- Supplementary Methods.....	page 88
- Experimental animals.....	page 88
- Parameters calibration for the mathematical model of ischemia simulation.....	page 89
- Supplementary Figure legends.....	page 90
3.2. Real-time video kinematic evaluation of the in situ beating right ventricle after pulmonary valve replacement in patients with tetralogy of Fallot: a pilot study.....	page 94
3.2.1. Abstract.....	page 95
- Objectives.....	page 95
- Methods.....	page 95
- Results.....	page 95
- Conclusion.....	page 96
3.2.2. Introduction.....	page 96
3.2.3. Materials and Methods.....	page 97
- Surgical methods.....	page 99
- Experimental Protocol.....	page 100
- Video kinematic Evaluation of right ventricle function....	page 100
- Statistical analysis.....	page 101
3.2.4. Results.....	page 101
- Clinical outcome.....	page 101
- Intraoperative video kinematic evaluation of right ventricle function in patients with tetralogy of Fallot.....	page 102
3.2.5. Discussion.....	page 105
3.2.6. Limitations.....	page 108
3.2.7. Conclusions.....	page 108
3.2.8 Supplementary data.....	page 109
3.3. In-situ optical assessment of rat epicardial kinematic parameters reveals frequency-dependent mechanic heterogeneity related to gender.....	page 111
3.3.1. Abstract.....	page 111
- Background.....	page 111
- Methods.....	page 111

- Results.....	page 112
- Conclusion.....	page 112
3.3.2. Introduction.....	page 112
3.3.3. Materials and methods.....	page 115
- Experimental animals.....	page 115
- In-vivo atrial stimulation.....	page 115
- In-situ optical assessment of kinematic parameters.....	page 117
- Systolic and diastolic area and time.....	page 118
- Statistical analysis.....	page 118
3.3.4. Results.....	page 119
- Frequency of epicardial torsion obtained via Particle Image Velocimetry.....	page 120
- Geometrical spatiotemporal variation at different BCL.....	page 121
- Rising stimulation frequency unmasks gender difference at the single cardiac cycle.....	page 122
3.3.5. Discussion.....	page 123
3.3.6. Conclusions and limitations.....	page 125
3.4. Unpublished Results.....	page 126
3.4.1. Tetralogy of Fallot.....	page 126
- Results.....	page 126
- Discussions.....	page 129
3.4.2. Hypoplastic Heart Syndrome.....	page 130
- Results.....	page 130
- HLHS patients.....	page 131
- HRHS patients.....	page 133
- Discussions.....	page 135
3.4.3. Treatments for the Heart Failure.....	page 136
3.4.3.1. Left Ventricular Assist Device (LVAD) implantation.....	page 136
- Results.....	page 136
- Discussions.....	page 138
3.4.3.2. Heart Transplantation evaluation.....	page 139

- Results.....	page 139
- Patient#1 (58 years), VAD_Bridge to Transplant.....	page 141
- Patient#2 (56 years).....	page 142
- Discussions.....	page 142
3.4.4. Case studies.....	page 144
- Results Case Study Patient #1.....	page 144
- Discussions Case Study Patient #1.....	page 145
- Results Case Study Patient #2.....	page 146
- Discussions Case Study Patient #2.....	page 147
4. DISCUSSIONS.....	page 148
4.1. CABGs.....	page 148
4.2. ToF.....	page 149
4.3. Gender differences.....	page 151
4.4. Hypoplastic Heart Syndromes.....	page 151
4.5. LVAD.....	page 152
4.6. Heart Transplantation.....	page 153
5. LIMITATIONS.....	page 155
6. CONCLUSIONS.....	page 155
7. REFERENCES.....	page 157
 ACKNOWLEDGEMENTS.....	 page 170

1. INTRODUCTION

1.1. Cardiac Imaging

Thanks to the technological development of the last 20 years, a lot of efforts have been spent to implement novel imaging technologies accelerating the translation from the research bench to patient bedside especially in the cardiac field.

The main idea behind every technique must be the safety for the patients, ease in the analysis and the cost reduction. The concept of a single technology able to evaluate every cardiac pathological situation is still a utopia. However, the multitude of techniques around the cardiac field is the best way to provide the clinicians different points of view to extend the knowledge of the pathology and its course and minimizing the invasive surgical procedures when possible.

The most important imaging branches in cardiology are:

1. Echocardiography
2. Nuclear Cardiology
3. Cardiac Computer Tomography
4. Magnetic Resonance [1]

Brief but detailed information on those techniques will be presented in the following chapters.

1.1.1. Echocardiography (ECHO)

The Echocardiography is based on the use of ultrasounds to create an image of the heart. Ultrasound results from a phenomena called the “piezoelectric effect”, a peculiar feature of some crystals to transform electrical oscillations into mechanical oscillations (sound) and *vice versa* [2]. The Echo machinery functioning is based on the piezoelectric crystal transducer. When a current is applied to it, the crystal vibrates emitting ultrasounds. Afterwards, the ultrasounds bounce on the object and return to the transducer, hitting and distorting the crystal. The distortion generates an electrical signal that is analyzed by the Echo machinery. In summary, the crystal emits ultrasounds and then “listens” for the reflections [3].

The Echocardiogram can be performed in many ways, but the most common are:

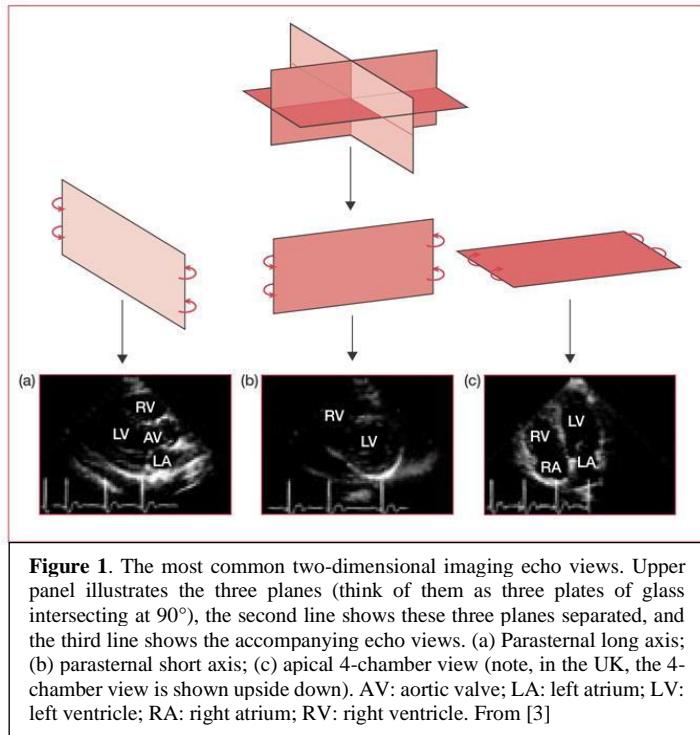
- Transthoracic (TTE)
- Transesophageal (TEE)

The transthoracic is the most used for heart check-ups and for pathology diagnosis, while the transesophageal is commonly used during cardiac surgery to check the intervention phases and the correct heart functionality before the patient’s chest closure. In the TEE, the Echo probe is inserted in the anesthetized patient’s esophagus until it reaches the heart position. This is particularly useful to visualize the posterior side of the heart (Left Ventricle; LV).

There are several different functions in every Echo machinery, and each gives a different heart point of view.

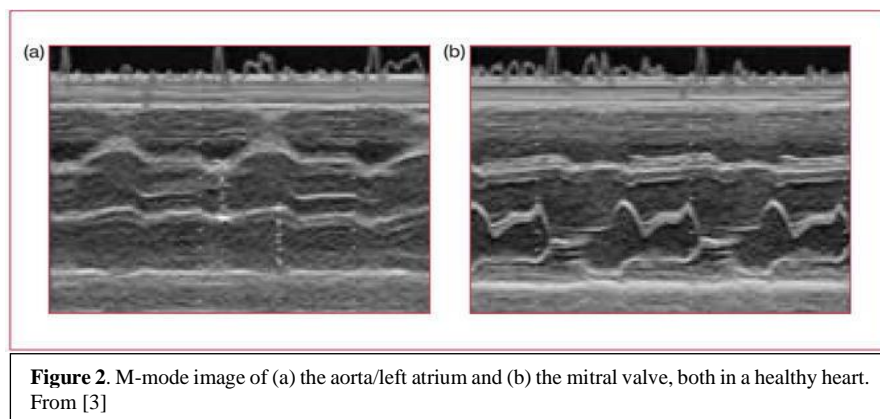
- Two-dimensional (2D) imaging
- M-Mode imaging
- Doppler imaging
- 3D echocardiography

2D imaging is the most used echo mode; it allows the detection of abnormal anatomy or abnormal movement of structures [4]. The most common cross-sectional views are the parasternal long axis, the parasternal short axis, and the apical view (Figure 1). These axes are only referred to the TTE. For the TEE, there are different views, the



midesophageal four-chamber, the midesophageal short- and long-axis, and the transgastric views.

M-mode (Figure 2) is a 1-dimension echocardiography derived from an M line superimposed on a cross-sectional image. It shows the time as the second dimension. Controlling the sweep speed gives access to accurate measurements of cardiac cycle intervals and thanks to the high-repetition frequency of the technique, precise measurements of mural thickness and cavitary size are obtained. In this way, the derived information is superior to the one obtained from cross-sections. M-mode echocardiography is commonly used for the evaluation of left ventricular



function, using short- or long-axis cuts through the left ventricle, and the timing of cardiac events such as left ventricular ejection time, using a long-axis cut through the aortic valve [5].

Doppler Imaging merges the Doppler Effect with the imaging. The Doppler Effect is the change in the frequency of a wave emitted by a moving source in relation to the observer, caused by the different sound wavelengths (frequencies) travelling in the air. The same approach is used to measure the blood flow velocity by comparing the frequency change between the transmitted and reflected sound waves [4]. In cardiac ultrasound, Doppler is used in three ways:

- Continuous-wave (CW) Doppler
- Pulsed wave (PW) Doppler
- Color-flow mapping (CFM) or Color Doppler

CW Doppler (Figure 3) does not provide spatial information since one crystal transmitting continuously and another recording continuously to read reflected signals. It estimates the severity of valve stenosis or regurgitation.

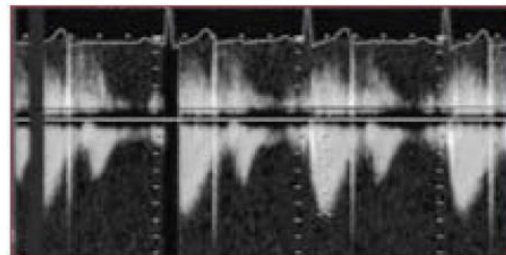
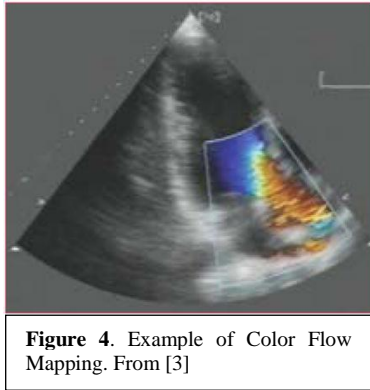


Figure 3. Example of Continuous wave doppler signal. From [3]

PW Doppler was created to overcome the spatial information limit on CW Doppler. It simply consists in a transducer emitting intermittently and reading returning signals in the time interval between two waves. This provides spatial information like conventional 2D mode while recording the blood flow velocities. The limitation of this modality lies in the pulse velocities that is limited by the returning signals time. If the transducer emits faster than the signal returns, the Aliasing effect will occur [5]. PW Doppler is used to assess ventricular in-flow patterns, intra-cardiac shunts and to make precise measurements of blood flow at valve orifices [4].



Color-flow mapping (CFM) or Color Doppler displays the blood direction and flow velocities superimposed on the image. A color is assigned to the flow direction; blue if the flow is going away from the transducer and red if the flow is going towards the transducer (Figure 4). The velocity of flow is displayed in blue and red shades; the faster the flow, the brighter the color. CFM is a modality

of PW Doppler, so it doesn't avoid the limitation of the Aliasing effect [5].

Echocardiography has been used since 1953 thanks to the collaborations between Edler and Hertz [6]. Echocardiography is the gold standard for cardiac imaging and diagnostic evaluation. It is very hard to find limitations in such an old and upgraded technology. However, technological imaging evolution is running faster, especially concerning spatial and temporal resolution. From this point of view echocardiography suffers from significant limitations due to the very low framerate and limited image resolution [5]. Some Echo machineries have been developed to overcome those limitations, but the costs make them affordable only to prestigious health care centers. Therefore, the standard cheap echo machinery, with all its limitations, remains the most used. Another echo limitation is the skill-based parameters evaluation, considering the sensibility and difficulty to properly set the probe. This results in different values from the same heart based on the technician's skill. Finally, during the surgical procedures the only available echo is the TEE that provides useful Left Ventricle information while only providing qualitative information of the Right Ventricle [7]. Moreover, TEE leads to misinterpretations on patient's prognosis, especially in those with Right Ventricle based pathologies, i.e. most of the congenital heart diseases. In some limited case the TEE can cause ventricular fibrillation after the probe insertion in the esophagus, due to the mechanical stimulation of cardiac structures [8].

3D echocardiography is used to overcome the above-mentioned limitations. It offers the possibility of having 3D heart images from any spatial point of view. This is possible thanks to the particular “array” 3D probe (Figure 5) that uses thousands of fully sampled elements for 360-degree focusing and steering. 3D echocardiography provides information about volumes and functionality of heart chambers [9].

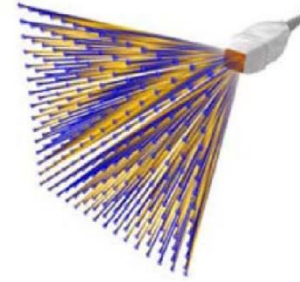


Figure 5. Example of 3D echo transducer array functioning. Modified from “Basics of Real Time 3D Echocardiography” Erasmus MC University Medical Center of Rotterdam.

The 3D echo is usable in both TTE and TEE, with two main advantages compared to the conventional 2D echo and M-mode evaluation (Figure 6):

- Quantification of absolute cardiac chambers volumes (LV and RV), and left atrial (LA) volumes and their function [9].
- Visualization of 3D structures and dynamic motion images of the heart, especially of heart valve conformations [9].

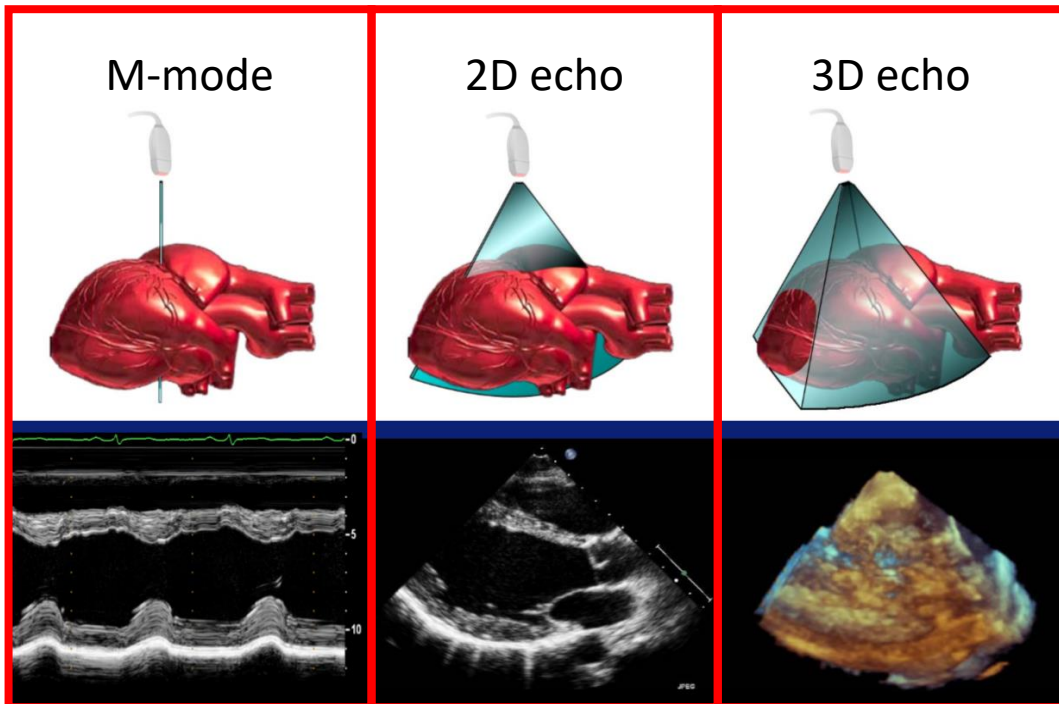


Figure 6. Functionality comparison between the linear M-mode evaluation (Left panel), conventional 2D Echo (middle panel) and 3D echo (right panel). Modified from “Basics of Real Time 3D Echocardiography” Erasmus MC University Medical Center of Rotterdam.

These two fundamental advantages could open new prospective on heart structures and functionality. However, 3D echo entails some strong limitations derived from the ultrasound procedures. As for 2D echo, the 3D echo image quality is limited by the acoustic windows. The spatial and temporal resolution of current 3D echo technology are still inferior to the 2D echo.

There are two different 3D data acquisition modes.

- The multi-beat acquisitions
- Real-time 3D mode

Multi-beat acquisition allows faster acquisition of a thin section of a 3D pyramidal volume. However, it requires four cardiac cycles and gated capture to reconstruct the 3D image. Therefore, it is prone to stitch artifacts in patients with rhythm disturbance and respiratory motion [10].

Real-time imaging captures the entire heart movement in a single beat overcoming the limitations of multi-beat mode, but suffering deteriorations in spatio-temporal resolution [10].

Because of these limitations, the use of 3D echo remains an uncommon and little widespread practice. This leads to a limited number of 3D echo specialists further reducing its use.

1.1.2. Nuclear Cardiology

Nuclear cardiology is based on the injection of a radioactive dye in the patient's body. An imaging machine (gamma camera, Figure 7), sensible to radioactive elements, creates pictures of the blood flow. The test is performed in resting and/or exercise state to evaluate possible areas with reduced blood flow or damage [11, 12].



Figure 7. Example of a gamma camera and the results it provides. After the injection of a radioactive dye, a patient is evaluated by a gamma camera (left panel). The data provided from the machinery (right panel) give estimation of cardiac blood flow. Moreover, the right panel shows the differences between two radioactive dyes used in two different techniques the SPECT (top panel) and the PET (bottom panel): F-18 flurpiridaz PET (FLUR) versus Tc-99m MIBI SPECT (MIBI). *“Reversible perfusion defect in the anterior and antero-septal wall is readily seen in a patient with left anterior descending coronary artery occlusion using F-18 flurpiridaz PET but the perfusion abnormality is not clearly appreciated using Tc-99m MIBI SPECT.”* Modified from [10].

According to the American Society of Nuclear Cardiology, there are several uses for this imaging branch. The most important are:

- Myocardial perfusion scintigraphy (MPS)
- Evaluation of Cardiac Function with Radionuclide Ventriculography (RNV)
- Assessment of Myocardial Injury, Infarction and Infection
- Imaging of the Nervous System of the Heart
- Positron Emission Tomography (PET)

Myocardial perfusion scintigraphy is the mainstay of the nuclear cardiology for the coronary artery health evaluation. It is performed by the use of single-photon emission computer tomography (SPECT; Figure 7, right panel, MIBI) evaluated by a gamma camera [12]. This test is usually performed in resting conditions and then

during exercise (stress test) to assess differences in cardiac function. In patients with respiratory disorders, the stress test is performed with pharmacological administration such as dipyridamole, adenosine, regadenoson or dobutamine [12, 13]. If there is a blockage in the coronary artery, the blood flow supply will be inefficient to support the exercise. The gamma machinery detects (nowadays automatically) the decrease in the blood flow.

The Evaluation of Cardiac Function with Radionuclide Ventriculography (RNV)

is a non-invasive test to assess the pumping function of the heart (Figure 8). This technique can also provide information about the function of the valves, the integrity of the cardiac chambers and can be used to monitor the effect of different drugs on the heart muscle. RNV is still one of the gold

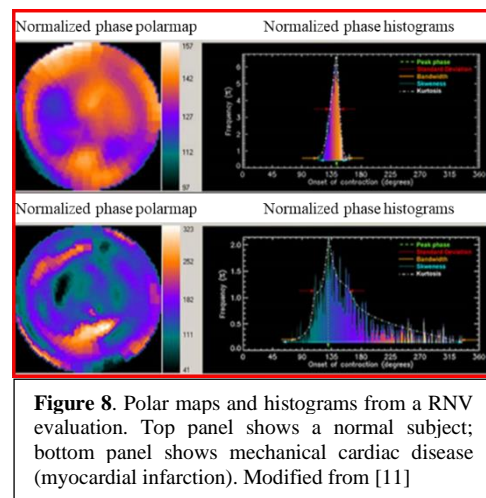


Figure 8. Polar maps and histograms from a RNV evaluation. Top panel shows a normal subject; bottom panel shows mechanical cardiac disease (myocardial infarction). Modified from [11]

standard methods for the measurement of LV ejection fraction (LVEF).

Assessment of Myocardial Injury, Infarction and Infection. Limited blood supply or inflammation can heavily or irreversibly impair cardiac cellular function. Nuclear cardiology techniques can be used to determine which areas of the heart muscle have been damaged by infection or by a stroke (Figure 7, STRESS FLUR, SHORT AXIS, MID).

Imaging of the Nervous System of the Heart. The cardiac nervous system is crucial for its proper functioning. When there is a damage in the heart muscle, the nervous system can be impaired with an abnormal function of the electrical system, possibly leading to Ventricular Tachycardia (VT). An abnormal heart rate and disarray of the normal cardiac rhythm can reveal this abnormality.

Positron Emission Tomography (PET) was developed to be more precise than SPECT and, nowadays, is used to provide information about either the blood supply to the heart muscle and the metabolic activity of the heart [14]. To date, there are different opinions concerning which technology gives the most reliable and precise data. Accordingly to Dr. Daniel J Bell, lead for radiology 2014-18 at the North Middlesex University Hospital (London), the main differences between SPECT and PET are the following:

PET:

- Very expensive. A PET CT-scanner is around \$2 million
- Uses positron-emitting radioisotope as tracer, in detail the fluorine-18 (FDG) (Figure 7, FLUR)
- Better contrast and spatial resolution (Figure 7)

SPECT:

- Lower cost. A SPECT scanner gamma camera costs from \$400,000 to \$600,000
- Uses gamma-emitting radioisotope as tracers; in detail technetium-99m (Figure 7, MIBI), iodine-123, iodine-131
- Less contrast and spatial resolution (Figure 7)

For most of the clinicians, “PET is just a bit better than SPECT” but it costs too much which is the reason why PET still has not replaced SPECT as the Gold standard for the Nuclear Cardiology.

Nuclear Cardiology has been the main nuclear base technique in medicine for several decades. The development of new imaging technologies like CT, as well as MR, has raised the question about the usefulness of Nuclear Cardiology. In the recent guidelines for Nuclear Cardiology [13], the effect of radioactive dyes on patients has been highlighted as well as the pharmacological impact, to mimic the stress test, in subjects with respiratory impairment. Another strong limitation for

both SPECT and PET is the poor contrast and spatial resolution. However, the Nuclear Cardiology has accomplished remarkable achievements and, also thanks to the development of novel radiopharmaceuticals, still holds promise as one of the major imaging techniques in medicine.

1.1.3. Cardiac Computed Tomography

Cardiac computed tomography (CT) scan uses x-rays to make detailed pictures of the heart [15]. The picture is created merging different 2D radiographic images (slices) rotating on the same axis to create a full 3D cross-sectional image [15]. There are several types of CT scanners and the basic difference is the number of slices the machinery can reproduce per second (64, 256 or 320). More slices, it means the highest image quality. The 320 slices cost around two and half times the 64 slices (\$2.5 million vs \$1 million) and whether it is worth it or not, is still a matter of debate in the clinical community.

The routinely use of cardiac CT concerns the evaluation of cardiac or coronary anatomy, to diagnose the coronary artery disease (CAD), to monitor coronary artery bypass surgery and/or implanted coronary stents and finally to calculate chambers volumes and cardiac function (including ejection fraction) [16].

The main analyses performed by the cardiac CT are:

- Calcium scoring
- Coronary CT angiography
 - o Retrospectively ECG-gated cCTA protocols
 - o Prospectively ECG-gated cCTA protocols
- Ventricles Function

Calcium scoring. Coronary artery calcium results from the sedimentation of substances over time which have hardened and become calcified. This is well documented in coronary atherosclerosis, where atherosclerotic plaques become calcified in the latest stages of the pathology leading to CAD [17].

A calcium score is obtained using a validated algorithm. The algorithm is based on the Agatston score who introduced a useful application to CT scan back in 1990 [16].

The score is calculated using the area and a weighted value related to the density of calcification.

A structure with an area of at least 1 mm² and a density greater than 130 Hounsfield unit (HU) is considered a calcified locus. If the locus corresponds to an anatomical position of a coronary, it represents a calcified

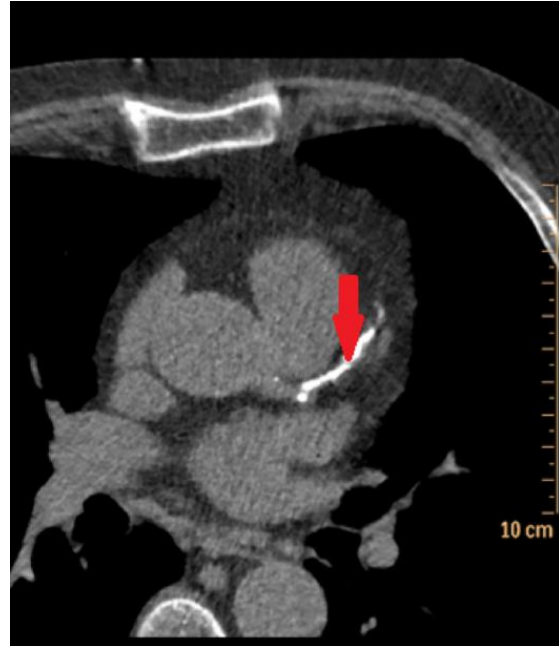
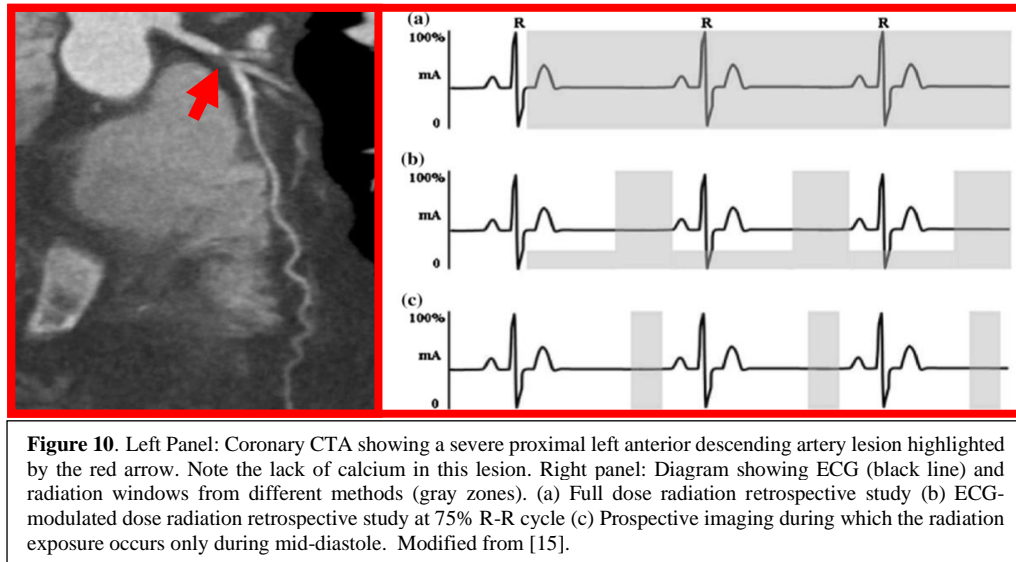


Figure 9. Coronary calcium within the left anterior descending artery. The calcium is seen as bright white and is highlighted by the red arrow. Modified from [15].

CAD plaque (Figure 9). A score of 1 is assigned for a value of 130–199 HU, a score of 2 for 200–299 HU, 3 for 300–399 HU, and a score of 4 for values of 400 HU and higher. The weighted score is multiplied by the area of the coronary to obtain the Agatston score [16]. Although this technique does not give any hemodynamic information about stenosis, the Agatston score is very useful to calculate the early risk stratification for patients. Patients with a score above 160 have an increased risk for a major adverse cardiac event. Moreover, results from a large Multi-Ethnic Study of Atherosclerosis (MESA) showed that a calcium score twofold higher than normal increased the probability of major coronary events by approximately 25% [18].

Coronary CT angiography can show coronaries without the risks associated with invasive treatments. It provides information on their anatomy highlighting the possible non- or obstructive CAD and plaque characteristics (Figure 10, left panel). CT angiography is possible due to the injection of a contrast fluid into the bloodstream. When the fluid reaches the anatomical site under examination, a picture is taken. Images are usually acquired based on patient's electrocardiogram (ECG) phases (Figure 10, right panel).

Indeed, for most patients, the best moment to acquire images is when the heart is fully relaxed; in the ECG this phase is approximately at 75% of the R-R interval (the distance between two R peaks) in mid-diastole (Figure 10, right panel, b, c) [16]. Methods of image acquisition can be Retrospective or Prospective.



Retrospective studies use X-Ray beams during the R-R interval with a full dose of radiation (Figure 10, right panel, a). Due to the high level of radiation on the patients, nowadays it is common to use ECG-modulated dosage consisting in basal low dosage increased when the 75% along the R-R cycle is reached (Figure 10, right panel, b). This upgrade provides high-quality images while decreases the amount of radiation emitted [16].

Retrospective studies use a standard spiral CT acquisition. The heart rhythm is detected, and the machinery scans the whole heart during multiple cardiac cycles. Finally, information from different phases of the cardiac cycle is obtained and used as trigger for the radiation emission.

Prospective studies use prediction of R wave timing to the image acquisition and the radiation emission. It allows to have a fixed table without spiral CT and most of all to limit the radiation on the patient only at the 75% of the R-R cycle (Figure 10, right panel, c). The main issue of the prospective study is that it requires a stable heart rate, otherwise image acquisition may not occur at every heartbeat. Consequently, there may be a longer acquisition time and radiation exposure than

in retrospective studies, making it more sensible to heart rate and breathing artefacts and so less useful [16].

Ventricles Function

With the advent of the new technological expansion in the last 20 years, a lot of improvements to CT have been made. Dual-source CT scanners allow to acquire in a modality called High-pitch. It permits to have an image just with a single high source of radiation triggered with ECG, in the same way of the prospective study, in less than a second. In combination with reconstruction technique (such MRI or SPECT) it is possible to measure chambers functional parameters such as left and right ventricular end-diastolic and end-systolic volumes, stroke volume, ejection fraction, and myocardial mass during the entire heartbeat [15] (Figure 11).

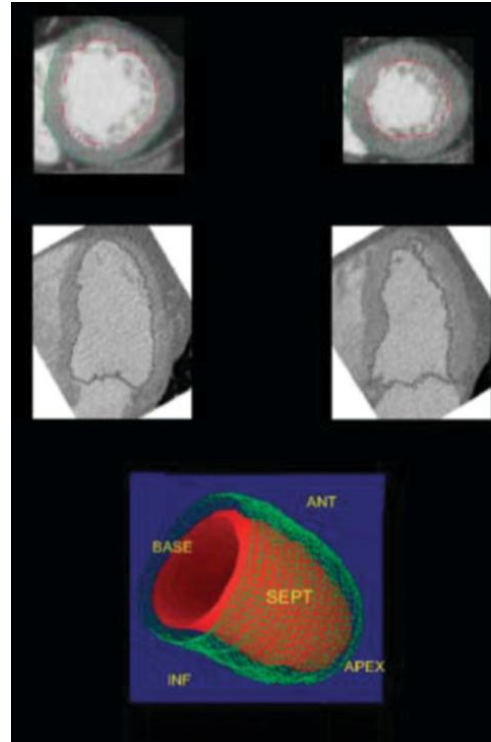


Figure 11. Evaluation of left ventricular function and volume via dual-source CT scanner. By tracing endocardial contours (red line in both top left and right images) of end-systolic and end-diastolic short- and long-axis views, left ventricular volumes and left ventricular ejection fraction can be derived from multidetector row computed tomography reconstruction. Modified from [14].

Even if the CT scan is widely used in clinic, it shows several limitations. The first one is the radiation emission that, even in the prospective studies, where the emission is limited to a short period of time, is correlated with lifetime attributable risk (LAR) of cancer development in both simulation study and patients [19, 20]. As it concerns the machinery accuracy the 64-slices imply 5 to 10 seconds to acquire images leading to possible artefacts and diagnostic positive- negative-false due to the patients' motion, arrhythmias and breath-hold failure. The introduction of new but extremely expensive 256- 320-slices with faster rotation and short scanning time has improved but not eliminated the tendency for artefacts.

Other limitations with cardiac CT are the use of pharmaceutical drugs for every scanning method like beta-blockers and sublingual nitrate, potential allergic reactions to the injected contrast fluid as well as its renal toxicity and finally poor contrast filling of distal vessels that could lead to diagnostic uncertainty [15].

1.1.4. Magnetic Resonance

Magnetic resonance imaging (MRI) is a scanning technique able to provide detailed images of the inner body structures. The technology is based on a strong magnetic field and radio waves to generate images. The human body is roughly composed for 70% of water which contains hydrogen nuclei (protons) that become aligned in a magnetic field. An MRI scanner applies a strong magnetic field (usually 1.5 Tesla), which aligns the proton "spins". This alignment (or magnetization) is next perturbed by the application of an external Radio Frequency (RF) energy. The protons absorb the energy from the magnetic field and flip their spins. When the field is turned off, the protons gradually return to their normal spin (relaxation process) producing a radio signal that can be measured by receivers in the scanner and converted into an image [21].

The MRI in the cardiac field (named CMR) is used for assessing infarcted regions and their relative late wall thinning, LV volumes, distortion of LV shape and compensatory hypertrophy of non-infarcted myocardium [22]. MRI is also used for ischemic/non-ischemic heart diseases, as well as heart failure and congenital heart disease [23, 24].

Tissues can be characterized by two different relaxation times, T1 and T2.

- T1 (longitudinal relaxation time) is the time constant which determines the rate at which excited protons return to equilibrium. It is a measure of the time taken for spinning protons to realign with the external magnetic field.
- T2 (transverse relaxation time) is the time constant which determines the rate at which excited protons reach equilibrium or go out of phase with each other [25].

The most used modality for CMR is the pulse mode or pulse sequence.

A pulse sequence is a series of RF pulses to produce MRI signals. Different types of pulses generate different image contrasts due to different T1 or T2 values. The two major pulses sequences are:

- Spin-Echo (SE) sequence
- Gradient-Echo (GRE) sequence [21]

Spin-Echo sequence. In this modality, a 90° RF is firstly applied to rotate the magnetization. When the proton relaxation starts, another 180° RF or a series of 180° RF impulses are applied to refocus the decaying transverse magnetization and produce a signal, called spin echo.

The most important parameters in the SE are echo time (TE) and repetition time (TR); TE is the time from the application of the 90° RF pulse to the formation of the spin echo, and TR is the time from the 90° RF pulse to the next 90° RF pulse.

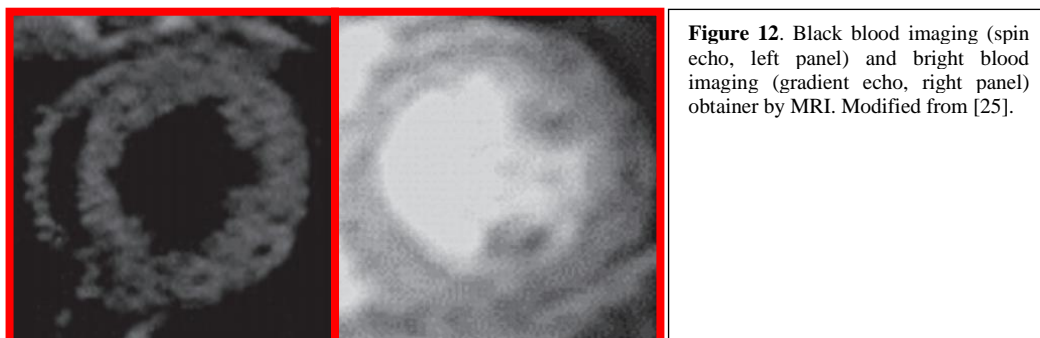
Those parameters are useful because:

- short TR and short TE produce T1-weighted contrast
- long TR and long TE produce T2-weighted contrast
- long TR and short TE produce proton-density-weighted contrast.

Spin echo-sequence requires time to acquire an image, resulting in a blur effect when fitting one beat in one image, thus requiring to merge different images to obtain an entire beat. It is used primarily for the Dark Blood imaging (Figure 12, left panel) to evaluate LV chamber [21, 26].

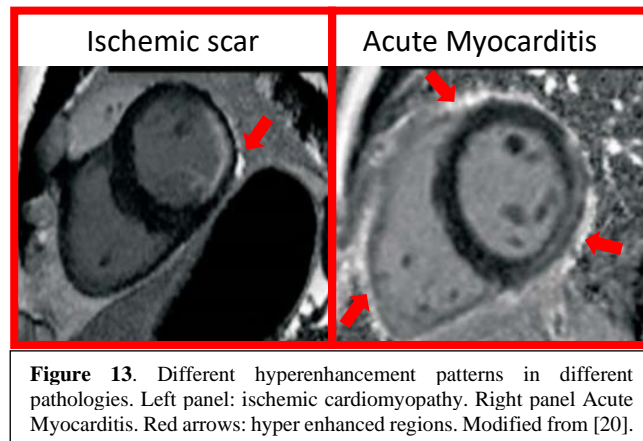
Gradient-Echo (GRE) sequence uses a weaker RF pulse, compared to that of SE, to move the magnetization by a small angle and refocus the decaying transverse magnetization through a bipolar magnetic gradient. The echo signal produced by the GRE sequence is called the gradient echo or field echo. These modifications allow TR in the GRE sequence to be as short as tens of milliseconds or less in the upgraded machinery.

It is used primarily for Bright Blood imaging (Figure 12, right panel) to evaluate global and segmental LV function. It has been used for measurements of LV mass, myocardial perfusion, blood flow and coronary anatomy [21, 26].



Cine MRI modality is made to capture a sequence of images in motion of the cardiac cycle, displaying the cardiac motion in a cine loop way. Differences between the myocardium and blood allow visualizing changes in the cardiac chambers and ventricular walls. Thus, it allows an easy quantification of the ventricular function and local wall motion and provides important information about the cardiac function. Accurate quantification of the RV is important for congenital heart disease, such as Tetralogy of Fallot, transposition of great arteries and arrhythmogenic RV dysplasia. [21]

Perfusion MRI (Late gadolinium enhancement MRI; LGE-MRI). As stated before, the human body is roughly composed for 70% of water and this is the focal basis of the MRI functioning. For this reason, the best choice for a contrast agent is a water-soluble one. Gadolinium (Gd) is a water-soluble chelated agent that lies in the intravascular space and permeates the interstitial space of tissues except for the brain (due to the blood brain barrier). Therefore, with Gd injection it is possible to assess the myocardium state. A healthy tissue will display different Gd concentration curves compared to a pathological one due to the different kinetics. Moreover, pathological myocardium has larger interstitial space, compared to the healthy one, due to the loss of intact myocardium in infarcted/scarred hearts. Since the Gd is a contrast agent that predominantly shortens the longitudinal relaxation time (T_1) of the proton spins, abnormal myocardium with increased Gd concentration will show signal enhancement on MRI images (hyperenhancement) (Figure 13) [21, 26].



Myocardial T1 mapping. LGE-MRI alone is not efficient to evaluate fibrosis because the signal intensity of the affected myocardium is not enhanced. Therefore, the quantification of T1 relaxation time is used to provide information about fibrosis. The modified Look-Locker inversion recovery (MOLLI) sequence is a novel pulse sequence that allows T1 quantification of the myocardium [26].

Using the Gd injection as contrast agent, T1 of healthy and pathological myocardium shows different behaviors, with normal myocardium displaying high T1 compared to the pathological one or LV cavity [27]. T1 values similar or lower than the LV cavity blood are used as index of abnormal Gd accumulation in the myocardium due to a higher level of fibrosis.

The main limitation of T1 mapping lies in the results highly dose dependent. Therefore, clinicians need to standardize the optimal dose, especially in patients with impaired kidney or chronic renal diseases [26]. Another important limitation consist in the lack of standard physiological values approved by the scientific community.

Myocardial T2 mapping. T2 relaxation time evaluation is used to reconstruct a parametric image. As stated before, the accumulation of water in the myocardium is associated with pathology. Studying the T2 relaxation time could be useful to identify myocardial regions with water accumulation or edema, specific characteristics of Acute Myocardial Infarctions (AMI). This is important to identify salvageable myocardial tissue that is highly associated with short- and long-term survival after AMI [21, 26].

MRI has introduced a very important upgrade in the cardiac imaging field especially for its safety avoiding radiations and contrast agents with adverse reactions. However, MRI machineries are very expensive and it takes long time to perform a proper investigation. Furthermore, the lack of standard examination protocols limits the possible comparisons in different studies to set proper clinical guidelines [21].

1.2. Video Kinematic Evaluation (Vi.Ki.E.)

1.2.1. Introduction

The cardiac imaging field has grown faster in the last three decades reaching a very accurate diagnostic and prognostic capability. However, even if there is a fully comprehension in both diagnosis and prognosis, there is still a big gap in the intraoperative evaluation of cardiac parameters. As well as the patients lie down unconscious on the surgical table, the cardiac evaluation during surgery is suspended. None can evaluate intraoperative cardiac parameter in surgery that requires aortic clamping with the consequent cessation of the heart beats. However, all the normothermic surgeries performed at beating heart, as well as heart transplantation or LVAD implantations, impacts immediately and strongly on heart.

Will these heavy and invasive procedures have an impact directly on the heart functionality? Will the cardiac modifications (patches, VAD, transplanted heart) lead to the future development of pathological situations?

Is it really necessary to preventively operate young patients or it would be better to postpone the surgery by waiting the pathology progression?

To date there are no answers and many clinical trials are trying to figure out which parameters should be used as diagnostic/prognostic markers, like a sort of “Holy grail” rush.

Video Kinematic Evaluation has been developed to provide a novel point of view trying to answer some of the above questions.

1.2.2. Vi.Ki.E. functioning

Vi.Ki.E. technology is as simple as innovative. It only consists of a high-speed camera (from 200 fps in humans, up to 1700 fps in animals) positioned above the open chest (Figure 14, a) recording cardiac cycles after the pericardial suspension. A virtual tracking allows to follow the epicardial movement of the heart in the recorded video (Figure 14, b), providing its trajectories (Figure 14, c) and Video Cardiograms (ViCGs) (Figure 14, d). Furthermore, a custom-made algorithm evaluates trajectories and ViCGs, converting them into kinematic parameters, based on Hamiltonian mechanics (Table 1). All the parameters are shown in real-time to surgeons in the operating room, providing data about mechanical performance progression of the heart [28, 29].

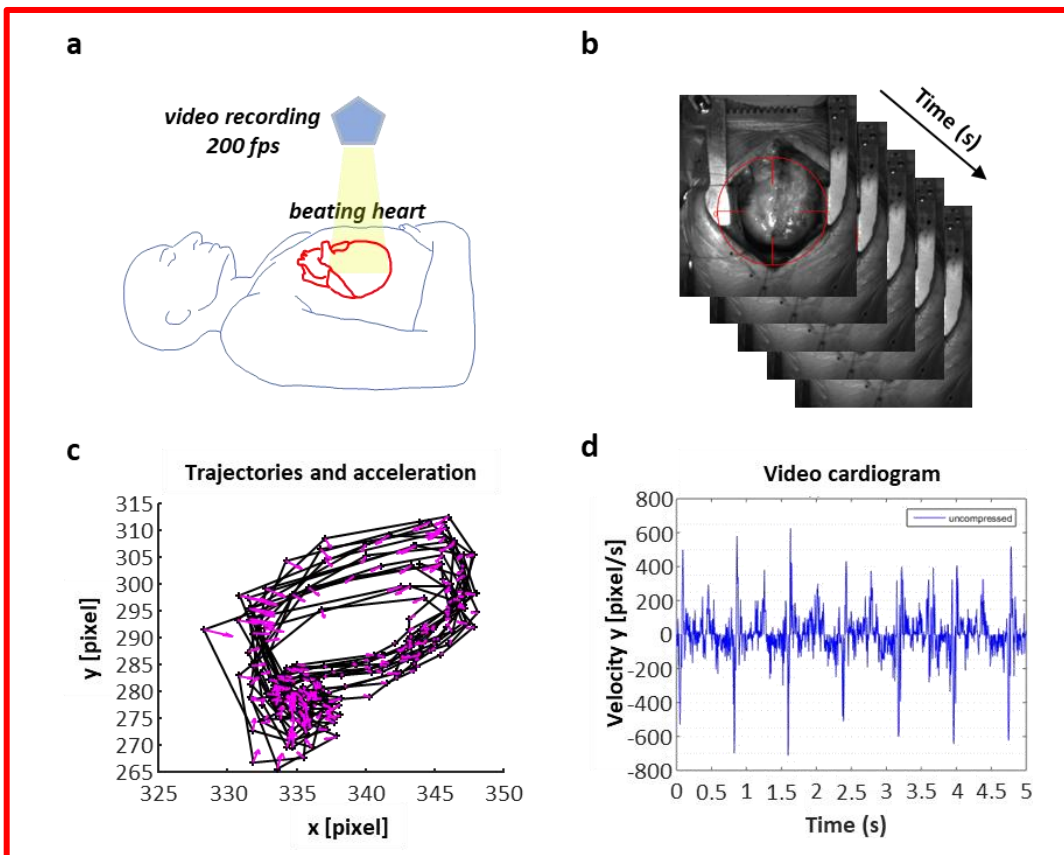


Figure 14. Workflow with video camera positioning, video recording, evaluation of the systolic and diastolic phases and Vi.Ki.E. parameters. (a) Schematic representation of the camera positioned using an extensible tripod on top of the open chest. (b) Sequence of video frames captured at 200 fps from a human beating heart with the video marker (red circle) 'anchored' to the cardiac tissue while moving in x-y directions. (c) Counterclockwise trajectories of contraction (left to right) and relaxation (right to left) for every cardiac cycle with related acceleration vectors (pink arrows). (d) Video cardiogram (ViCG) showing the velocity of a selected video marker with contraction/relaxation peaks and peak-to-peak intervals.

Parameter name	Formula	Physiological meaning
Displacement [pixel]	$U=dx$	Marker displacement between 2 consecutive video frames: it estimates the instantaneous movement of the cardiac tissue and builds the marker trajectory.
Velocity [pixel/s]	$v=dx/dt$	Marker velocity between 2 consecutive video frames: it estimates the instantaneous motility or contractility of the cardiac tissue and builds the marker trajectory.
Kinetic energy [pixel ² /s ²]	$E=1/2v^2$	Marker kinetic energy between 2 consecutive video frames: it estimates the consumption of ATP to generate the cardiac movement.
Frequency [Hz]	$f=\text{beat number}/\text{video duration}$	Contraction frequency calculated from the cardiac beats identified.
Acceleration [pixel/s ²]	$a=dv/dt$	Marker acceleration between 2 consecutive video frames: it estimates the instantaneous variation of the motility of the cardiac tissue and builds the marker trajectory.
Force [N]	$F=ma$	Cardiac force moving the mass m.

Table 1. Table displaying kinematic and dynamic parameters calculated with their physiological meaning. According to classical and Hamiltonian mechanics, $x(t)$ is the position vector (pixel) in the coordinate system (x, y) of an orthonormal Euclidean space, where t is the time (s).

1.2.3. Camera speed selection

The camera speed selection is crucial. In this work, two different cameras have been used. A 200 fps camera for the operating room, and a fast 500 to 1000 fps camera for the experimental animals [30]. The selection of a slower camera for patients' evaluation and a faster one for the experimental animals is due to two main aspects:

- In the operating room, the spaces are limited, thus the necessity to use a small camera, working with a USB 3.0 linked to a laptop. Furthermore, the human heart counts approximately 75 beats/minute, usually lowered by anesthesia (around 1 beat per second). Therefore, 200 frames in one second lead to a very high accuracy sampling (1 image every 5ms) that is extremely accurate to study human phenomena like mechanical ventricular systole (300-400ms) and diastole (400-500ms).
- In the laboratory, there is almost no space limitation, thus, the possibility to use a 500 to 1000 fps camera which requires a very complex and bulky series of equipment connections to properly work. Furthermore, the rat heart, under anesthesia, has in average 240 beats/minute, approximately 1 beat every 250ms. Therefore, the sampling is 1 image each ms (1000 fps) or 1 every 2ms (500 fps), that are both accurate to record mechanical ventricular systole (80-90ms) and diastole (140-150ms).

In the first Vi.Ki.E. publication [28], it was highlighted, in a rat model, the effect of different frame rates on trajectories, and consequently on data, as shown in Figure 15.

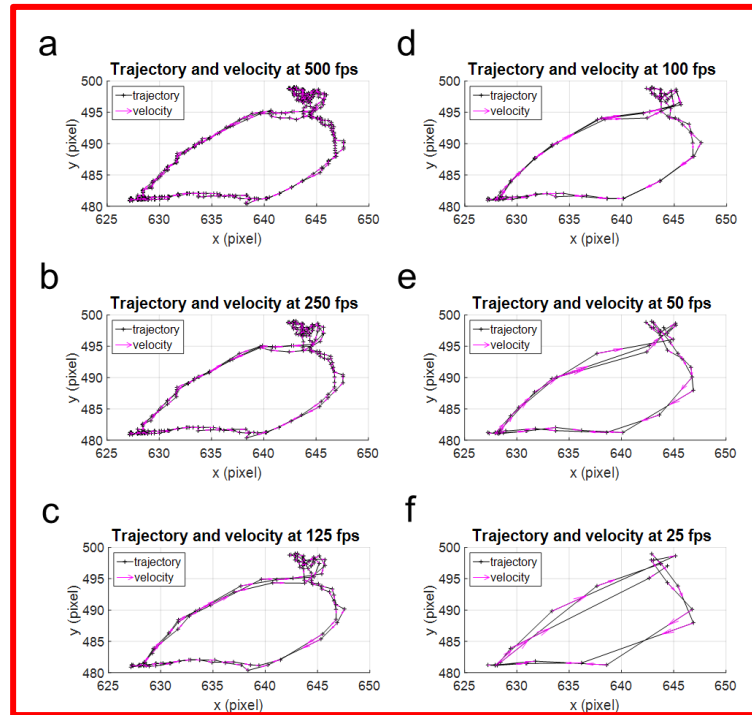


Figure 15. Marker's trajectories and the related velocity vectors obtained at different acquisition rates. The rate of 500 fps (a) gave the best trajectory details, the rates of 250 (b), 125 (c), 100 (d), and 50 (e) could be considered acceptable, whereas the other lower rates (≤ 25 fps in f) were significantly affected by the aliasing phenomenon with loss of trajectory details.

1.2.4. Trajectories and Video cardiograms: a qualitative point of view

The cardiac tracking software provides a .csv file that, after its conversion in .txt format, is ready to be open by the custom-made algorithm in MATLAB (The MathWorks, Inc., Natick, MA, USA).

Trajectories and ViCGs are, respectively, the main information on cardiac cycle and marker movement and all the Vi.Ki.E. parameters are calculated from them.

The visualization of both Trajectories and ViCGs, however, is mainly qualitative. Indeed, Trajectories provides information about cardiac cycles as shown in Figure 16. The cardiac cycles overlapping denotes a conserved mechanic of the beats (Figure 16, B, top panel). On the contrary, a spread trajectory denotes an impaired cardiac mechanics (Figure 16, A, top panel). Furthermore, trajectories provide information on systolic and diastolic phase, but they differ according to the position of the camera upon the heart (Human: left to right systole, Figure 14, c; Animals: left to right diastole, [30])

Video cardiograms provide information about Marker velocities and/or acceleration, and their visualization can be used for qualitative speculation. As shown in Figure 16, A, middle and bottom panel, it is challenging for a beginner, and some time even for experts, to distinguish beats from spikes or noise signals, denoting an impaired cardiac mechanics. The opposite occurs in B, middle and bottom panels of the same figure, where the peaks are clear, with a constant distance between them, denoting a good mechanical behavior.

Even if these parameters can help the operators to have a global idea on mechanical heart behavior, they cannot assess the cardiac function. In several cases, as LVAD implantation, trajectories are strongly impaired by the implantation, limiting the cardiac movement, and resulting in useless data.

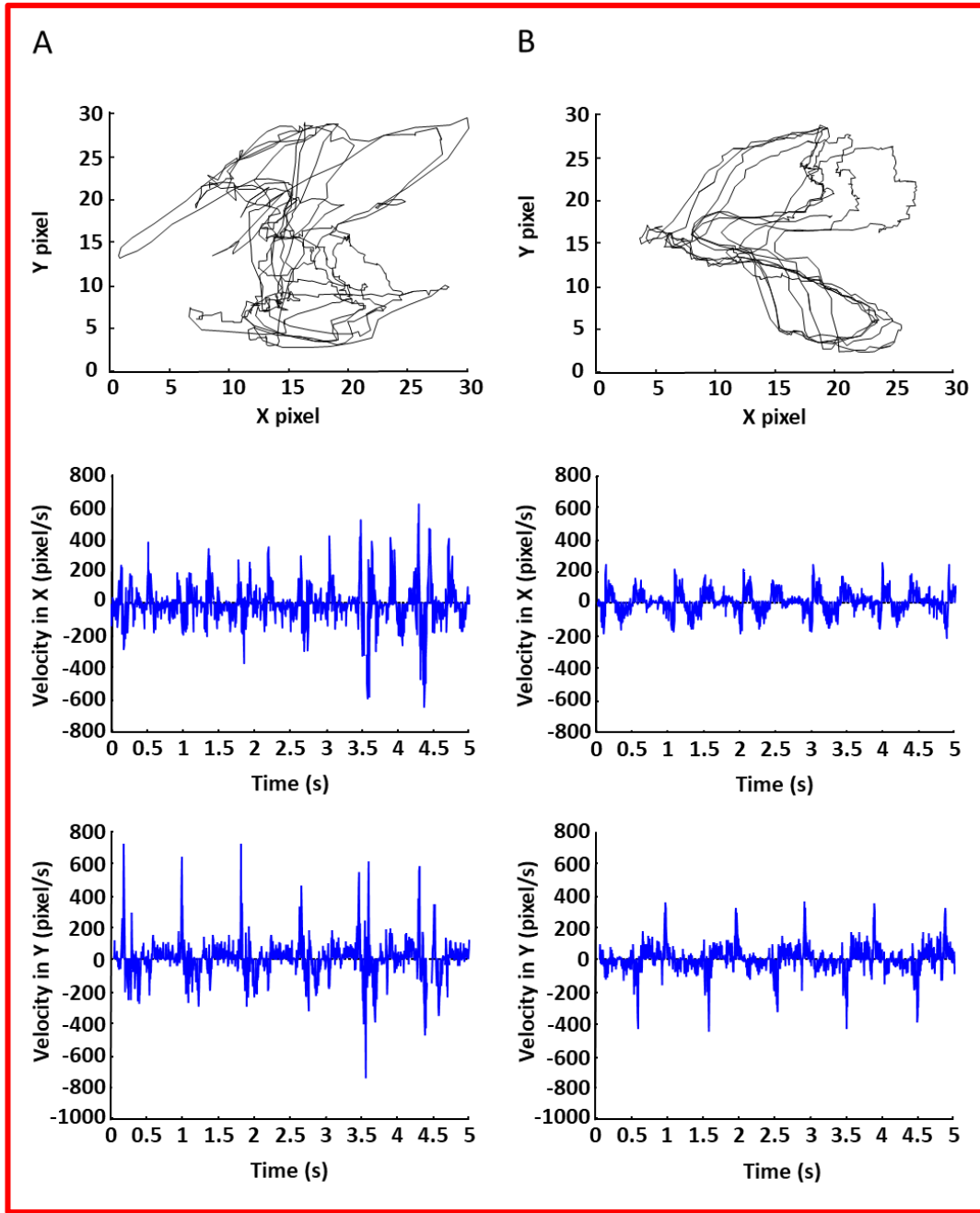


Figure 16. Visualization of epicardial marker trajectories in a patient before surgery (column A) and after surgery (column B) and their related video cardiograms. Top panels: trajectories. Middle panels: video cardiograms on X axis. Bottom panels: video cardiograms on Y axis. To note trajectories in B are more conserved, even if shifted, compared to A where they are randomized. The same observation can be made for the repetitive patterns of video cardiograms in B column compared to A column.

1.2.5. Mechanical parameters explanation and physiological meaning

The quantitative measures of the video kinematic evaluation are based on the Hamiltonian mechanics, thus based on the Kinetic Energy. Briefly, the Newtonian equation of motion ($F=m*a$) can be easily obtained not from the acceleration (which is easy to understand, but challenging to apply), but from the gradient of the total energy of the mechanical system. The total energy, also called “Hamiltonian function” is the sum of the kinetic and potential energies. In the Vi.Ki.E. specific case the potential energy of the heart system is supposed to be uniform in space since the concentration of ATP inside the tissue is uniform [31]. Therefore the mechanical force F is just the gradient (first derivate) of the kinetic energy.

The Vi.Ki.E. algorithm, uses those formulas to obtain precise values starting from trajectories and Video Cardiograms, in other words, from the marker position and its velocity and acceleration in each frame.

As stated in Table 1 the main parameters are:

- Displacement (pixel); the instantaneous movement of the cardiac tissue in x and y directions; it builds the temporal-spatial trajectory.
- Velocity (pixel/s); the instantaneous motility or contractility of the cardiac tissue; it builds the temporal-spatial trajectory.
- Kinetic Energy (pixel²/s²); an estimation of the consumption of ATP for the generation of cardiac movement.
- Frequency (Hz); contraction frequency calculated from the identified cardiac beats.
- Acceleration (pixel/s²); the instantaneous variation of the cardiac tissue motility; it builds the temporal-spatial trajectory.
- Force (N); cardiac force moving a mass [28].

The most relevant parameters for both clinical and experimental fields are the Energy and the Force.

The Energy, as stated in before, is an estimation of the ATP consumption [31]. This is very important because it can be used as a prognostic marker.

Force is expressed in Newton, and it implicates a “mass” and an “acceleration” ($F=m*a$). In the next chapter, it will be explained in detail how the force was validated, but briefly, a note mass was attached on the epicardium and followed with the video Marker.

In human surgery, it is not impossible to attach some mass onto the epicardium, especially for a whole ventricle evaluation. For this reason, the light is used as the “mass” to follow with video Marker, assuming that the weight of the light is unitary. Therefore, the Force is equal to the acceleration.

In the clinical bench, the Force is not the real heart force of contraction because, as stated, we do not consider the real mass of the heart. However, Force parameter provides an evaluation of Cardiac Fatigue that can be very useful as a clinical marker.

1.3. Particle Image Velocimetry (PIV)

In this work, a modified version of the well-known Particle Image Velocimetry (PIV) tool was adopted, in some cases, to further investigate the epicardial deformation of the heart. This software is used in literature to evaluate the motion of liquids “particle by particle” [32]. Adapting the software to the cardiac surface, as it would be a fluid, is useful to obtain interesting data about the epicardial velocity and the rotation frequency of its vectors that estimates the epicardial torsion as shown in Figure 17.

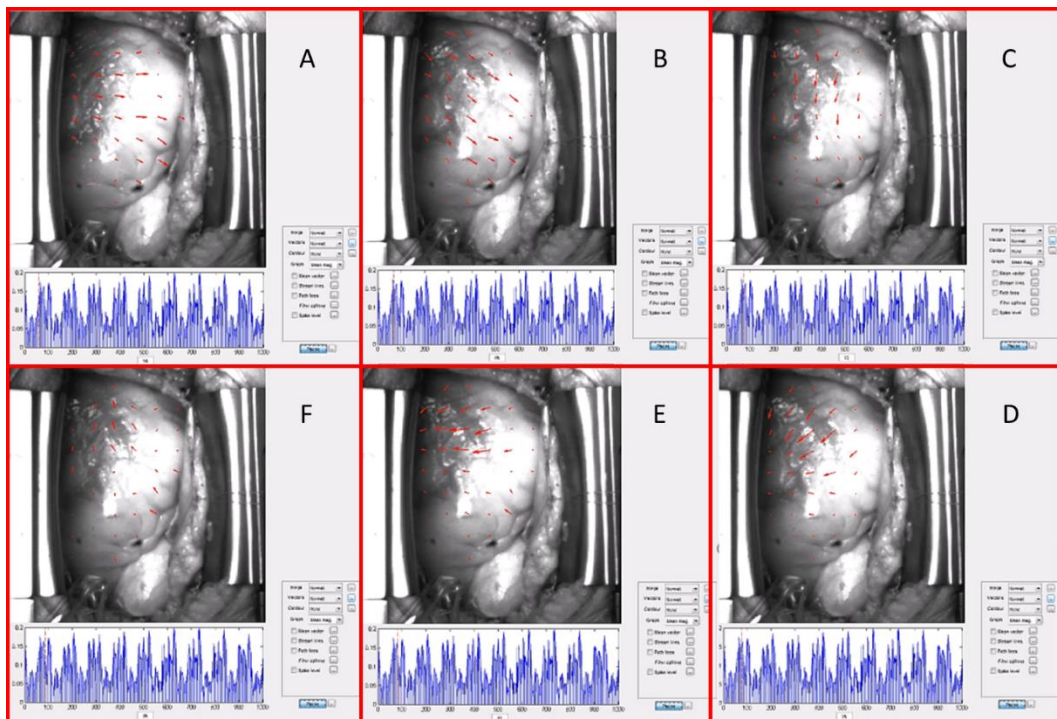


Figure 17. PIV visualization of epicardial torsion. Six different frames from a video evaluation made by PIV (From A to F). Red arrows: velocity vectors. Blu Graph: visualization of the mean velocity for each frame visualized by the red dashed line.

To note the rotational behavior of the Velocity vectors through the frames. This provide an estimation of epicardial torsion.

1.4. The Vi.Ki.E. competitive advantage

In this chapter a summary of all the pros and cons of the technologies explained above will be presented, and it will be displayed which competitive advantage the Vi.Ki.E. approach can contribute to the cardiac imaging theater.

Echography

- Transthoracic Echocardiography:
 - Pros: Non-invasive
 - Gold standard for the diagnostic evaluation
 - Detects four-chambers anatomy and function in addition to wall thickness and cavitary sizes
 - Provides information about blood flow
 - Cons: Not possible to use during cardiac surgery
 - Highly skill dependent
 - Requires time to obtain diagnostic data
 - Low image spatial and temporal resolution

- Transesophageal Echocardiography:
 - Pros: Gold standard for the cardiac evaluation during surgery
 - Optimal LV evaluation (anatomy, function, wall thickness, cavitary sizes)
 - Provides information about blood flow
 - Cons: Invasive
 - Risk of adverse events (ventricular fibrillation)
 - Does not evaluate the RV (provides only qualitative information)
 - Highly skill dependent
 - Requires time to obtain diagnostic data
 - Low image spatial and temporal resolution

Nuclear Cardiology

- Pros: Gold standard for the artery health evaluation (SPECT-MPS) and provides information about both the blood supply to the heart muscle and the metabolic activity of the heart (PET)
Detects chambers anatomy, valve function, and ventricles pumping function with RNV
Assessment of Myocardial Injury, Infarction and Infection
Imaging of the Nervous System of the Heart
- Cons: Side effects due to the radioactive dye injected
Limited use since the advent of CT and MRI
Low image spatial and temporal resolution

Cardiac Computer Tomography

- Pros: Calcium sedimentation in the coronaries (Calcium scoring)
Coronaries blood flow evaluation (Coronary CT angiography)
Provides chambers functional parameters (High-pitch CT scan)
- Cons: Radiation emission correlated with LAR of cancer development
Side effects correlated to the drugs introduced to perform a proper CT evaluation (i.e. sublingual nitrate, beta blockers)
Takes time to grab images resulting in artifacts especially in patients with arrhythmias and/or respiratory impairments (even in the new 360-slices models)
Very expensive machineries

Magnetic Resonance

- Pros: Optimal chambers evaluation (anatomy, function, wall thickness, cavitory sizes)
Provides information about blood flow and coronary anatomy
Assesses the pathological state of the heart with a contrast agent (hyperenhancement)
Evaluates the fibrosis (T1 mapping MOLLI) and the AMI (T2 mapping)

- Cons: Takes long time to perform a proper evaluation
 No T1 mapping standard examination protocols (T1 mapping results are dose dependent) and Lack of standard physiological values
 Very expensive machineries

Video Kinematic Evaluation

- Pros: Non-invasive
 Innovative approach based on epicardial motion, and consequent novel set of useful clinical data, highlighting unexplored aspects of the cardiac function
 Fast evaluation
 Algorithm-based evaluation (no technical skill required, high data reproducibility)
 Quantitative RV evaluation
 Translational technology, with low costs in each field (cellular, basic research, clinic)
 High spatial and temporal resolution (up to 1000fps)
- Cons: Only applicable during open chest surgeries
 Lack of standard physiological values
 Limited number of cases evaluated
 Only RV evaluation in human

The medical technological evolution always carries innovative, less invasive, and cheaper approaches, leading to a constant amelioration of patients' outcome and recovery. However, most of the times, the innovative approaches are barely comparable with the old technologies, and, when possible, only some aspects of the novel techniques can be comparable. Video Kinematic Evaluation suffers this complication. In fact, as stated before, the main limitation in all the current technologies in the heart imaging field is the spatial and temporal resolution. Vi.Ki.E has been developed to overcome this gap. The high speed cameras adopted allow to precisely evaluate every physiological aspect of the cardiac beat (i.e. the systolic/diastolic phase only, the atrial kick, the ventricular distension) without

artifacts and/or technician's interpretations. Moreover the epicardial kinematic approach is unique in the cardiac field and cannot be compared with any of the other current techniques, except in some cases where a simple data linear regression can be performed.

In the Vi.Ki.E. contest the most comparable technique is the TEE, since they are both intra-surgical approaches. The coupling of Vi.Ki.E. with TEE can provide a "360 degrees" heart evaluation, optimal in the surgeries implying both ventricles as LVAD implantation.

2. METHODS

2.1. Instrumentation

The setup adopted in this work is approximately the same for both clinical and basic research approaches, with some small differences, as cited above, due to the different heart size and rate between patients and experimental animals.

Vi.Ki.E. Clinical instrumentation.

- Extensible tripod holding the camera on top of the patient's chest.
- Low-speed camera: full HD (1920×1080 total pixel area) camera Samsung S10 (with an internal SD memory of 256 MB and internal rechargeable battery)
- High-speed camera Basler acA1300-200um USB 3.0 with the ON Semiconductor PYTHON 1300 CMOS sensor, (1280×1024, Ahrensburg, Germany)
- Edmund Optics 6mm compact fixed focal length lens (Barrington, NJ, USA)
- High-performance PC Intel core i7-6700HQ 2.6GHz, 16GB DDR4 2133MHz SDRAM, 1TB HDD 7200 RPM With 128GB SSD PCIE ×4
- Acquisition software: Pylon 5 Camera Software Suite 5.0.5 for Microsoft Windows (Ahrensburg, Germany).

Vi.Ki.E. Experimental instrumentation.

- Low-speed camera: full HD (1920×1080 total pixel area) camera Samsung S10 (with an internal SD memory of 256 MB and internal rechargeable battery)
- High-speed camera Baumer HXC13 (Baumer Italia, S.r.l. , Milano, IT) camera with full CameraLink® interface (1280×1024 total pixel area for 500 fps or 1020×600 for 1000 fps)
- Macro objective Kowa Industrial Lenses LM35XC, F = 1:2.0, f = 35 mm, picture size 13.8-18.4 mm (RMA Electronics, Hingham, MA, USA).

- The acquisition software was custom made in LabVIEW Visual Programming Language (National Instruments, Assago, Milano, Italy)
- Frame grabber acquisition board PCIe 1433 (National Instruments, Italy) adapted into a Workstation HP Z220 (Crisel Instruments, Italy) with 24 GB RAM.

2.2. Settings and placement of the marker

To obtain reliable results, it is fundamental to place and set up the marker correctly. The tracking program implied is Video Spot Tracker (VST), an open-source software from CISMM (Computer Integrated Systems for Microscopy and Manipulation) University of Chapel Hill, North Carolina (<http://cismm.web.unc.edu/software/>).

To start the tracking, it is necessary to open the video recorded or the sequence of images in the software. Figure 18 shows the workspace and the first video frame.

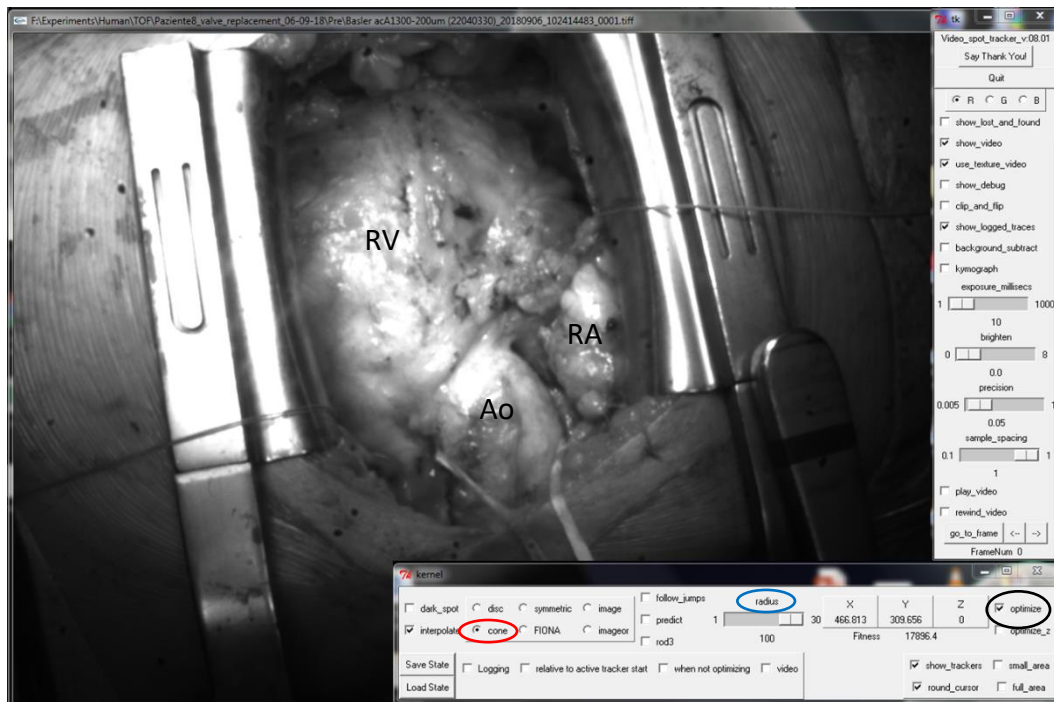


Figure 18. VST workspace and first frame of the video. Colored ellipsis show the most useful sections of the “kernel” workspace. RV: Right Ventricle. Ao:Aorta. RA: Right Atrium

The first setting step is to select the kernel (Figure 18, red ellipse). A kernel is the algorithm implied in the tracking. In this work, the “cone” was the optimal selection in all the evaluation (both patients and experimental animals) due to its capability

to follow the brightest spots on the images. Other kernels track different aspects like shadows, edges, fluorescent dyes, and many others.

The second step is the selection of the marker radius (Figure 18, blue ellipse), different radius provides different trajectories due to the number of points tracked (Figure 19). The radius selection is based on the required evaluation. As shown in Figure 19 (in the left column), the marker appears too small for an entire RV evaluation. The opposite is shown in Figure 19 (right column) where the marker includes both Aorta (Ao) and Right Atrium (RA) light spots, thus mediated in the trajectory. The Middle column, on the contrary, shows an optimal marker position where the most mobile region of the RV is tracked [33]. The third step is the marker optimization (Figure 18, Black ellipse), allowing the software to automatically fit the best marker starting area based on the selected kernel.

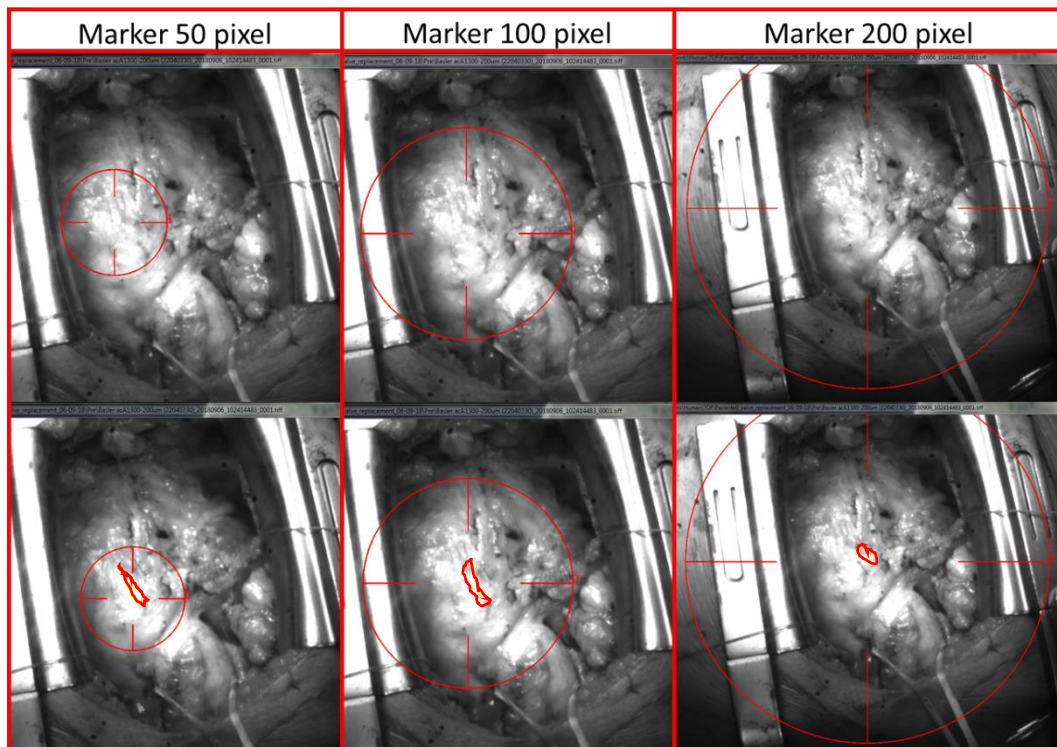
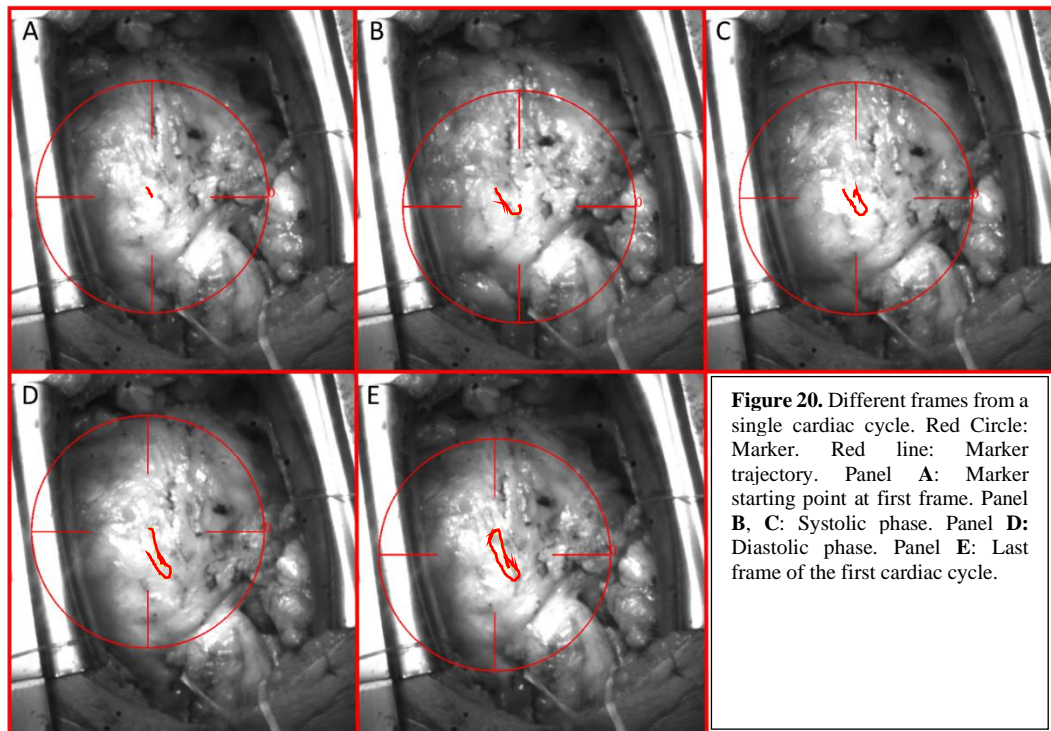


Figure 19. Different marker radius and trajectories. Left column: Marker radius 50 pixels with marker optimization (top panel) and marker trajectory (bottom panel). Middle and Right column same as Left but for marker radius of 100 pixels and 200 pixels, respectively.

As stated before, the “cone” kernel is based on the light changes on the epicardium, thus the importance of the light placing step. This should be extremely accurate to allow the best reproducibility of the data, especially in the “Before-After surgery” data comparison where both the light and the marker radius should be as similar as possible.

Figure 20 shows different frames of the same cardiac cycle to focus the attention on how the light is moving upon the epicardium. The changes in light are a consequence of the blood flow inside the chambers. When the “main spot” of light moves near the Aorta (Figure 20, A-B) it means that the epicardium in the heart base is in the nearest position to the light source. This is due to the augmented blood filling in the base of the heart compared to the apex; typical phenomena occurring during systole. On the contrary, when the “main spot” of light is moving further from the Aorta (Figure 20, C-D), the diastolic phase is underway. In the panel E of the Figure 20, the cardiac cycle reaches the same position of panel A and the cardiac cycle is closed.



The light positioning can be very challenging in some cases. Figure 21 shows a wrong light positioning in which the “main spot” of light is placed on the chest divaricator leading to a jump in the marker. During a marker jump, the acceleration is tending to infinite thus corrupting the kinetic values. Marker jumps can occur any

time when two or more “main spot” of light appears during the cycle. Therefore, the importance to check the light positioning before the recording.

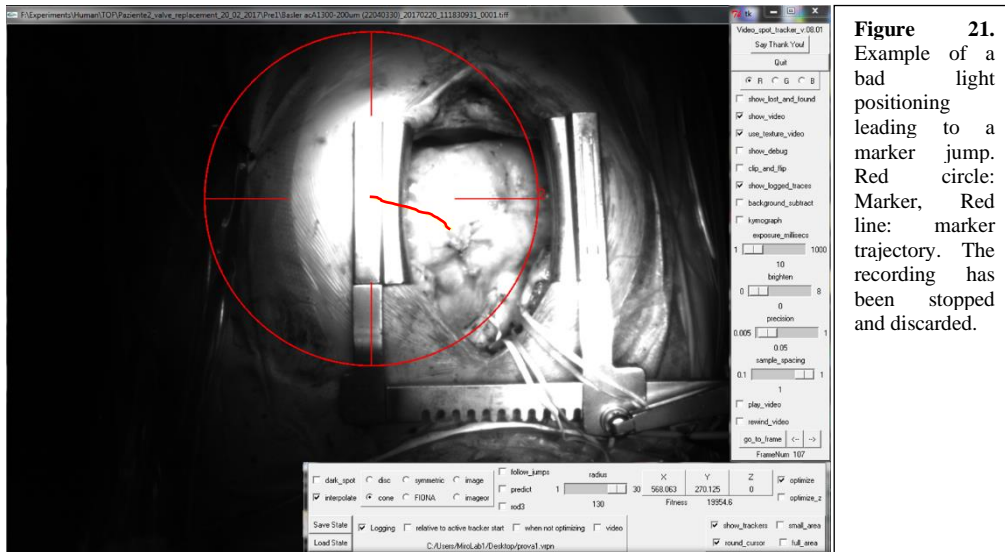


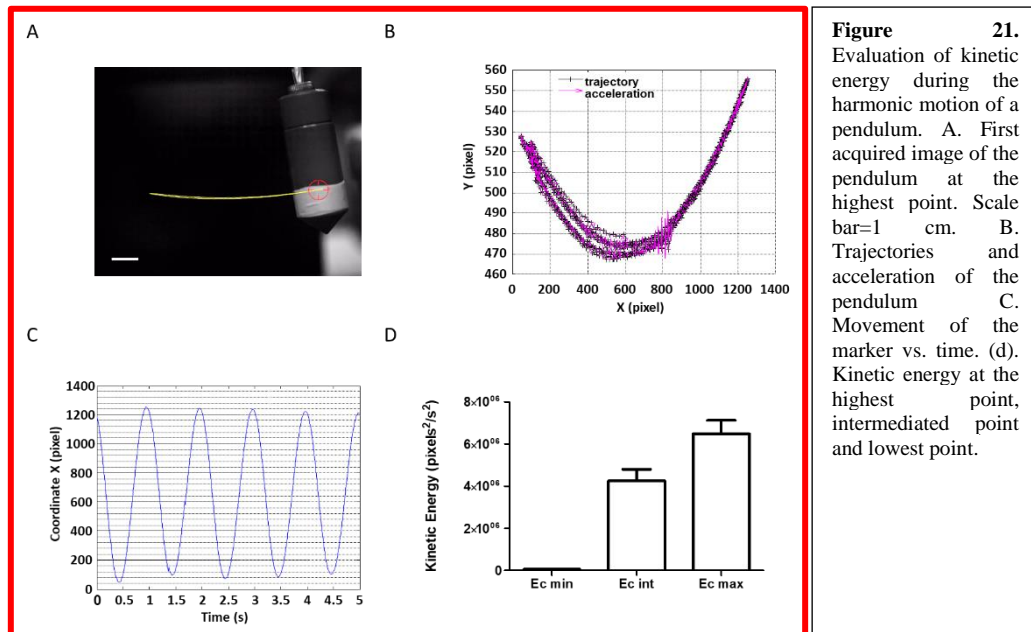
Figure 21. Example of a bad light positioning leading to a marker jump. Red circle: Marker, Red line: marker trajectory. The recording has been stopped and discarded.

2.3. Vi.Ki.E. Validation

The Vi.Ki.E. technology is new and custom made, so it was necessary to perform a proper validation for each parameter especially for the clinical practice use.

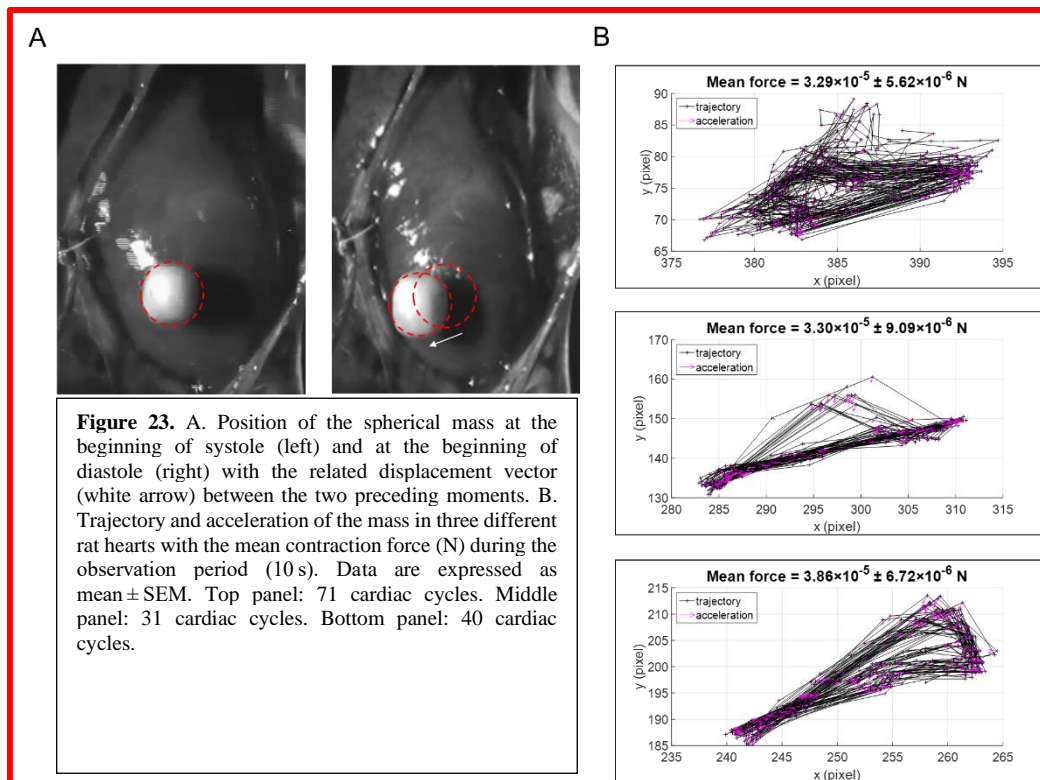
2.3.1. Kinetic Energy validation

The kinetic energy evaluation was performed by acquiring videos of the periodic motion of a pendulum (mass of 200 g) oscillating (Figure 22). The pendulum was connected to an arm by a 21.5 cm non-stretchable string and the motion was acquired at 200 fps for five seconds. The video marker was anchored onto the white area of the pendulum and displayed the trajectories (Figure 22, A), the coordinate x vs. time (Figure 22, C) and the kinetic energy at the highest, intermediate and lowest positions (Figure 22, D). As expected, the marker movement was an arc. When the coordinate x was displayed vs. time, it drew a periodic wave. The kinetic energy measured for five consecutive frames in the three positions was ca. zero at the highest position (all the energy is potential; $h = 17$ cm) and maximal at the lowest position (all the energy is kinetic; $h = 11.5$ cm). In the intermediate position, the kinetic energy was in between the other two measurements [28].



2.3.2. Force validation

The Force evaluation was made by anchoring a known spherical mass (0.035 g, diameter = 3 mm) onto the epicardial surface in three different rat hearts (Figure 23, A). The use of a mass connected to the cardiac tissue allowed a switch from a description in terms of acceleration (pixel/s²) to the International System of Units and, consequently, we calculated the contraction force (N) accelerating the mass and the related ViCG in terms of displacement and velocity. In all three rats, the Force was about the same, suggesting that every cardiac cycle, even if in different animals, exerts a well-conserved force of contraction. We also observed, for every beat, a well-conserved contraction-relaxation trajectory (Figure 23, B), which was a kind of hysteresis loop due to the intrinsic viscoelastic properties of the myocardium [28, 34].



2.3.3. Validation of data during the time

The Vi.Ki.E. validation during the time was evaluated by acquiring 1-second video recording of sinus rhythm at 1000 fps in three healthy rat hearts, every 10 min for 1 h (Figure 24). The video marker was anchored in the same position and monitored changes in Velocity, Kinetic Energy, Force, and Displacement over time. We observed minimal percentage variations (likewise physiological) for the four parameters, suggesting a good reproducibility of our data over time.

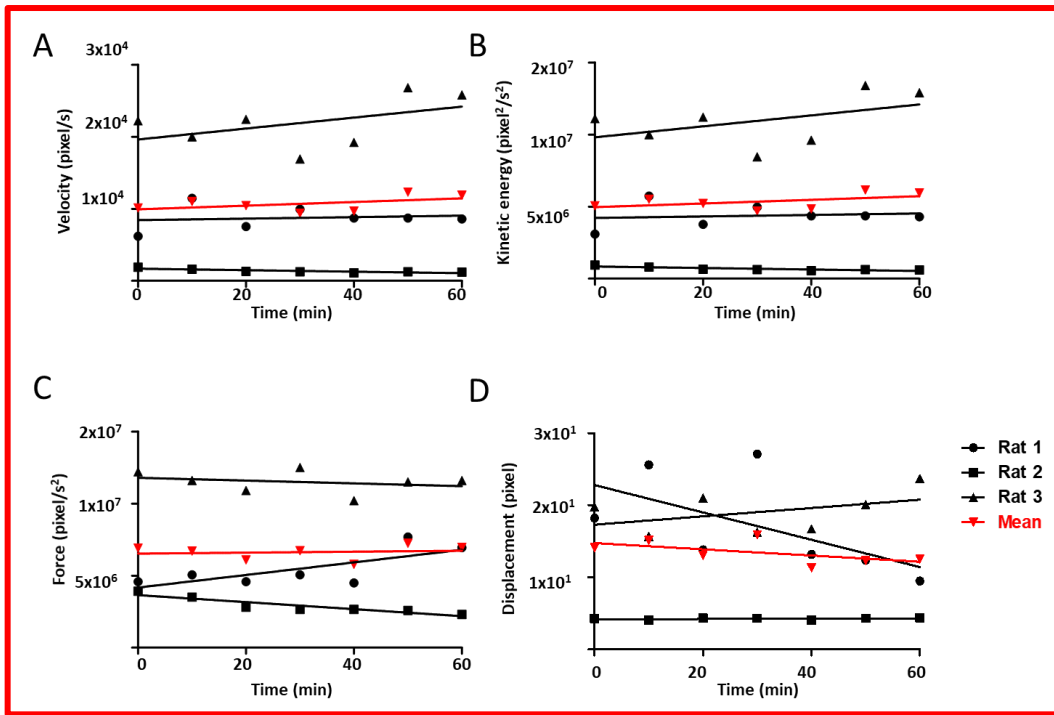


Figure 24. Reproducibility of the acquired data. A. Velocity (pixel/sec) monitored every ten minutes for one hour at 1 kHz temporal resolution. B. Same as A for kinetic energy (pixel²/s²). C. Same as A for acceleration (pixel/s²). D. Same as A for displacement (pixel). Marker radius: 60 pixels. n=3.

2.3.4. Validation in a computer model

The Vi.Ki.E. algorithm effectiveness, of the obtained data, was evaluated through a numerical simulation based on the cardiac electro-mechanical coupling (EMC) model. This model described the interplay between the spread of electrical excitation in the cardiac tissue and the consequent contraction/relaxation process. The EMC model consisted of four sub-components, two for the bioelectrical activity and two for the mechanical response of the cardiac tissue. The two bioelectrical components were the Bidomain model for the electric current flow [35] and the ten Tusscher human ventricular model [36] for the cellular membrane dynamics.

Briefly, the Bidomain model takes into account the electrical properties of cardiac muscle, of both the intracellular and extracellular spaces, through an anisotropy perspective. The ten Tusscher model, takes into account the action potential of human ventricular cells, including a high level of electrophysiological detail (i.e. the fast sodium, L-type calcium, transient outward, rapid and slow delayed rectifier, inward rectifier currents, basic calcium dynamics, calcium transients, calcium current inactivation, and the contraction staircase)

As it concerns the mechanical sub-components, stretch-activated channels were incorporated in the membrane model according to [37]. The macroscopic description of the mechanical activity was based on the equations of finite elasticity, where the passive mechanical properties of the myocardium were assumed to be transversely isotropic, hyper-elastic, and nearly incompressible, defined by an exponential strain energy function derived from [38]. The EMC model was finally closed by the active tension generation model developed describing the process of calcium binding to troponin C and cross-bridge cycling triggered by calcium release from the intracellular calcium stores during the electrical activation of a myocyte. The active tension generated by this model entered as input in the non-linear elasticity equations yielding the active component of the stress tensor.

The intracavitary blood pressure p in the left ventricular (LV) cavity was described by a pressure-volume loop model [39], based on the following four phases:

- Isovolumetric LV contraction phase, where p increased from the end-diastolic pressure (EDP) value of about 2 kPa to 10 kPa;
- Ejection phase, where the pressure-volume relationship was described by a two-element Windkessel model, until the volume reduction stopped;
- Isovolumetric LV relaxation phase, where p decreased to 1 kPa;
- Filling phase, where p increased linearly to EDP.

The model was modified incorporating a transmural ischemic region of $1 \text{ cm} \times 1 \text{ cm}$ with the sequent parameters:

- The intra (i)- and extra (e)- cellular conductivity coefficients of the Bidomain model, along (l) and across (t) the fiber direction, were $\sigma_{il} = 3$, $\sigma_{el} = 2$, $\sigma_{it} = 0.31525$, $\sigma_{et} = 1.3514$, all in $\text{m}\Omega\text{-1cm}^{-1}$. The parameters of the strain energy function were the same of the original paper [39] apart from the bulk modulus, which amounted to 200 kPa
- From the bioelectrical point of view, ischemic conditions were modeled modifying the following parameters of the ten Tusscher model [40]. The extracellular potassium concentration was increased from 5.4 mM to 8 mM; the maximal conductance of the I_{Na} and I_{CaL} currents was decreased by 25%; the parameters of the I_{KATP} current were modified as in [41] for ischemia stage 2.
- From the mechanical point of view, ischemic conditions were modeled by reducing the active tension and passive tissue stiffness by 10% and 25% compared to their normal values, respectively.

The excitation process was initiated by stimulating three endocardial anterior apical sites and one endocardial posterior apical site, mimicking an idealized Purkinje network. Two simulations were performed, one for a healthy tissue (HEALTH) and one for a tissue with a transmural ischemic region (ISCH). In both cases, three beats

were simulated, at a basic cycle length of 500ms. Figure 25 (left panels) display the epicardial distributions of transmembrane and extracellular potentials computed in the HEALTH and ISCH simulations, during the plateau phase of the heartbeat (ST segment, $t = 120\text{ms}$). The ISCH transmembrane potential distribution showed a minimum in the ischemic region, whereas the ISCH extracellular potential distribution showed a maximum (ST elevation) in correspondence of the ischemic region. The kinematic evaluation applied to the experimental data was validated on the simulated data related to the healthy and ischemic tissue. Right panels of Figure 25 report that ischemia decreased of about 20% in: i) the maximum displacement module (Figure 25, right panel, a), ii) the mechanical behavior of the cardiac tissue, with a reduction of the maximum velocity module (Figure 25, right panel, b) and iii) the mean kinetic energy (Figure 25, right panel, c). These theoretical findings validated the use of kinematic parameters markers as indices of cardiac mechanical performance.

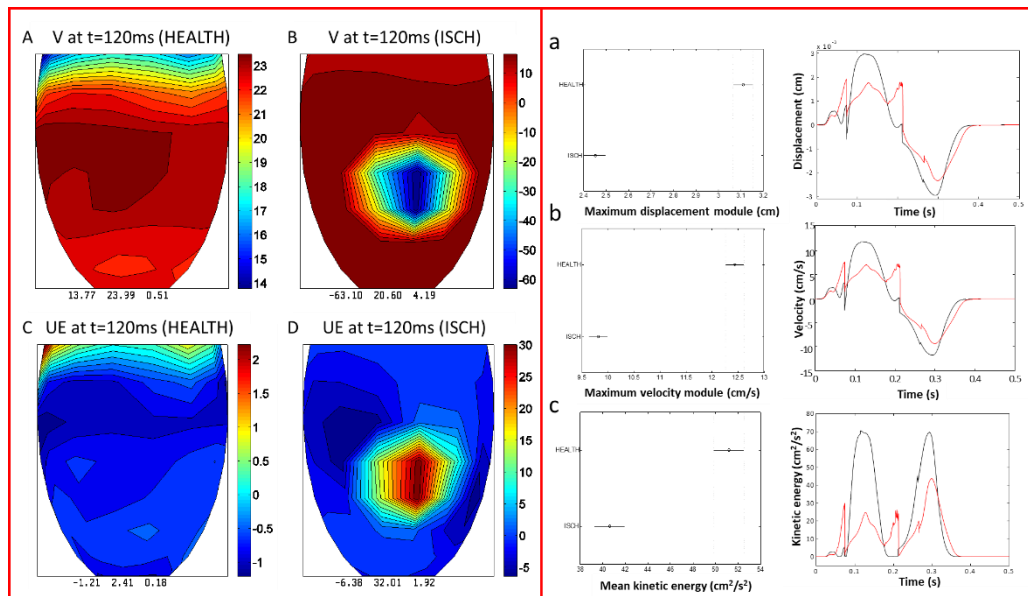


Figure 25. Numerical simulation results of epicardial transmembrane (V) and extracellular (UE) potential distributions. **Left panel.** (A). V distribution at $t = 120\text{ms}$ after the onset of stimulation in the healthy tissue (HEALTH). (B). V distribution at $t = 120\text{ms}$ after the onset of stimulation in the tissue with transmural ischemia (ISCH). (C) UE distribution at $t = 120\text{ms}$ after the onset of stimulation in the healthy tissue. (D). UE distribution at $t = 120\text{ms}$ after the onset of stimulation in the tissue with transmural ischemia. **Right panel.** (a) Left. Maximum displacement module, as defined in Table 1, in marker trajectories (frame distance = 0.25ms), which was averaged across 48 (HEALTH) and 48 ischemic (ISCH) sites. Data are expressed as mean \pm SEM. Right. Time evolution of the displacement of a single sample marker; comparison between healthy (black) and ischemic (red) site. (b) Same as (a) for the maximum velocity module. (c) Same as (a) for the mean kinetic energy. * $p < 0.05$, calculated from one-way ANOVA, LSD post-hoc. No overlapping bars have statistical significance.

2.4. Conversion curve from pixels to millimeters

The necessity to have comprehensible parameters usable by clinicians directly in the operating room forced the conversion of the Vi.Ki.E. pixel values in the SI millimeters unit.

To do that, pictures of a millimeter paper was taken at different heights from 5cm to 60cm with a step of 5cm, counting how many millimeters fitted each image. Three different spots were counted, for both columns and rows, and an average measure for x and y axes was calculated. Since the resolution of the camera was known, it was possible to reconstruct a calibration curve (pixel to mm) as shown in Figure 26.

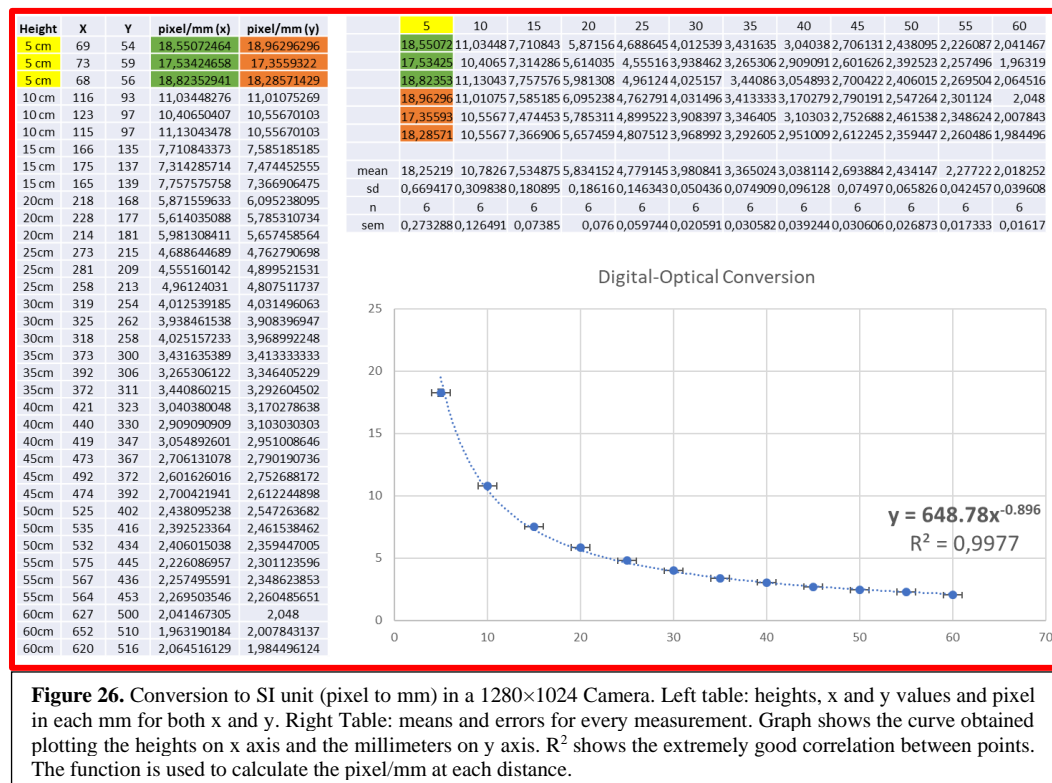


Figure 26. Conversion to SI unit (pixel to mm) in a 1280×1024 Camera. Left table: heights, x and y values and pixel in each mm for both x and y. Right Table: means and errors for every measurement. Graph shows the curve obtained plotting the heights on x axis and the millimeters on y axis. R² shows the extremely good correlation between points. The function is used to calculate the pixel/mm at each distance.

In order to obtain precise values, the camera is usually placed, at the same distance from the heart before and after the surgery. However, it can occur to place the camera at different heights during the surgery due to some clinical necessities leading to a bias of the parameters evaluated. This is the reason why it was created the function to calculate the pixel/mm conversion (Figure 26) at every height in the range between 5 to 60cm. Knowing the camera distances from the heart makes all the parameters comparable.

2.5. Protocols

Human Surgical Protocols.

The human surgical protocols for CABG, GLENN, FONTAN, valve replacements, LVAD implantation, and Heart Transplantation followed the ESC guidelines.

Vi.Ki.E. clinical protocols

All methods and experiments were carried out in accordance with relevant guidelines and regulations set by the Institutional Review Board (IRB) of the Azienda Ospedaliera Universitaria Integrata of Verona, where all the experiments were done (approved protocol from ethics committee on 16th March 2016, # 847CESC Protocol # 13371). All patients signed up an informed consent.

In this work, several different pathological conditions have been monitored starting from Coronary Artery Bypass Grafting (CABG, N=10), Tetralogy of Fallot (TOF, N=12), Congenital Valvulopathy (N=1), Hypoplastic Heart Syndromes (HHS, N=6), Ventricular Assist Devices implantation (VAD, N=6) and finally Heart Transplantation (N=2). The Vi.Ki.E. protocol adopted was approximatively the same to obtain comparable data.

Initially, two time-points were established to record cardiac cycles.

The first time-point was recorded right after the chest opening and the pericardial suspension, where the heart is settled in the pericardial cradle without any compression or mechanical stimuli that can lead to a bias in the evaluation. The second time-point was recorded at the end of the surgery, before the chest closure. A third time-point, was recorded in-between the surgery at the ECC (Extra-Corporeal Circulation) exit, and it was added after the CABG study just to understand the mechanical behavior of the heart in a different pathophysiological state.

For each time-point the extensible tripod, holding the camera connected to the PC, was placed with the camera perpendicular to the heart at approximately 40 cm (Figure 27). Four consequent recordings of 5 seconds at 200 fps were performed.

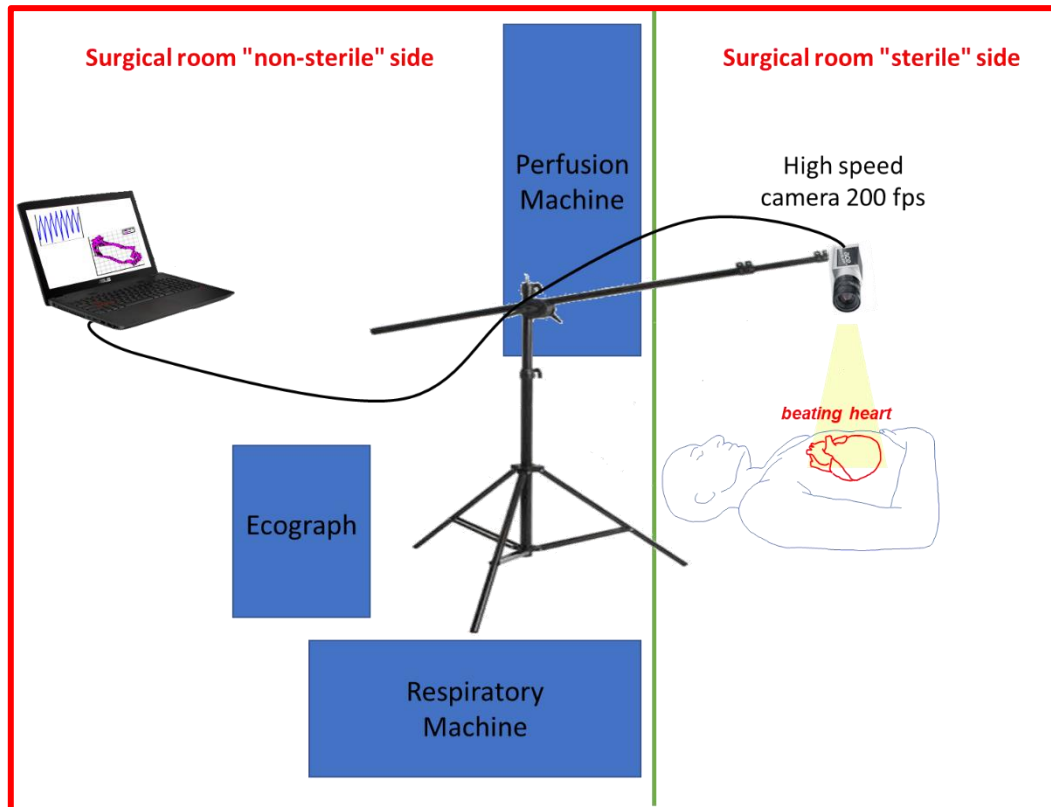


Figure 27. Schematic intra-operative setup. The operating room is divided in a “non-sterile” side, where perfusionists, anesthetists and students can assist the surgery and in a “sterile” side, where only surgeons and assistants can access and perform the surgery. The extensible tripod is in the “non-sterile” side of the operating room and it is just extended for some centimeters in the “sterile” side. This process is very accurate to avoid any touch with the surgical bed or other sterile objects interaction.

In order to optimize the procedure, due to the long buffer time to download the images in the PC memory, leading in more than two minutes of surgeon inactivity and possible loss of focus, a single recording of 20 seconds at 200 fps was performed. The buffer time to download the images in this way is slower but it is performed in post-processing, avoiding surgeon inactivity and loss of focus. Later the videos were split in 4 recordings of 5 seconds each.

Animal surgical protocols

The study was conformed to Italian (D.L.4/3/2014) and European guidelines (2010/63/UE).

The animals were kept in single-sex groups of four individuals from weaning (4 weeks after birth) until the onset of the experiments, in a temperature-controlled room at 20-24°C, with the light on between 7:00 AM and 7:00 PM. The bedding of the cages consisted of wood shavings; food and water were freely available.

Animals were anesthetized either with a mixture of ketamine chloride 40 mg/kg (ip) (Imalgene, Merial, Milano, Italy), or with 0.20 mg/kg (ip) of a mixture of tiletamine hydrochloride and zolazepam hydrochloride (Zoletil; Virbac S.r.l., Carros, France) and medetomidine hydrochloride 0.15 mg/kg ip (Domitor, Pfizer Italia S.r.l., Latina, Italy) for the *in vivo* experiments. The heart was exposed through a median thoracotomy and suspended in a pericardial cradle under artificial ventilation (RoVent® Small Animal Ventilator, Kent Scientific, CT, USA), performed through tracheotomy. Body temperature was maintained constantly at 37 °C thanks to a heat lamp radiation, and further doses of anesthetic were administered as needed during the experiment.

Vi.Ki.E. experimental protocols

The approved protocols, by the Veterinary Animal Care and Use Committee of the University of Parma and conformed to the National Ethical Guidelines of the Italian Ministry of Health, were the following: 41/2009, 59/2012, 281/2017, 989/2017. For each of the underlying protocols, the camera was placed at approximately 17 cm from the heart.

- Measurement of contraction Force. The ventricular force was measured by anchoring a known spherical mass (0.035 g, diameter = 3 mm) onto the epicardial surface in three different rat hearts (Figure 23, A). We then recorded, for each heart, 10 seconds video recording with a low-speed camera at 30 fps.
- Reproducibility of the data acquired. The mechanical parameters were evaluated during time by acquiring 1-second video recording of sinus

rhythm at 1000 fps onto three healthy rat hearts, every 10 min for 1 h. We anchored the video marker in the same position and monitored changes in displacement, velocity, acceleration, and energy over time.

- Ischemia/Reperfusion. Videos of *in-situ* rat hearts, undergoing an acute cardiac ischemia/reperfusion injury model, were recorded at 500 fps for 1 second. The beating heart was recorded in normal conditions followed by anterior descending coronary ligation. The surgical needle was left within the performed knot as this allowed the removal of the ligation without damaging the tissue. Then, after waiting for 6 min and 12 min, other two videos of the beating heart (now ischemic) were recorded. The same procedure was followed after the removal of the ligation (i.e., two video files were recorded after 6 min and 12 min).
- Induced AV block. A flexible cannula (0.8 mm diameter), firmly fixed to a three-axes manipulator, was adopted and positioned ca. 5 mm above the pulmonary cone. A gentle air-pressure flow (20 kPa) was delivered for 1 second using an electro-valve (Asco Numatics, Bussero, Milano, Italy) remotely controlled by a stimulator (Crescent Electronics, Sandy, UT, USA). During the air delivery, a video of 2 seconds at 30 fps was recorded and the changing in the mechanical parameters after an AV block was evaluated.
- Atrial Stimulation. The heart was stimulated with a cathodal suprathreshold train of stimuli (10 Vpp) at different basic cycle length (BCL: 390 ms, 330 ms, 290 ms, 260 ms, 230 ms, 210 ms, 190 ms, 170 ms, 160 ms) by driving the right atrium with a silver electrode (0.05 mm) with one end connected to a stimulus generator (SIU-102, Warner Instruments CT, USA) and the other hooked to the atrial auricle appendage. The current return silver electrode has been placed in the right forearm. The stimulus generator was triggered by a function generator (Aim-TTi TG310, RS Components, Milano, IT). A video of 2 seconds at 500 fps was recorded for each BCL (Figure 28).

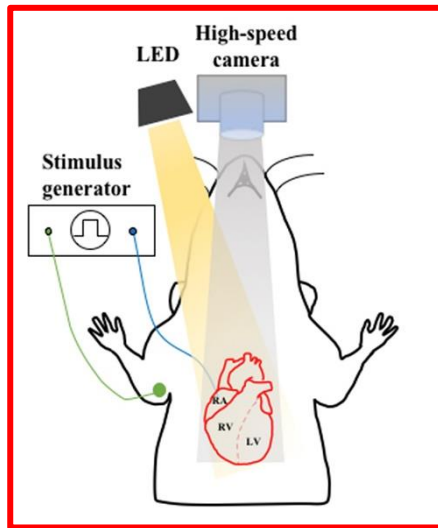


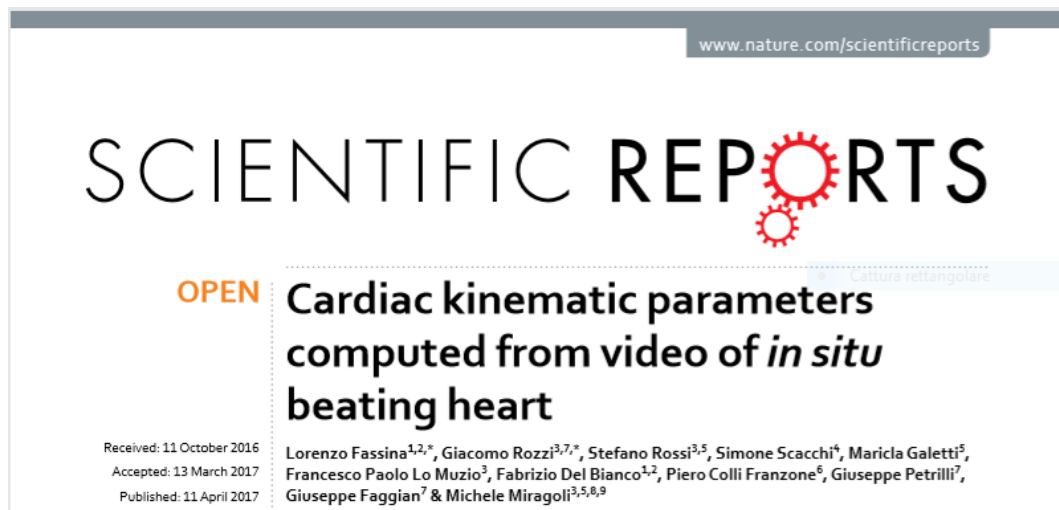
Figure 28. Schematic representation of the experimental setup. A. The heart (red cartoon) is exposed after median thoracotomy. One end of the stimulating electrode (blue line) is hooked on the Right Atrial (RA) auricle appendage to perform atrial stimulation, while the other end is connected to a stimulus generator (black rectangular box). The current return electrode (green line) is placed on the right forearm. The high-speed camera is placed perpendicular to the heart to record anterior epicardial kinematic. The grey shaded region represents the video camera field of view. The LED is placed beside the camera. The yellow shaded region represents the light beam. RV, Right Ventricle; LV, Left Ventricle; dashed red line, interventricular septum.

The complete analysis of the mechanical parameters was performed, for both clinics and basic research, as cited above. Once acquired, the video has been opened with VST, and the light was tracked through the epicardial surface. Finally, the .csv file was evaluated with a custom-made algorithm in MATLAB (Mathworks, USA).

3. RESULTS

The results shown in this work will be presented in a chronological order to offer to the reader the feeling of a growing project able to gradually evaluate more complex situations. Chapters 3.1, 3.2 and 3.3 will report the entire publications as they are, including images and references.

3.1. Cardiac Kinematic parameters computed from video of *in situ* beating heart [28].



3.1.1. Abstract

Mechanical function of the heart during open-chest cardiac surgery is exclusively monitored by echocardiographic techniques. However, little is known about local kinematics, particularly for the reperfused regions after ischemic events. We report a novel imaging modality, which extracts local and global kinematic parameters from videos of *in situ* beating hearts, displaying live video cardiograms of the contraction events. A custom algorithm tracked the movement of a video marker positioned ad hoc onto a selected area and analyzed, during the entire recording, the contraction trajectory, displacement, velocity, acceleration, kinetic energy and

force. Moreover, global epicardial velocity and vorticity were analyzed by means of Particle Image Velocimetry tool. We validated our new technique by i) computational modeling of cardiac ischemia, ii) video recordings of ischemic/reperfused rat hearts, iii) videos of beating human hearts before and after coronary artery bypass graft, and iv) local Frank-Starling effect. In rats, we observed a decrement of kinematic parameters during acute ischemia and a significant increment in the same region after reperfusion. We detected similar behavior in operated patients. This modality adds important functional values on cardiac outcomes and supports the intervention in a contact-free and non-invasive mode. Moreover, it does not require particular operator-dependent skills.

3.1.2. Introduction

Myocardial ischemic injury, resulting from severe impairment of the coronary blood flow, is usually related to thrombosis or other acute alterations of coronary atherosclerotic plaques [42]. Cardiovascular surgery re-establishes the blood flow in the downstream ischemic tissue by percutaneous coronary intervention (PCI) [43, 44] or coronary artery bypass graft (CABG) [45, 46]. While several imaging techniques are present for post-operative evaluation of cardiac function (e.g., CT-scan [46], MRI [47], SPECT [48]), only trans-esophageal echocardiography (TEE) can directly assist surgeons during open-chest surgery assuring, before closing the chest, an assessment of good-prognosis [49]. TEE can be combined with other imaging techniques also in the context of structural heart disease [50]. However, TEE handling requires essential skills for the operator [51] and primarily returns information only about global left ventricle function.

Almost 3% of CABG patients undergo to a second open-chest operation, mainly due to vein graft failure alone or combined with other causes such as restenosis [52], perioperative ischemia/myocardial infarction [53] and ventricular aneurisms [54, 55]. Information about the kinematic parameters specifically from the re-vascularized cardiac regions (i.e., once the blood flow is restored after reperfusion) is missing. To date, several efforts have been devoted to measuring the kinematics of local cardiac regions following the movement of a radio-opaque marker

glued/sewed on the cardiac tissue by a biplane cineradiography [55, 56]. The only reported video-tracking acquisition on the motion of a beating heart is related to mechanical compensation of a robotic arm movement during endoscopic CABG [57]. During open-chest procedures, all cardiac surgeons should confirm that a direct real-time rapid and contactless measurement of kinematic parameters, strictly related to a localized portion of the heart (i.e., ischemic or suffering regions), would be a benefit.

We show, using a commercial low-speed full HD video camera (in ~60-bpm human hearts during CABG) as well as a high-speed video camera (in ~180-bpm rat hearts that underwent ischemia/reperfusion protocol), the tangible possibility to acquire a video (from few seconds to a minute) and display a video cardiogram (ViCG) and its related kinematic parameters in a contactless modality. An algorithm runs in post-processing mode by directly displaying the trajectories of selected tissue video markers and by computing their related kinematic parameters (such as frequency, displacement, velocity, acceleration, kinetic energy and force) during cardiac cycles. From the same video the algorithm, via an adapted Particle Image Velocimetry (PIV) tool, calculates the velocity and the vorticity (i.e., the rotation frequency of the velocity vectors) [32, 58] during systolic and diastolic phases. Recently, we have validated and acquired in vitro similar kinematic parameters in beating 2D syncytia of cultured cardiac cells [31] or in iPSCs-derived cardiomyocytes [59]. An application of in situ beating heart has never been proposed. Thus, the aim of this study is to introduce a contactless and user-friendly technology that can return, together with conventional gold standard techniques, important local and global functional parameters useful from experimental to clinical benches.

3.1.3. Results

Both low-speed and high-speed cameras have been positioned above the heart in open-chest (Fig. 3.1.1a, left panel) Wistar rats [60] or patients, which underwent CABG [61]. The camera and the related optical macro-objective maximized the visualization of the heart, which was covered by the entire field of view.

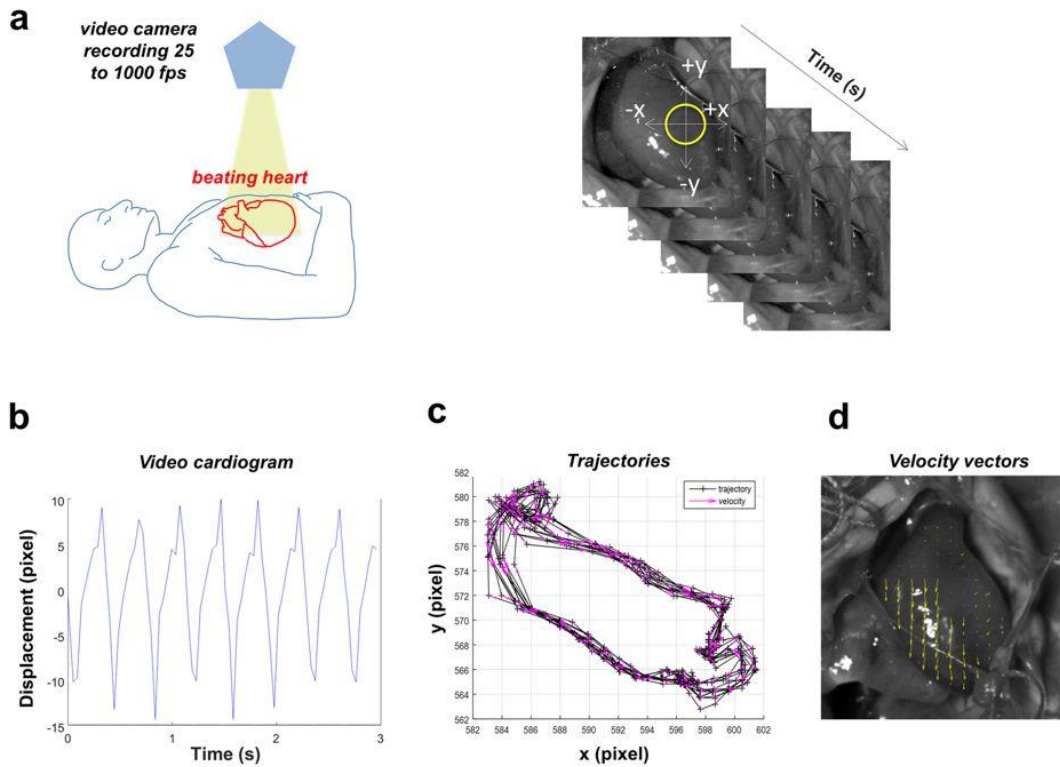


Figure 3.1.1: Workflow with video camera positioning, video recording and evaluation of the systolic and diastolic phases. (a) Left. Schematic representation of the camera positioned using an articulating arm on top of the open chest. The authors drew the scheme. Right. Sequence of video frames captured at 500 fps from a beating heart with the video marker (yellow circle) 'anchored' to the cardiac tissue while moving in x-y directions. (b) Video cardiogram (ViCG) showing the displacement of a selected video marker with contraction/relaxation peaks and peak-to-peak intervals. (c) Counterclockwise trajectories of contraction (left to right) and relaxation (right to left) for every cardiac cycle with related velocity vectors (pink arrows). The graph shows a typical overlapping in the x-y movements of the selected video marker. (d) Particle Image Velocimetry (PIV) showing the velocity vectors (yellow arrows) of the beating cardiac tissue.

- Validation of the measured parameters in rat hearts

Using Video Spot Tracker (VST, CISMM, Computer Integrated Systems for Microscopy and Manipulation, UNC Chapel Hill, NC, USA), we tracked the spatial-temporal coordinates x , y and t of the chosen video marker, in each frame (Fig. 3.1.1a, right panel) [31]. Coordinates were analyzed by a custom algorithm implemented with Matlab Programming Language (The MathWorks, Inc., Natick, MA, USA). The algorithm computed tissue displacements both in the x and y directions (Fig. 3.1.1b) and, consequently, obtained the following parameters: the contraction peaks, the relaxation peaks, the beat-to-beat intervals, the systolic and diastolic phases, and the tissue trajectory (Fig. 3.1.1c). In particular, we took in consideration the following physical quantities (Table 3.1.1):

Parameter name	Formula	Physiological meaning
Displacement (pixel)	$\mathbf{U} = d\mathbf{x}$	Marker displacement between 2 consecutive video frames: it estimates the instantaneous movement of the cardiac tissue and builds the marker trajectory.
Velocity (pixel/s)	$\mathbf{v} = d\mathbf{x}/dt$	Marker velocity between 2 consecutive video frames: it estimates the instantaneous motility or contractility of the cardiac tissue and builds the marker trajectory.
Kinetic energy (pixel ² /s ²)	$E = \frac{1}{2}\mathbf{v}^2$	Marker kinetic energy between 2 consecutive video frames: it estimates the consumption of ATP to generate the cardiac movement.
Frequency (Hz)	$f = \text{beat number}/\text{video duration}$	Contraction frequency calculated from the cardiac beats identified.
Acceleration (pixel/s ²)	$\mathbf{a} = d\mathbf{v}/dt$	Marker acceleration between 2 consecutive video frames: it estimates the instantaneous variation of the motility of the cardiac tissue and builds the marker trajectory.
Force (N)	$\mathbf{F} = m\mathbf{a}$	Cardiac force moving the mass m .

Table 3.1.1: Kinematic and dynamic parameters calculated from video marker tracking with their physiological meaning. According to classical and Hamiltonian mechanics, $\mathbf{x}(t)$ is the position vector (pixel) in the coordinate system (x,y) of an orthonormal Euclidean space, where t is the time (s).

- (i) Displacement (pixel); the instantaneous movement of the cardiac tissue in x and y directions; it builds the temporal-spatial trajectory.
- (ii) Velocity (pixel/s); the instantaneous motility or contractility of the cardiac tissue; it builds the temporal-spatial trajectory.
- (iii) Kinetic energy (pixel²/s²); an estimation of the consumption of ATP for the generation of cardiac movement.
- (iv) Frequency (Hz); contraction frequency calculated from the identified cardiac beats.
- (v) Acceleration (pixel/s²); the instantaneous variation of the cardiac tissue motility; it builds the temporal-spatial trajectory.
- (vi) Force (N); cardiac force moving a mass.

The calculus of the preceding quantities was subjected to a de-noising procedure via wavelet compression (near symmetric wavelet: Symlets 4; decomposition level: 3; compression method: global threshold leading to recover 99% of the signal energy).

To study the cardiac cycle, we obtained fields of velocity vectors (Fig. 1d) in diastole and in systole by means of PIV. Consequently, it was possible to evaluate the mean rotation frequency of the velocity vectors (i.e., the mean vorticity in Hz) and the mean velocity module (calculated with respect to space and time).

- Temporal and spatial resolution

During the initial setting, we studied the effect of both video marker radius and rate effect ('frame number per second' or fps) of the video acquisition on the returned data quality. In Supplementary Fig. 3.1.1, we reported the temporal graphs of the velocity marker in the x direction (the y direction produced similar results and therefore it is not shown) in normal (HEALTH) heart. The radius equal to 15 pixels was the minimum required to correctly follow ventricular epicardial surface movements and, then, to correctly identify cardiac beats.

In Supplementary Fig. 3.1.2a–f, we displayed trajectory and velocity vectors, which were obtained at different acquisition rates (500, 250, 125, 100, 50, and 25 fps). As expected, the rate of 500 fps gave the best trajectory and velocity results (Supplementary Fig. 3.1.2a). The rates between 250 and 30 fps could be considered acceptable (Supplementary Fig. 3.1.2b–e). However lower rates (≤ 25 fps, Supplementary Fig. 3.1.2f) were significantly affected by the aliasing phenomenon with loss of trajectory and velocity details and thereby not used in the present study.

- Reproducibility of the acquired data

We evaluated the aforementioned parameters during time by acquiring 1-s video recording of sinus rhythm at the highest possible temporal resolution (1 kHz) onto three healthy rat hearts, every 10 min for 1 h (Supplementary Fig. 3.1.3, Supplementary Video 1). We anchored the video marker in the same position and monitored changes in displacement, velocity, acceleration and energy over time.

We observed minimal percentage variations (likewise physiological) for the four parameters, suggesting a good reproducibility of our data.

- Kinetic energy acquisition in a controlled and simple system

We then evaluated the kinetic energy parameter by acquiring videos of the periodic motion of a pendulum (mass of 200 g) oscillating for small displacements (Supplementary Fig. 3.1.4a). The pendulum was connected to an arm by a 21.5 cm not-stretchable string and the motion was acquired at 200 fps for five seconds. We selected the video marker onto the white area of the pendulum and displayed the trajectories (Supplementary Fig. 3.1.4b), the coordinate x vs. time (Supplementary Fig. 3.1.4c) and the kinetic energy at the highest, intermediate and lowest positions (Supplementary Fig. 3.1.4d). As expected, marker movement is an arc. When the coordinate x was displayed vs. time, it drew a periodic wave. The kinetic energy we measured for five consecutive frames in the three aforementioned positions was ca. zero at the highest position (all the energy is potential; $h = 17$ cm) and maximal at the lowest position (all the energy is kinetic; $6.49 \times 10^6 \pm 6.01 \times 10^5$ pixel²/s², $h = 11.5$ cm). In the intermediate position, the kinetic energy was $4.26 \times 10^6 \pm 5.40 \times 10^5$ pixel²/s².

- Measurement of the contraction force

We then measured the ventricular force by anchoring a known spherical mass (0.035 g, diameter = 3 mm) onto epicardial surface in three different rat hearts (Fig. 3.1.2a, Supplementary Video 2). The use of a mass connected to the cardiac tissue allowed a switch from a description in terms of acceleration (pixel/s²) to the International System of Units and, consequently, we calculated the contraction force (N) accelerating the mass (Fig. 3.1.2b) and the related ViCG in terms of displacement and velocity (Fig. 3.1.2c). The ViCG was also useful to recognize the diastolic and systolic phases.

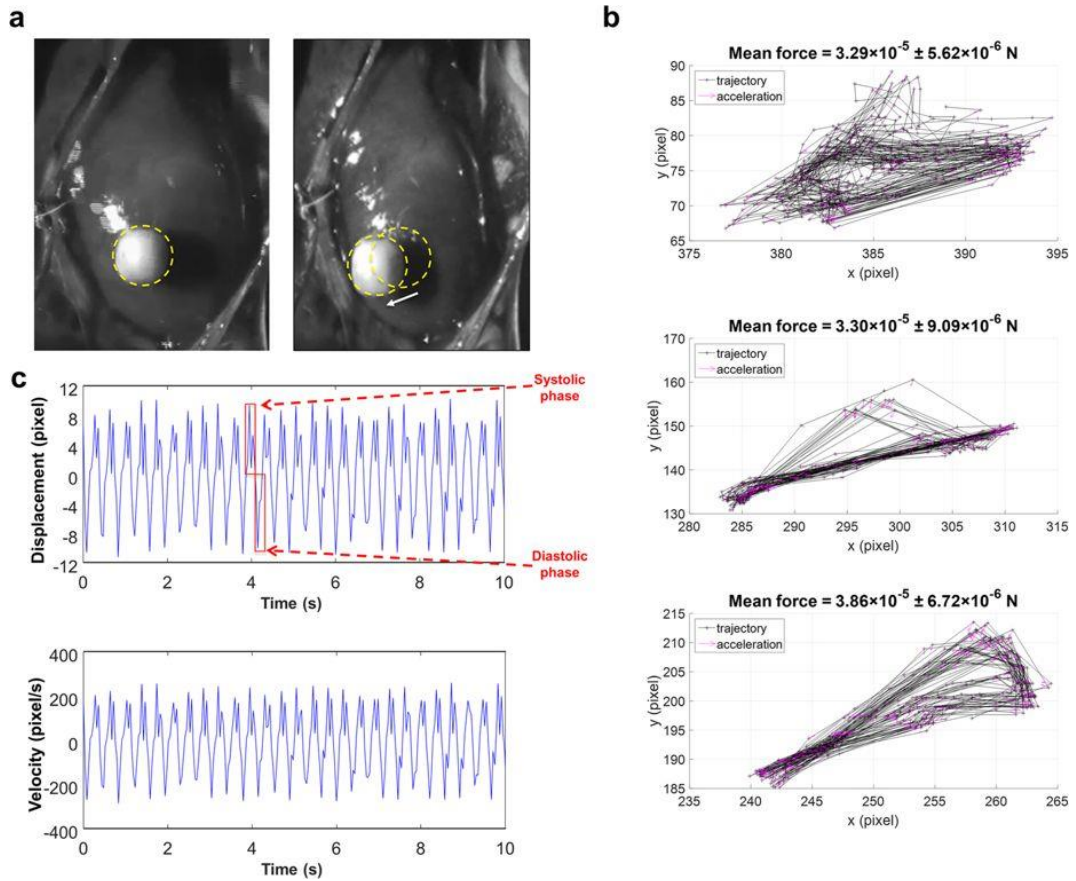


Figure 3.1.2: Validation of contraction force measured with a known spherical mass anchored onto the epicardial surface. (a) Position of the spherical mass at the start of systole (left) and at the start of diastole (right) with the related displacement vector (white arrow) between the two preceding moments. **(b)** Trajectory and acceleration of the mass in three different rat hearts with the mean contraction force (N) during the observation period (10 s). Data are expressed as mean \pm SEM. **(c)** Video cardiograms of displacement vs. time (top) and of velocity vs. time (bottom). Systolic and diastolic phases are underlined in red.

We found the following mean contraction forces (Fig. 3.1.2b): i) $3.29 \times 10^{-5} \pm 5.62 \times 10^{-6}$ N (n of beats = 72); ii) $3.30 \times 10^{-5} \pm 9.09 \times 10^{-6}$ N (n of beats = 31); and iii) $3.86 \times 10^{-5} \pm 6.72 \times 10^{-6}$ N (n of beats = 40), suggesting that every cardiac cycle exerts a well-conserved force of contraction.

We also observed, for every beat, a well-conserved contraction-relaxation trajectory, which was a kind of hysteresis loop due to the intrinsic viscoelastic properties of the myocardium [34].

- Simulation of kinematic parameter measurement in ischemic contractile hearts

We evaluated the effectiveness of our algorithm on data obtained from numerical simulations based on the cardiac electro-mechanical coupling model. We incorporated a transmural ischemic region of $1\text{ cm} \times 1\text{ cm}$. The excitation process was initiated by stimulating three endocardial anterior apical sites and one endocardial posterior apical site, mimicking an idealized Purkinje network. Two simulations were performed, one for a healthy tissue (HEALTH) and one for a tissue with a transmural ischemic region (ISCH). In both cases three beats were simulated, at a basic cycle length of 500 ms. Supplementary Fig. 5 displays the epicardial distributions of transmembrane and extracellular potentials computed in the HEALTH and ISCH simulations, during the plateau phase of the heartbeat (ST segment, $t = 120\text{ ms}$). The ISCH transmembrane potential distribution showed a minimum in the ischemic region, whereas the ISCH extracellular potential distribution showed a maximum (ST elevation), in correspondence of the ischemic region. The kinematic evaluation applied to the experimental data was validated on the simulated data related to the healthy and ischemic tissue. The results reported in Fig. 3.1.3 show that ischemia reduced of about 20%: i) the maximum displacement module (Fig. 3.1.3a), ii) the mechanical behavior of the cardiac tissue, with a reduction of the maximum velocity module (Fig. 3.1.3b) and iii) the mean kinetic energy (Fig. 3.1.3c). These theoretical findings validated the use of kinematic parameters as indices of cardiac mechanical performance.

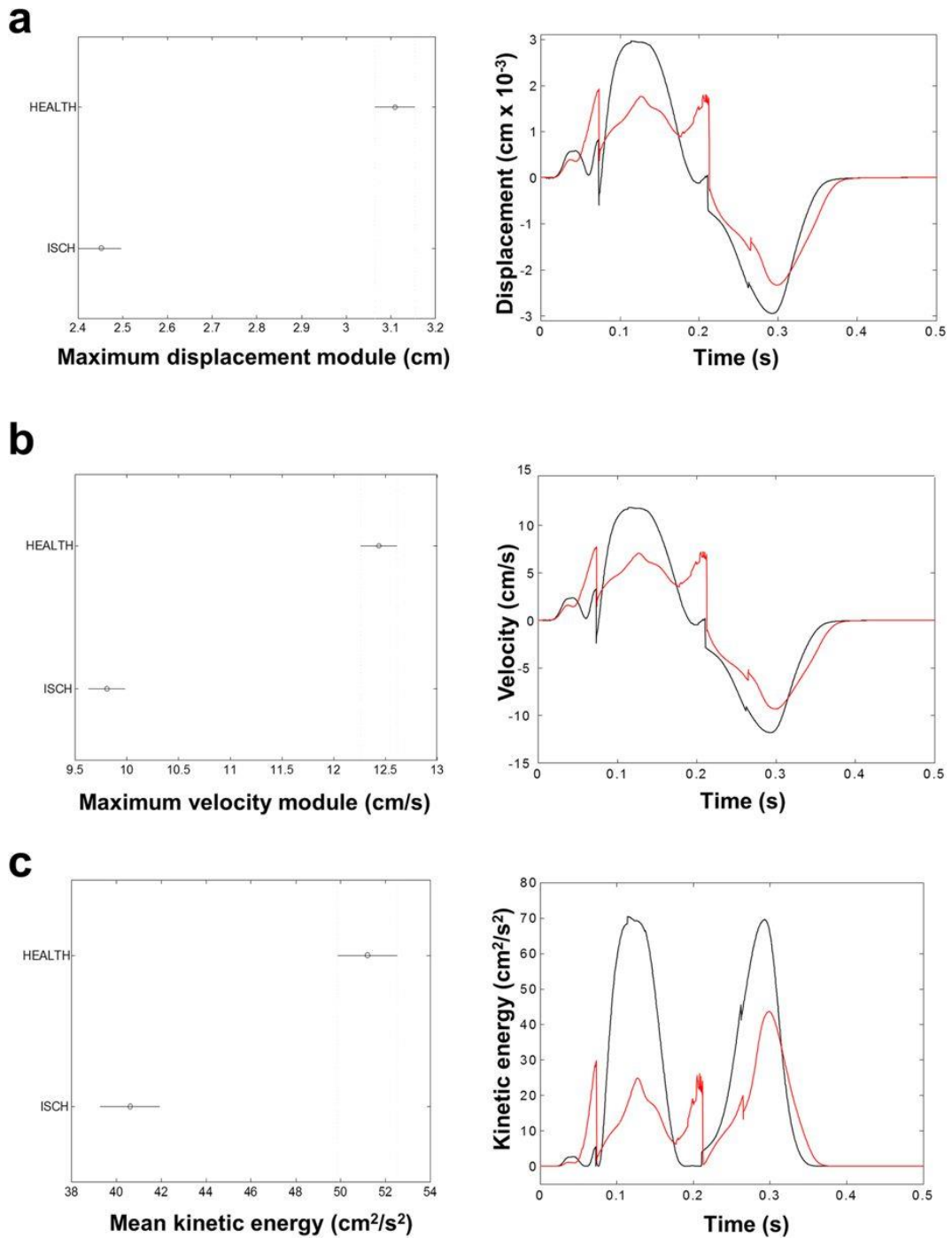


Figure 3.1.3: Simulation of kinematics in ischemic heart. (a) Left. Maximum displacement module, as defined in Table 1, in marker trajectories (frame distance = 0.25 ms), which was averaged across 48 healthy (HEALTH) and 48 ischemic (ISCH) sites. The horizontal bars are the 95% confidence intervals for the differences between means according to one-way ANOVA and LSD (Least Significant Difference) post hoc test. There is a statistically significant difference between the means with non-overlapping bars ($p < 0.05$). Right. Time evolution of the displacement of a single sample site; comparison between healthy (black) and ischemic (red) site. (b) Same as (a) for the maximum velocity module. (c) Same as (a) for the mean kinetic energy.

- Video kinematic parameters in ischemic and reperfused rat hearts

We then acquired videos of six in situ rat hearts before an acute cardiac ischemia/reperfusion injury model [62] with a high-speed camera (acquisition rate = 500 fps) for 1 s in control (HEALTH), ischemic (ISCH, 6 min) and reperfused (REP, 6 min) conditions.

Figure 3.1.4 showed the data only at 6 min following reperfusion as the data at 12 min were comparable. We selected always the same video marker on the well-defined region beneath the ligation (Fig. 3.1.4b, left panel). We only extracted data where the ischemic tissue turned from deep red to trans-lucid white, as a sign of a nearly complete coronary occlusion. Alike the simulation results, the system captured that the brief ischemia patently corrupted the mechanical performance of the ischemic region in terms of trajectories, ViCGs (Fig. 3.1.4a) and kinematic parameters (Fig. 3.1.4b, right panel), while the reperfusion caused significant improvements of those parameters.

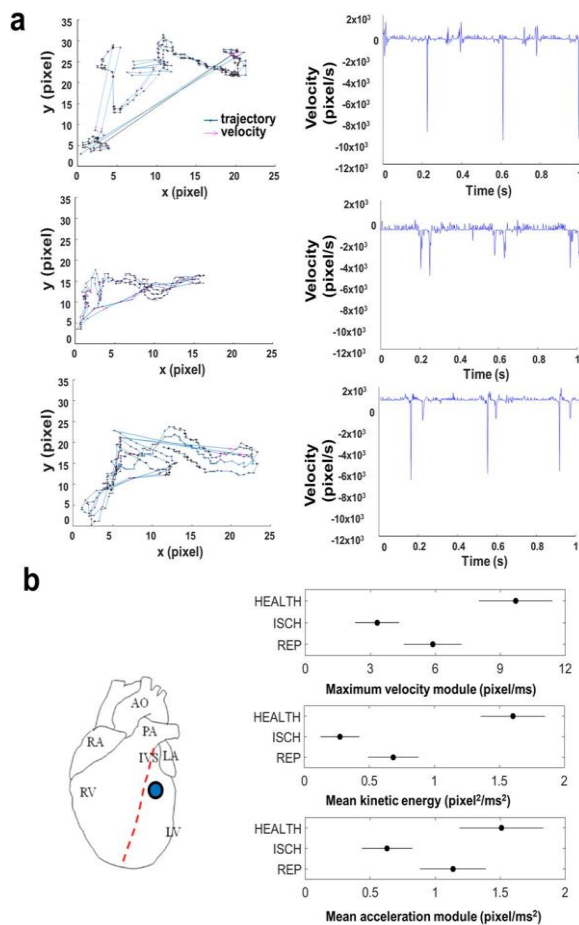


Figure 3.1.4: Kinematic parameters and ViCGs obtained by using a high-speed video camera during ischemia/reperfusion protocol in rats. (a) Left column. Trajectories and velocities measured from a 1-s recording at 500 fps during ischemia/reperfusion protocol. Top: healthy tissue. Middle: ischemic tissue, 6 min after coronary ligation. Bottom: reperfused tissue, 6 min after reperfusion. Right column. Video cardiogram of velocity vs. time in the three conditions: healthy (top), ischemic (middle) and reperfused (bottom) tissue. (b) Left. Representative video marker position (blue circle) on a schematic rat heart. A video marker with a radius of 20 pixel was selected onto the tissue underneath the coronary ligation. Right. Top. Maximum velocity module measured in healthy (HEALTH), ischemic (ISCH) and reperfused (REP) tissue. Middle. Same for mean kinetic energy. Bottom. Same for mean acceleration module. See the text for statistical significances. The horizontal bars are the 95% confidence intervals for the differences between means according to one-way ANOVA and LSD (Least Significant Difference) post hoc test. There is a statistically significant difference between the means with non-overlapping bars ($p < 0.05$). $n = 6$.

We found that the maximum velocity module was significantly reduced during ischemia from 9.71 ± 3.09 pixel/ms to 3.32 ± 1.05 pixel/ms ($p < 0.05$ vs. healthy tissue), while, after 6 min of reperfusion, this parameter showed significantly higher and more physiological values (5.88 ± 1.95 pixel/ms, $p < 0.05$ vs. ischemic tissue, $p < 0.05$ vs. healthy tissue).

We observed an analogous behavior for the mean kinetic energy. Specifically, it significantly decreased during ischemia from 1.60 ± 0.68 pixel²/ms² to 0.27 ± 0.11 pixel²/ms² ($p < 0.05$ vs. healthy tissue), whereas, after 6 min of reperfusion, this parameter showed significantly higher and more physiological values (0.68 ± 0.16 pixel²/ms², $p < 0.05$ vs. ischemic tissue, $p < 0.05$ vs. healthy tissue).

The mean acceleration module significantly decreased during ischemia from 1.51 ± 0.84 pixel/ms² to 0.63 ± 0.16 pixel/ms² ($p < 0.05$ vs. healthy tissue), whereas, after 6 min of reperfusion, this parameter showed physiological and significantly higher values (1.14 ± 0.22 pixel/ms², $p < 0.05$ vs. ischemic tissue, not significant vs. healthy tissue). In addition, the mean frequency of contraction was also decreased in the ischemic heart in comparison with the healthy one (from 4.08 ± 1.81 Hz to 3.64 ± 0.45 Hz, $p > 0.05$), whereas the reperfusion did not change the contraction frequency in comparison with ischemia ($p = 0.21$). The same experiment was performed for the non-ischemic regions (right ventricles) in the HEALTH, ISCH and REP conditions and we did not find significant differences for the aforementioned parameters (data not shown).

During the same protocol, PIV was used to study some physical parameters of the cardiac cycle. In particular, as example of PIV imaging, we have reported the velocity vector field (pixel/s) in diastole (Fig. 3.1.5a, left panels) and in systole (Fig. 3.1.5a, right panels).

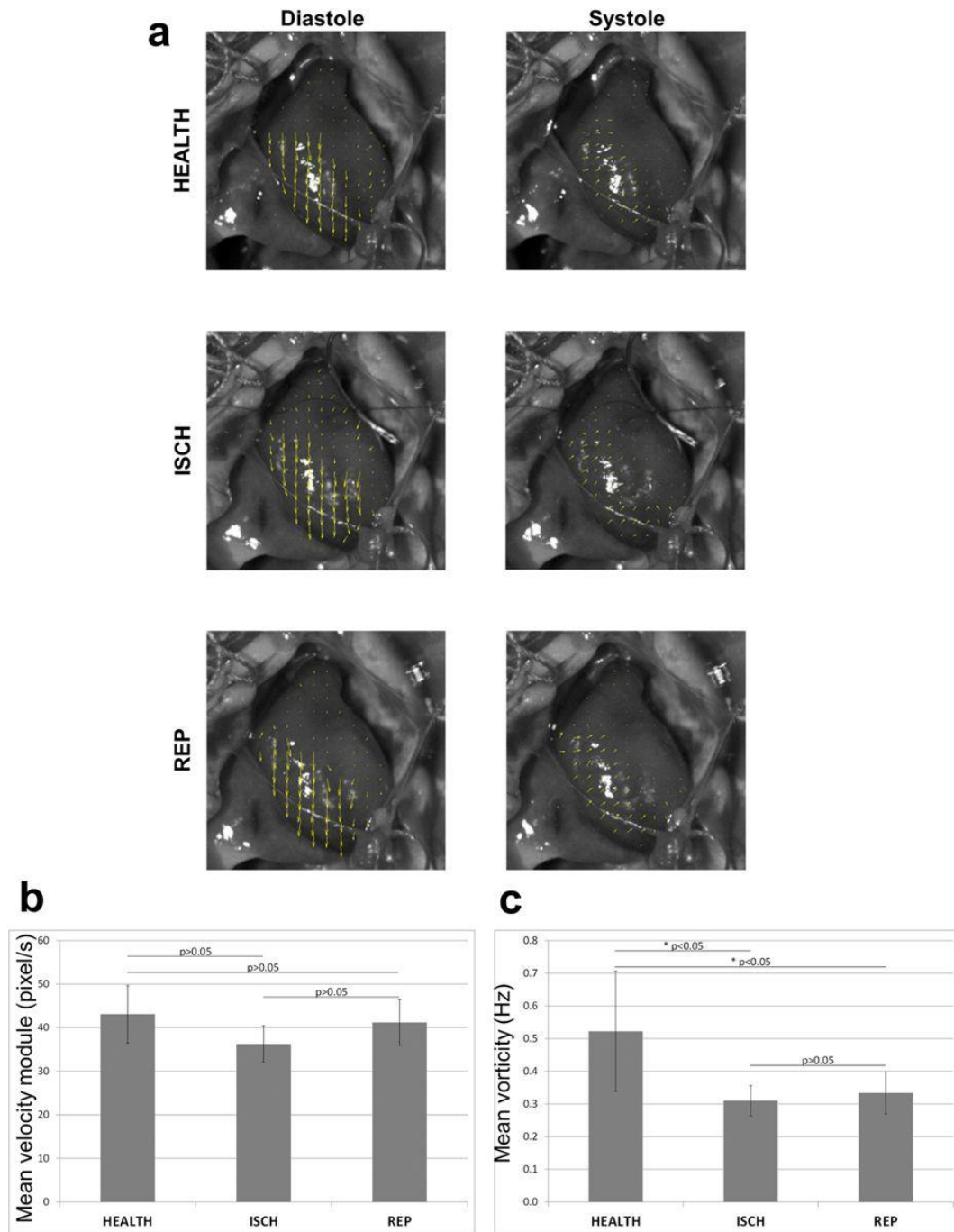


Figure 3.1.5: Particle Image Velocimetry (PIV) analysis in ischemic/reperfused rat hearts. (a) PIV showing the velocity vectors for a rat heart as example in diastole (left column) and in systole (right column) for the HEALTH, ISCH and REP conditions. (b) Velocity module calculated by PIV analysis in the three aforementioned conditions. (c) Same as (b) for vorticity. The p-value was * $p < 0.05$, calculated from Student's t test (paired). $n = 6$.

The mean velocity module was decreased in ischemia in comparison with the healthy heart (from 43.10 ± 6.56 pixel/s to 36.24 ± 4.18 pixel/s, $p > 0.05$, Fig. 3.1.5b); the reperfusion ameliorated, but not significantly, the mean velocity module (to 41.19 ± 5.23 pixel/s) in comparison to ischemia.

Compared with the initial value measured for the healthy heart, mean velocity module remained not significant ($p > 0.05$).

The mean vorticity was significantly decreased in the ischemic heart in comparison with the healthy one (from 0.52 ± 0.18 Hz to 0.31 ± 0.05 Hz, $p < 0.05$, Fig. 3.1.5c); the reperfusion ameliorated the mean vorticity (to 0.33 ± 0.06 Hz) in comparison to ischemia ($p > 0.05$) but we did not obtain the initial value of the healthy heart ($p < 0.05$).

- Video kinematic parameters in patients underwent CABG

We then moved to experimental medicine by adapting our system to an operating room with the purpose of recording the beating hearts of ten patients that underwent CABG (Fig. 3.1.6).

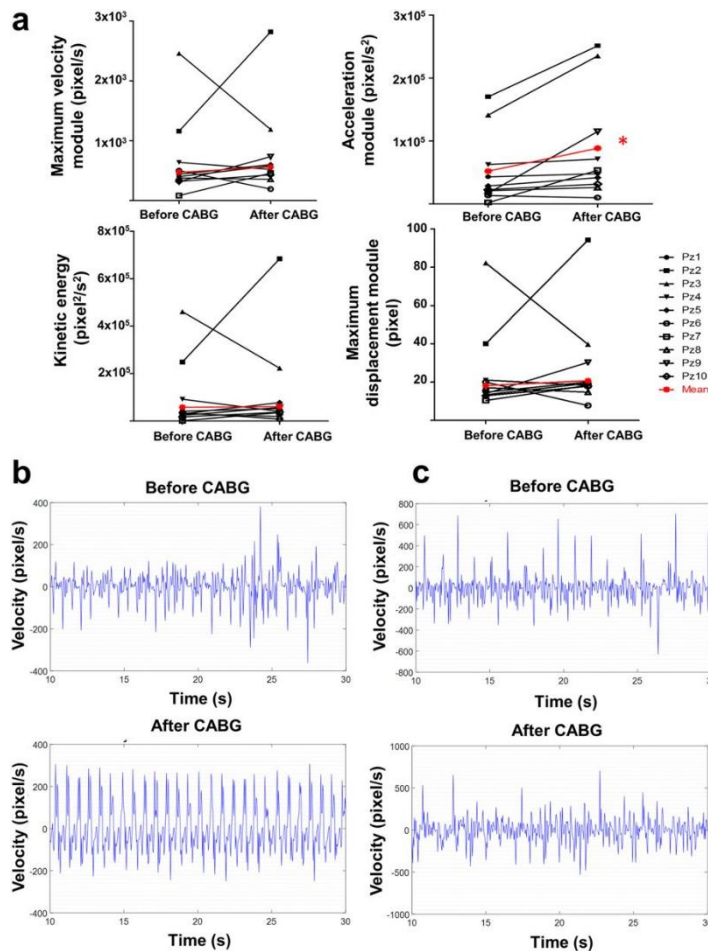


Figure 3.1.6: Kinematic parameters and video cardiograms in patients underwent coronary artery bypass graft (CABG). (a) Top. Maximum velocity module and acceleration module measured by using a low-speed video camera. Bottom. Same for kinetic energy and maximum displacement module. (b) Video cardiogram (velocity vs. time) for the patient #1 before (top) and after (bottom) CABG. (c) Same as (b) for patient #3.

In average, the coronary occlusion for ten patients was $86.1 \pm 2.5\%$. For all hearts, we selected a video marker (radius = 20 pixel) onto the epicardial surface beneath the region where CABG was performed. We performed three video recordings for each patient: i) at chest opening (at pericardium opening, time 0 min); ii) after CABG (but before protamine sulfate infusion with cannulated aorta, time 120–180 min); iii) before chest closing (time 140–200 min). The TEE showed a significant improvement for the mean ejection fraction (EF%, from 31.75 ± 4.80 to 46.70 ± 2.60 , $p = 0.004$) and a not significant increment for the mean fractional shortening (FS%, from 38.40 ± 6.10 to 50.27 ± 2.50 , $p = 0.08$) (Supplementary Fig. 3.1.6a). With our method, we did observe significant changes for the acceleration module ($p = 0.02$, Fig. 3.1.6a, Supplementary Fig. 3.1.6b) and a substantial improvement for the other three parameters: maximum velocity module ($p = 0.28$), kinetic energy ($p = 0.58$), and maximum displacement module ($p = 0.37$) (Fig. 3.1.6a, Supplementary Fig. 3.1.6b). However, when we looked at the individual patient's outcome, patient #3, despite increased acceleration module, denoted a substantial reduction in the other three parameters.

The corresponding ViCGs showed that cardiac cycles differed from each other for all patients before CABG. For the sake of comparison, we displayed the ViCG from patient #1 (which obtained an increment in all preceding parameters after surgery) (Fig. 3.1.6b, upper panel) and patient #3 (Fig. 3.1.6c, upper panel) before CABG. In both patients, we observed disturbed cardiac cycles and dissimilar contraction/relaxation trajectories (data not shown). After CABG, the cardiac cycles became more physiological for patient #1 (Fig. 3.1.6b, lower panel) but not for patient #3 (Fig. 3.1.6c, lower panel).

Similarly, PIV analysis, before and after CABG in diastolic and systolic phases, for aforementioned patients, showed that the mean velocity module significantly increased by 32% ($p < 0.05$) in patient #1 (Fig. 3.1.7c) and only by 9% in patient #3 (not significant, Fig. 3.1.7d). Accordingly, patient #3 received an inotropic agent and extra monitoring in the critical-care postoperative unit.

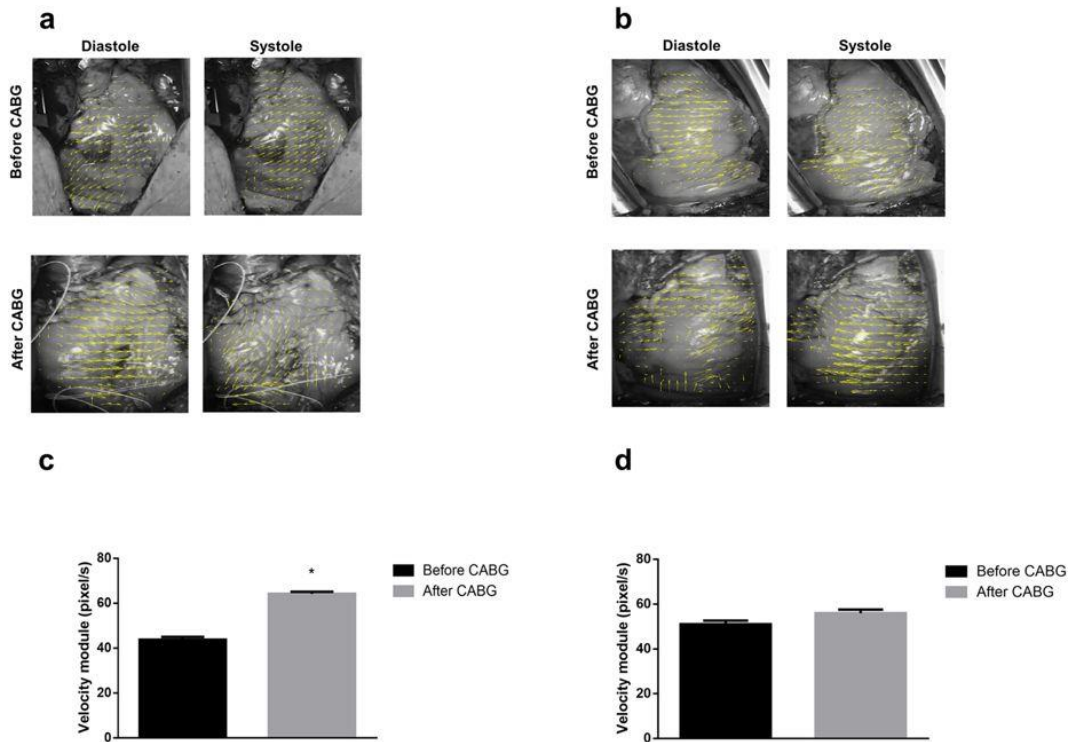


Figure 3.1.7: Particle Image Velocimetry (PIV) analysis in CABG patients. (a) PIV analysis for patient #1 before (top) and after (bottom) CABG for the diastolic (left) and systolic (right) phases. (b) Same as (a) for patient #3. (c) Velocity module calculated by PIV analysis for patient #1 before and after CABG (* $p < 0.05$). (d) Same as (c) for patient #3. Calculated from one-way ANOVA, LSD *post hoc* test. $n = 1,732$ video frames for patient #1 and $n = 992$ video frames for patient #3.

- Improved kinetic energy following atrioventricular block in rat and human hearts: the Frank-Starling effect

We ran a protocol whereby a gentle air-pressure mechanical stimulation (20 kPa for 1 s), delivered onto the rat atrioventricular (AV) regions, exerted a limited stretch-induced depolarization and caused AV blocks, resembling the condition of the commotio cordis [57, 63, 64]. This intervention delayed the preload and resulted in an increment of the end-diastolic volume. Following the Frank-Starling mechanisms, the stroke volume increased and therefore the required kinetic energy as well (Supplementary Video 3, Supplementary Fig. 3.1.7a–b) [65]. Our methodology detected, following the AV block, an increased kinetic energy from 0.003 to 0.025 pixel²/ms².

Similarly, we found a spontaneous increment of the end-diastolic volume in human heart (patient #2, Supplementary Fig. 3.1.7c–d) after CABG intervention but before protamine sulfate infusion. We observed an increment in kinetic energy after the pause from 0.084 to 0.149 pixel²/ms² before returning to 0.093 pixel²/ms².

3.1.4. Discussion

We report a video-based and contactless technique that can add, for the first time to our knowledge, precise cardiac kinematic information during open-chest procedures. Our technology can be adapted for both basic and clinical research and can work in conjunction with standard monitor procedures, without disturbing the intervention during open-chest cardiac surgery. We validated our kinematic parameters in the ‘physical’ case, i.e., tracking the movement of a pendulum during its periodic motion and in rats by connecting a known mass onto the epicardial surface and following its trajectories. The minimal differences we encountered in the force or acceleration measurements were only related to physiological changes in the kinematics of the cardiac tissue and were not an artifact of the measure (cf. Fig. 3.1.2). We also demonstrated the reproducibility of the data by monitoring over time our kinematic parameters from the same hearts (Supplementary Fig. 3.1.3). We were able to capture the contraction movement of the ischemic/reperfused tissue area and we computed the corresponding kinematic and dynamic parameters (such as displacement, velocity, kinetic energy, frequency, acceleration, force) which are undetectable via conventional TEE. We precisely interrogated the same epicardial areas before and after intervention i) *in silico* by modeling ischemic contractile hearts, ii) in an experimental rat model during ischemia/reperfusion protocol, and iii) in patients underwent CABG.

Our image processing technology allowed monitoring the progression of the intervention by analyzing the cardiac kinematic parameters (by video markers with a radius of at least 15–20 pixel and a temporal resolution of ≥ 30 fps, Supplementary Figs 3.1.1–2). These data can be extracted and presented in the operating room

before closing the patient's chest, permitting supplementary considerations about cardiac performance and prognosis. While the human heart beats at an intrinsic frequency of ca. 1.5 Hz, rat heart beats at ca. 4.5 Hz. Thus, we decided to use either a low-cost camera for human studies (full HD portable camcorder, built-in memory) with auto-zoom and low temporal resolution or a high-speed camera for animal studies (1000 fps with manual zoom, video acquisition connected to a fast PC via frame grabber). In all experiments, we never lost video marker tracking. We obtained data on patients before and after CABG (at the final check and after protamine sulfate infusion) showing that the acceleration of the reperfused tissue significantly increased (Fig. 3.1.6a). To note, also the other three parameters showed an increment in average.

The differences observed in rats vs. humans (i.e., statistical significance was achieved in all ischemic rat parameters) were possibly related to the artificial almost-complete coronary occlusion in healthy rat hearts vs. pathophysiological coronary occlusion of 86.1% occurring in the failing human hearts (inclusion selection for CABG vs. stent placement).

For human hearts, the local cardiac kinematics before and after CABG was extremely variable (cf. Fig. 3.1.6), possibly depending on the volume of ischemic region, age, gender, weight, lifestyle and medical records (i.e., when coronary occlusions have been detected). Moreover, we have to take into consideration that the field of view of open-chest human heart covers mainly the right ventricle compared to the rat heart where the left ventricular (LV) area, within the field of view, is larger.

There is clinical evidence supporting the concept that all patients undergoing CABG have different degrees of myocardial stunning [66], which occasionally requires inotropic support after surgery (i.e., patient #3), but not signs of myocardial infarction.

In animals, stunned myocardium has been detected after 15–30 min of coronary occlusion [67], which was not our case. Certainly, prolonged ischemia would be important for understanding whether the method can detect abrupt evidence of myocardial pathophysiological alterations [68]. Indeed pioneering studies indicate that, following brief episodes of ischemia, creatine phosphate [69] increases rapidly after reperfusion, suggesting that local kinetic energy rapidly increases as well [70].

The power of our technique is that the ViCG, which was obtained during ischemia/reperfusion protocol or before and after CABG, may return an overall view of the quality of the intervention from a mechanical perspective, especially in the reperfused regions, where the video markers were positioned. In addition, the ViCG can be combined with the conventional ECG by returning information on in vivo data of excitation-contraction coupling machinery.

The benefit of using high-fps acquisition in basic research (up to 1000 fps) is such that we can distinguish local contraction trajectories in a millimeter range during ventricular fibrillation (data not shown) in rat hearts or we can appreciate an increment of the kinetic energy after a mechanical stimulus inducing AV blocks (cf. Supplementary Fig. 3.1.7). The technique can be easily adapted to study other inherited or acquired cardiac complications at both laboratory and clinical levels by returning important physiological data on tissue contraction at open-chest stage.

In summary, our technology can monitor and examine several cardiac regions in open-chest beating hearts. This not only provides mechanical insights, but it also offers new prognostic values. Moreover, kinetic energy, as indirect measurement of ATP consumption [31], can be embraced as a clinical marker.

3.1.5. Limitations

Video kinematic evaluation performed from a single camera is not able to study the movement in the z direction thus resulting in bi-dimensional analysis of three-dimensional (3D) phenomena. Nevertheless, the designed and implemented

algorithm is already capable to acquire 3D motion and it was employed to study the 3D data of mathematical modeling. A further development for a stereoscopic/double camera acquisition as well as concurrent monitoring of electrical activity could solve the limitations. Acceleration and kinetic energy are obtained from the linear parameters (displacement and velocity), so they are per se prone to the measure noise. We compared our data from the same sampling rate, i.e., HEALTH vs. ISCH in animal studies or before and after CABG in human studies. Doing so, we avoided the aliasing phenomena by maintaining the same signal-to-noise ratio.

While we could measure kinematics on the left ventricle in animal studies, only the right ventricle is exposed in humans, thereby limiting our measurement at the closest regions near the CABG intervention.

3.1.6. Methods

- Experimental animals

The study population consisted of nine male Wistar rats bred in the animal facility of the Department of Life Science, University of Parma. The rats were 12–14 weeks of age and weighed 300–350 g. The investigation was approved by the Veterinary Animal Care and Use Committee of the University of Parma (Italy) (Protocol # 41/2009 and 59/2012) and it conformed to the National Ethical Guidelines of the Italian Ministry of Health and to the Guide for the Care and Use of Laboratory Animals (National Institute of Health, Bethesda, MD, USA, revised 1996). More information is detailed in the Supplementary methods section.

- Human patients

We performed video recording in patients during CABG surgery in the Azienda Ospedaliera Universitaria Integrita (Verona, Italy). Ten patients (9 males, 1 female) were enrolled from March to December 2016. Patients were selected for CABG as they presented coronary occlusion of 86.1% in average. No human tissue samples have been used. The video recording never interfered with the standard CABG

intervention, in accord with the guidelines for coronary artery bypass surgery [64]. All methods and experiments were carried out in accordance with relevant guidelines and regulations set by the Institutional Review Board (IRB) of the Azienda Ospedaliera Universitaria Integrata of Verona, where all experiments were done (approved protocol from ethics committee on 16th March 2016, # 847CESC Protocol # 13371). All patients signed an informed consent.

- Functional imaging

○ Low-speed video camera

A full HD (1920×1080 total pixel area) camera Samsung S10 (with an internal SD memory of 256 MB and internal rechargeable battery) has been used for the cardiac force measurement in rats and for the CABG recording in the operating room. The on-site monitor of the camera allowed the recording of the heart beating. Videos have been recorded for 60 s in full HD gray-scale mode at 30 fps. The hearts have been constantly illuminated with scialytic light by keeping it in the same position during video recording for both animals and patients.

○ High-speed video camera

A Baumer HXC13 (Baumer Italia, S.r.l., Milano, Italy) camera with full CameraLink® interface (1280×1024 total pixel area for 500 fps or 1020×600 for 1000 fps) was used for ischemia/reperfusion experiments in rats. The camera was equipped with a macro-objective Kowa Industrial Lenses LM35XC, $F = 1:2.0$, $f = 35$ mm, picture size 13.8–18.4 mm (RMA Electronics, Hingham, MA, USA). The acquisition software was custom made in LabVIEW Visual Programming Language (National Instruments, Assago, Milano, Italy). We ran 1-s acquisitions at either 1000 fps (reproducibility data) or 500 fps (ischemia/reperfusion data) allowing the recording of spontaneous beats in anesthetized rats. No pixel binning was used. The camera was connected with two CameraLink® cables to a frame grabber acquisition board PCIe 1433 (National Instruments, Italy) adapted into a Workstation HP Z220 (Crisel Instruments, Italy) with 24 GB RAM. The video file consisted of 1000 or 500 TIFF images (1.25 MB each) of the beating heart. For the

pendulum experiment, we ran an acquisition at 200 fps (1280 × 1024 total pixel area) for five seconds of recording.

- Video acquisition

- o Video kinematic evaluation in rats

In the anesthetized animals subjected to artificial ventilation (Rodent Ventilator, Ugo Basile, Italy), the heart was exposed through a longitudinal sternotomy and suspended in a pericardial cradle. Body temperature was maintained with infrared lamp radiation. In the present study, the camera was levelled at 17 cm above the spontaneously beating heart. A constant illumination was achieved using a scialytic lamp for laboratory (ElettroMedica, Italy). During recording, the ventilator was switched off to avoid motion artifacts and immediately re-switched on at the end of the recording. The distance between the camera and the heart, the focus and the heart's orientation were never changed during the experiments.

For the force measurement experiments, we employed known masses consisting of a pin-head with a 1 mm-long needle inserted on the epicardium surface. For the ischemia/reperfusion experiments, we recorded the beating heart in normal conditions followed by anterior descending coronary ligation, as recently described³³. We left the surgical needle within the performed knot as this allowed the removal of the ligation without damaging the tissue. Then, we waited for 6 min and 12 min before recording another video of the beating heart (now ischemic). The same procedure was followed after the removal of the ligation (i.e., two video files were recorded after 6 min and 12 min).

For the mechanically-induced AV blocks, we adopted a flexible cannula (0.8 mm diameter) firmly fixed to a three-axes manipulator and positioned ca. 5 mm above the pulmonary cone. A gentle air-pressure flow (20 kPa) was delivered for 1 s using an electro-valve (Asco Numatics, Bussero, Milano, Italy) remotely controlled by a stimulator (Crescent Electronics, Sandy, UT, USA), similar to what we had previously implemented for single cell mechanical stimulation [71].

- Video kinematic evaluation during CABG in human patients

In the operating room, the camera was positioned with an articulating arm at 40 cm above the open chests. We performed video recordings of beating hearts at chest opening (after pericardium opening, time 0 min), after CABG but before protamine sulfate infusion with cannulated aorta (data not shown, time 120–180 min), and before chest closing (time 140–200 min). All patients were in normal sinus rhythm during the intervention. Because, during CABG, the surgeons frequently move the operating table, we recorded the original position of the table and recalled it during video acquisitions. For the analysis (before and after CABG), we took into consideration additional anatomical markers, such as coronary vessels or skin edges for properly positioning the video marker.

- Quantitative analysis

Tracking of the cardiac contraction

Using VST program (<http://cismm.cs.unc.edu/downloads>), which tracks the movement of biological objects starting from the video recording of their displacements, we anchored a single video marker to the cardiac tissue or to a mass (0.035 g) firmly connected to that tissue. The x and y coordinates are expressed in pixel, whereas the t coordinate in second (s).

- Kinematics

Using a custom algorithm based on the Matlab Programming Language (The MathWorks, Inc., Natick, MA) and the tracked spatial-temporal coordinates of the cardiac contraction, we identified the heartbeats and then calculated the corresponding kinematic parameters (see Table 1 for the mathematical definitions and their physiological meaning).

- Particle Image Velocimetry

We employed ‘Particle Image Velocimetry’ (PIV) tool, which is a fluid flow visualization and quantification technique, in particular its Matlab Central implementation in PIVlab (<http://it.mathworks.com/matlabcentral/fileexchange/27659-pivlab-time-resolved->

particle-image-velocimetry-piv-tool?s_tid=srchtitle). We applied the PIV to study the cardiac cycle and we reported the images of the velocity vectors (pixel/s) in diastole and in systole. During the whole observation period, it was possible to evaluate the mean rotation frequency of the velocity vectors, that is, the mean vorticity (Hz) and the mean velocity module (pixel/s).

- Mathematical models

- o Numerical simulations

The numerical simulations were based on the cardiac electro-mechanical coupling (EMC) model. This model described the interplay between the spread of electrical excitation in the cardiac tissue and the consequent contraction/relaxation process. The EMC model consisted of four sub-components, two for the bioelectrical activity and two for the mechanical response of the cardiac tissue. The bioelectrical components were the Bidomain model for the electric current flow [35] and the ten Tusscher human ventricular model [36] for the cellular membrane dynamics. We disregarded the presence of an ischemic damage in the surviving layers at the border of the ischemic region. From the bioelectrical point of view, ischemic conditions were modeled modifying the following parameters of the ten Tusscher model [40]: the extracellular potassium concentration was increased from 5.4 mM to 8 mM; the maximal conductances of the I_{Na} and I_{CaL} currents were decreased by 25%; the parameters of the I_{KATP} current were modified as in [41] for ischemia stage 2. In the normal ventricular tissue, the same set of Bidomain anisotropic conductivities was assigned, yielding the physiological conduction velocities of about 0.065 and 0.03 cm/ms, when measured for wave front propagation along and across fiber, respectively, matching reported conduction velocities. Since we considered the early stage of myocardial ischemia, the conductivity coefficients inside the ischemic region were not modified, reflecting an unchanged distribution of connexin 43. From the mechanical point of view, ischemic conditions were modeled by reducing the active tension and passive tissue stiffness of 10% and 25% with respect to their normal values. Stretch-activated channels were incorporated in the membrane model according to [37]. The macroscopic description of the mechanical activity was based on the equations of finite elasticity, where the

passive mechanical properties of the myocardium were assumed to be transversely isotropic, hyper-elastic, and nearly incompressible, defined by an exponential strain energy function derived from [38]. Realistic fiber orientations were incorporated into both the conductivity tensors of the Bidomain model and the strain energy function. The EMC model was finally closed by the active tension generation model developed describing the process of calcium binding to troponin C and cross-bridge cycling triggered by calcium release from the intracellular calcium stores during the electrical activation of a myocyte. The active tension generated by this model entered as input in the non-linear elasticity equations yielding the active component of the stress tensor. The intracavitary blood pressure p in the left ventricular (LV) cavity was described by a pressure-volume loop model [39], based on the following four phases:

Isovolumetric LV contraction phase, where p increased from the end-diastolic pressure (EDP) value of about 2 kPa to 10 kPa;

Ejection phase, where the pressure-volume relationship was described by a two-element Windkessel model, until the volume reduction stopped;

Isovolumetric LV relaxation phase, where p decreased to 1 kPa;

Filling phase, where p increased linearly to EDP.

- Numerical methods

The space discretization was based on Q1 finite elements. The computational domain was a truncated ellipsoid representing the left ventricle geometry. The size of the major axis of the ellipsoid was 5 cm, while that of the minor axis was 2.7 cm. Two different meshes were used, a fine one to solve the Bidomain equations and a coarser one for the finite elasticity equations. The nodes of the electrical mesh were 3,631,488, while those of the mechanical mesh were 8,400. The time discretization was performed by a semi-implicit finite difference scheme. The time step size was 0.05 ms for the electrical components of EMC model and 0.25 ms for the

mechanical components. Our parallel code was based on the PETSc library (<https://www.mcs.anl.gov/petsc/>). The simulations were run on 256 cores of the Bluegene cluster Fermi of the CINECA laboratory (<http://www.cineca.it>). For further details on the numerical methods, we remand to [35, 72, 73]. Parameters calibrations are detailed in the Supplementary methods section.

- General statistics

Normal distribution of variables was checked by the Kolmogorov-Smirnov test. Statistics of normally distributed variables included mean \pm standard error of the mean (SEM), paired and unpaired Student's t test. Statistical significance was set at $p < 0.05$. For the ischemia/reperfusion experiments, one-way Analysis of Variance (ANOVA) was applied with post hoc Least Significant Difference (LSD) test, electing a significance level of 5% (the results are expressed as mean \pm 95% confidence intervals for the differences between means). Statistics was performed using GraphPad Prism v.6 (La Jolla, CA, USA).

3.1.7. Supplementary Information

- Supplementary Methods

o Experimental animals

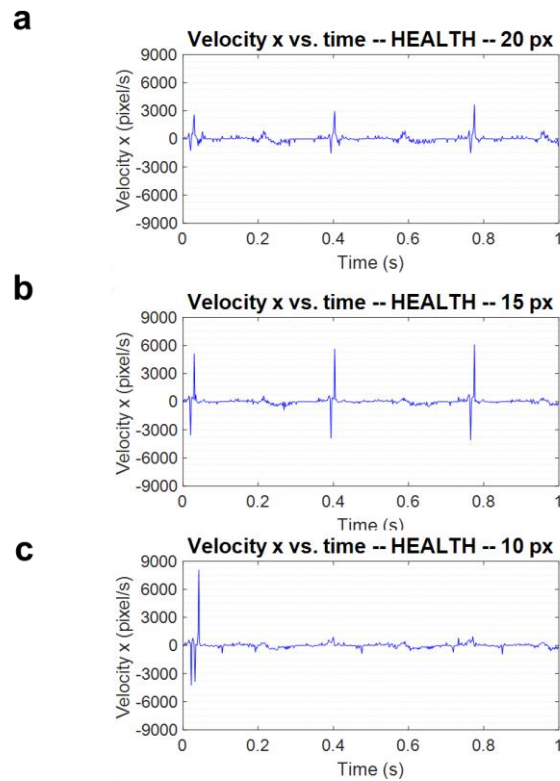
The animals were kept in single-sex groups of four individuals from weaning (4 weeks after birth) until the onset of the experiments, in a temperature-controlled room at 20-24°C, with the light on between 7:00 AM and 7:00 PM. The bedding of the cages consisted of wood shavings; food and water were freely available. Animals were anesthetized with a mixture of ketamine chloride 40 mg/kg ip (Imalgene, Merial, Milano, Italy) and medetomidine hydrochloride 0.15 mg/kg ip (Domitor, Pfizer Italia S.r.l., Latina, Italy) for the in vivo experiments; all efforts were made to minimize suffering. We used nine male rats in total. Six male rats were enrolled in i) the experiments related to the cardiac force measurement with a given mass ($n = 6$); ii) the same animals were used for the ischemia/reperfusion experiments ($n = 6$) and iii) three of them included in the “reproducibility”

experiments, monitoring parameters every ten minutes for 1 h before ischemia/reperfusion (n = 3). Three male rats were included in mechanically-induced AV block experiments. This study was carried out in accordance with the recommendations in the “Guide for the Care and Use of Laboratory Animals” of the Italian National Institute of Health. The protocol was approved by the Veterinary Animal Care and Use Committee of the University of Parma and conformed to the National Ethical Guidelines of the Italian Ministry of Health (Protocol # 41/2009 and 59/2012).

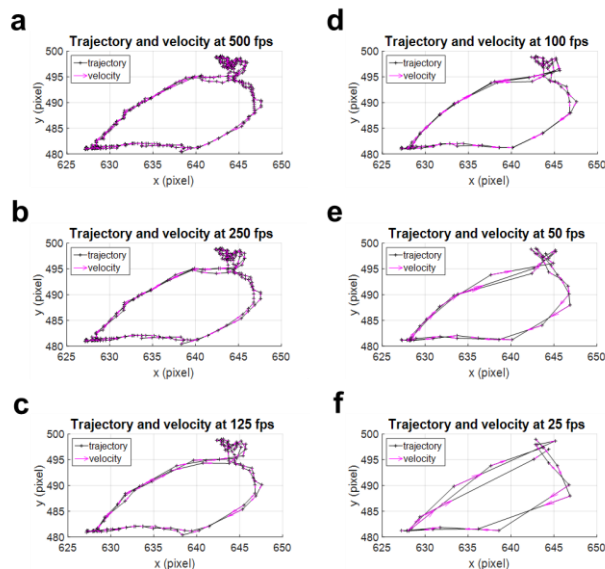
- Parameters calibration for the mathematical model of ischemia simulation

The intra (i)- and extra (e)- cellular conductivity coefficients of the Bidomain model, along (l) and across (t) the fiber direction, were $\sigma_{il} = 3$, $\sigma_{el} = 2$, $\sigma_{it} = 0.31525$, $\sigma_{et} = 1.3514$, all in $\text{m}\Omega\text{-1cm-1}$. The parameters of the strain energy function were the same of the original paper [39] except for the bulk modulus, which amounted to 200 kPa. The size of the ischemic region was $1 \text{ cm} \times 1 \text{ cm}$, developing along the whole transmural thickness, from the endocardial to the epicardial surface. From the bioelectrical point of view, ischemic conditions were modeled modifying the following parameters of the ten Tusscher model: the extracellular potassium concentration was increased from 5.4 mM to 8 mM; the maximal conductance of the I_{Na} and I_{CaL} currents was decreased of 25%; the parameters of the I_{KATP} current were modified as in [41] for ischemia stage 2. From the mechanical point of view, ischemic conditions were modeled by reducing the active tension and passive tissue stiffness of 10% and 25% with respect to their normal values, respectively. The excitation process was initiated by stimulating three endocardial anterior apical sites and one endocardial posterior apical site, mimicking an idealized Purkinje network. Two simulations were performed, one for a healthy tissue (HEALTH) and one for a tissue with a transmural ischemic region (ISCH). In both cases, three beats were simulated, at basic cycle length of 500 ms.

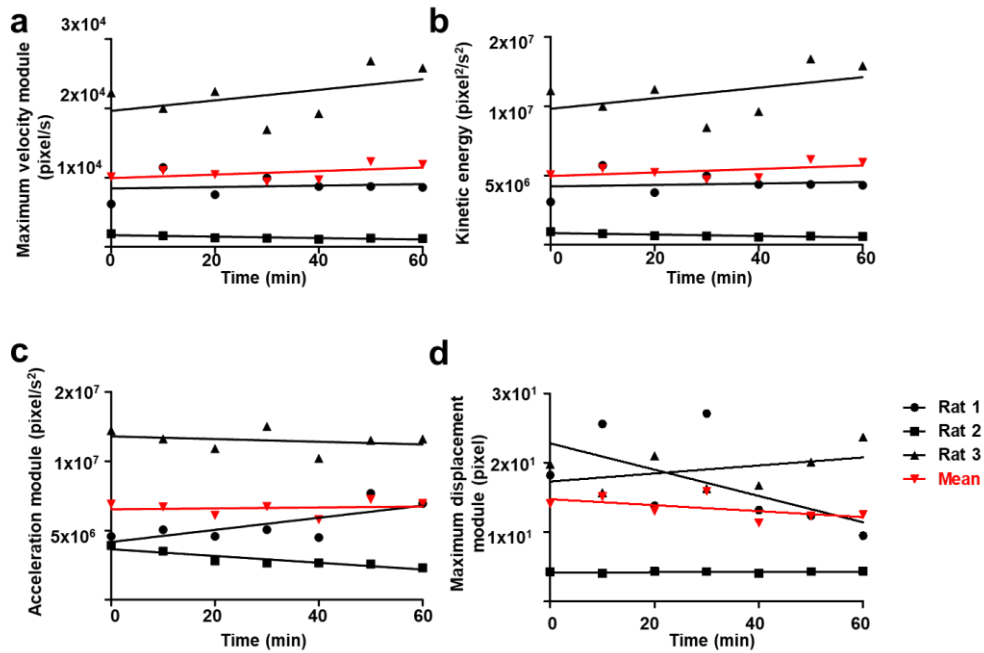
- Supplementary Figure legends.



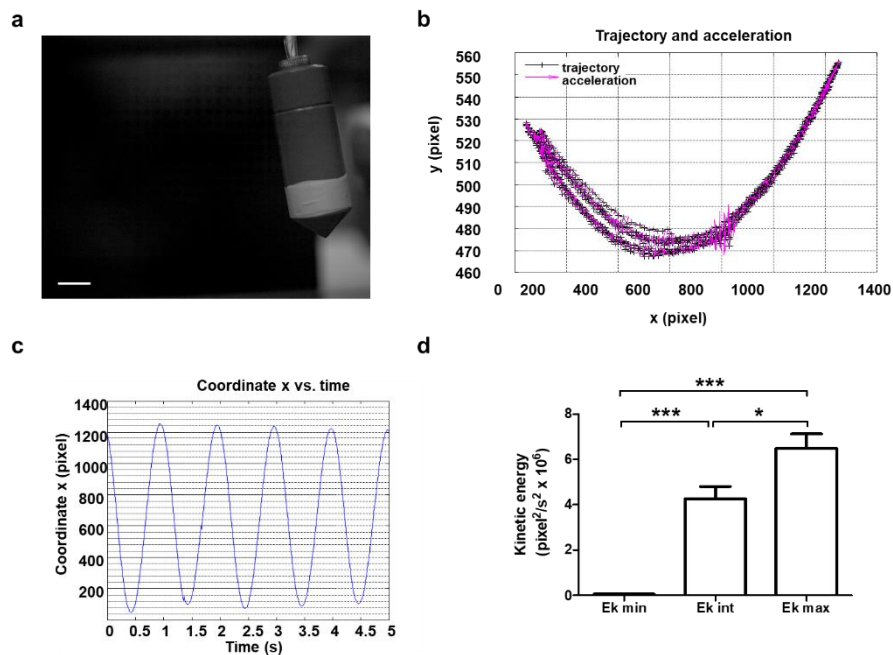
Supplementary Figure 3.1.1. Velocities in the x direction obtained at different marker radius. We used a video marker radius equal to 20, 15, or 10 pixel (px) for **a**, **b** and **c** respectively. We found that a radius equal to 15 pixel was the minimum required to correctly follow the ventricle's tissue and, then, to identify the cardiac beats. $n = 3$



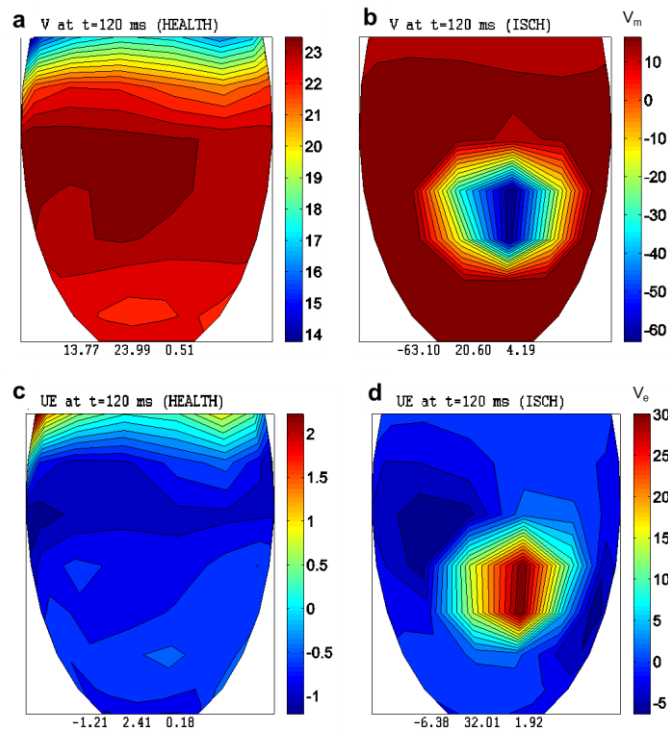
Supplementary Figure 3.1.2. Marker's trajectories and the related velocity vectors obtained at different acquisition rates. The rate of 500 fps (**a**) gave the best trajectory details, the rates of 250 (**b**), 125 (**c**), 100 (**d**), and 50 (**e**) could be considered acceptable, whereas the other lower rates (≤ 25 fps in **f**) were significantly affected by the aliasing phenomenon with loss of trajectory details and were excluded from this study.



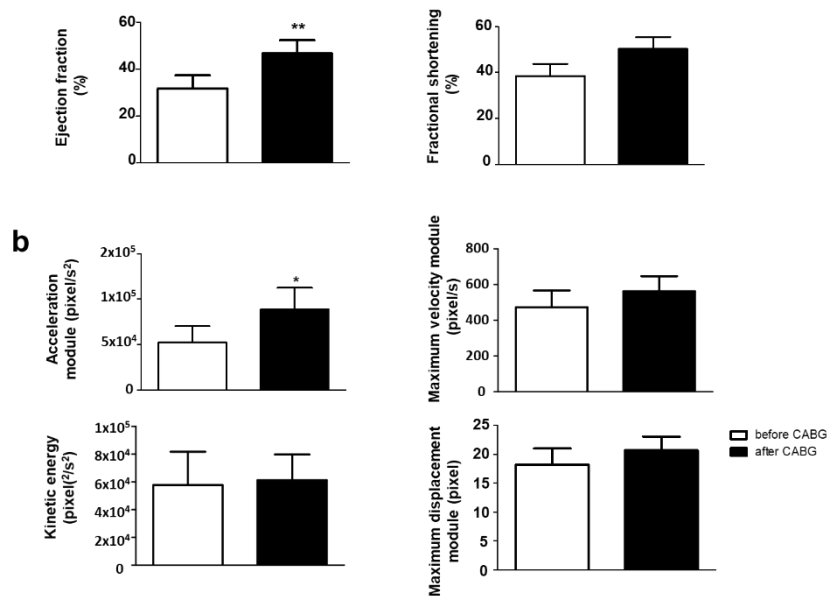
Supplementary Figure 3.1.3. Reproducibility of the acquired data in three different rat hearts. (a) Maximum velocity module (pixel/s) monitored every 10 min for 1 h at 1000 fps. (b) Same as (a) for kinetic energy (pixel²/s²). (c) Same as (a) for acceleration module (pixel/s²). (d) Same as (a) for maximum displacement module (pixel). Marker radius = 60 pixel. n = 3.



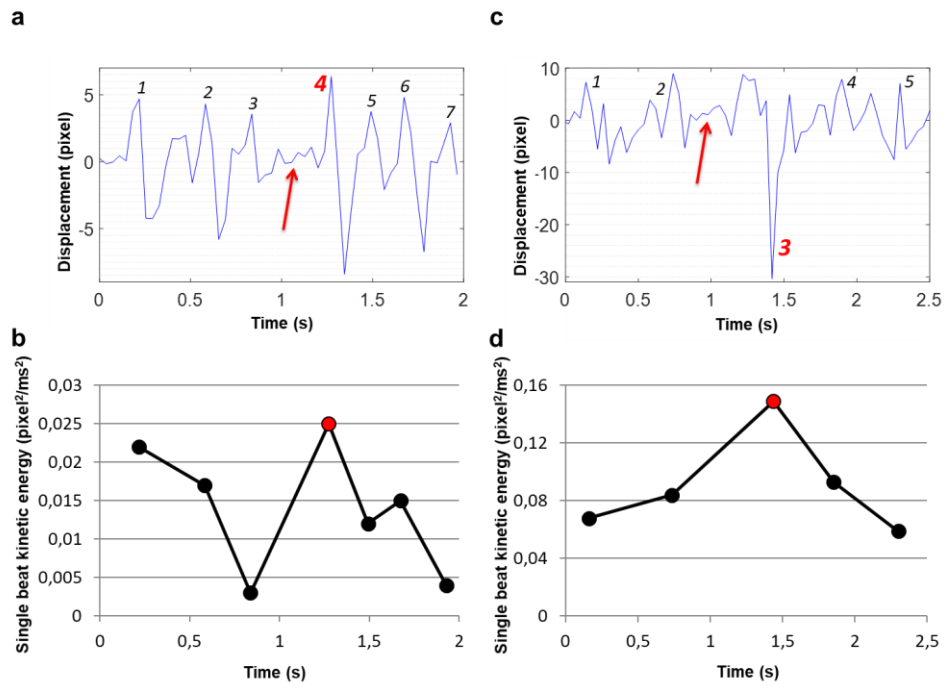
Supplementary Figure 3.1.4. Evaluation of the kinetic energy during the periodic motion of a pendulum. (a) First acquired image of the pendulum at the highest point. Scale bar = 1 cm. (b) Trajectories and accelerations during five seconds of recording (with a maximum inaccuracy of three pixels in the y direction). (c) Coordinate x vs. time. (d) Kinetic energy at the highest point (ca. zero, E_k min), at the intermediate point (E_k int, $p < 0.05$) and at the lowest point (maximum kinetic energy, E_k max, $p < 0.001$). The statistics was calculated with one-way ANOVA. Data are showed as mean \pm SEM. n = 10.



Supplementary Figure 3.1.5. Numerical simulation results of epicardial transmembrane (V) and extracellular (UE) potential distributions. (a) V distribution at t = 120 ms after the onset of stimulation in the healthy tissue (HEALTH). (b) V distribution at t = 120 ms after the onset of stimulation in the tissue with transmural ischemia (ISCH). (c) UE distribution at t = 120 ms after the onset of stimulation in the healthy tissue. (d) UE distribution at t = 120 ms after the onset of stimulation in the tissue with transmural ischemia. Numbers at the bottom of each panel represent the minimum value, the potential step and the maximum value respectively.



Supplementary Figure 3.1.6. Functional parameters of human beating hearts. (a) Mean ejection fraction (EF%, left, **p<0.01) and mean fractional shortening (FS%, right, p>0.05) of seven patients before and after CABG. (b) Acceleration module, kinetic energy, maximum velocity module and maximum displacement module before (white) and after (black) CABG (p<0.05 only for the acceleration module; the p-value was calculated from Student's t-test, normal distribution was checked by means of the Kolmogorov-Smirnov test).



Supplementary Figure 3.1.7. Kinetic energy related to the Frank-Starling effect following an AV block. (a) Video cardiogram (ViCG) for the marker displacement of spontaneously beating rat heart with an AV block between the third and the fourth beat; red arrow: mechanically induced AV block (20 kPa of air pressure delivered for 1 s). (b) Related kinetic energy measured for each cardiac cycle. Black dots: single beat kinetic energy measured for each cycle. Red dot: single beat kinetic energy after AV block. (c) Same as (a) for spontaneously beating human heart (patient #1). Red arrow: spontaneous AV block. (d) Related kinetic energy measured for each human heartbeat. Red dot: single beat kinetic energy after AV block.

The publication on Scientific Report led to an increased interest for Vi.Ki.E. applications in more complex cases, like congenital heart diseases, and especially in the Right Ventricle evaluation thanks to the direct “sight contact” of the camera with it. Therefore, a pilot study on the Right Ventricle evaluation, in hearts affected by Tetralogy of Fallot, was set up and published on Interactive Cardiovascular and Thoracic Surgery.



3.2. Real-time video kinematic evaluation of the *in situ* beating right ventricle after pulmonary valve replacement in patients with tetralogy of Fallot: a pilot study [29].

Interactive CardioVascular and Thoracic Surgery 29 (2019) 625–631
doi:10.1093/icvts/ivz120 Advance Access publication 9 June 2019

ORIGINAL ARTICLE

Cite this article as: Rozzi G, Lo Muzio FP, Sandrini C, Rossi S, Fassina L, Faggian G et al. Real-time video kinematic evaluation of the *in situ* beating right ventricle after pulmonary valve replacement in patients with tetralogy of Fallot: a pilot study. *Interact CardioVasc Thorac Surg* 2019;29:625–31.

Real-time video kinematic evaluation of the *in situ* beating right ventricle after pulmonary valve replacement in patients with tetralogy of Fallot: a pilot study

Giacomo Rozzi^{a,b,*}, Francesco P. Lo Muzio ^{a,b,*}, Camilla Sandrini ^a, Stefano Rossi^b, Lorenzo Fassina^c,
Giuseppe Faggian^a, Michele Miragoli^{b,d,*} and Giovanni Battista Luciani^{a,*}

^a Department of Surgery, Dentistry, Pediatrics and Gynaecology, University of Verona, Verona, Italy

^b Department of Medicine and Surgery, University of Parma, Parma, Italy

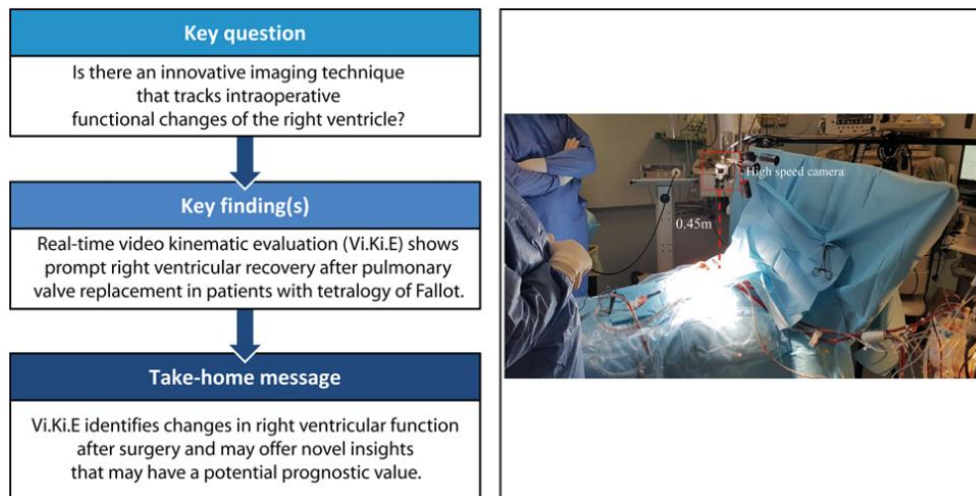
^c Department of Electrical, Computer and Biomedical Engineering, University of Pavia, Pavia, Italy

^d Humanitas Clinical and Research Center, Rozzano, Italy

* Corresponding author. Section of Cardiac Surgery, Department of Surgery, Dentistry, Pediatrics and Gynaecology, University of Verona, O.C.M. Piazzale Stefani 1, 37126 Verona, Italy. Tel: +39-45-8123303; fax: +39-45-8123308; e-mail: giovanni.luciani@univr.it (G.B. Luciani).

Received 15 October 2018; received in revised form 1 April 2019; accepted 14 April 2019

3.2.1. Abstract



- Objectives.

The timing for pulmonary valve replacement (PVR) after tetralogy of Fallot repair is controversial, due to limitations in estimating right ventricular dysfunction and recovery. Intraoperative imaging could add prognostic information, but transesophageal echocardiography is unsuitable for exploring right heart function. Right ventricular function after PVR was investigated in real time using a novel video-based contactless kinematic evaluation technology (Vi.Ki.E.), which calculates cardiac fatigue and energy consumption.

- Methods.

Six consecutive patients undergoing PVR at 13.8 ± 2.6 years (range 6.9–19.8) after the repair of tetralogy of Fallot were enrolled. Mean right ventricular end-diastolic and end-systolic volume at magnetic resonance imaging were 115.6 ± 16.2 ml/m² and 61.5 ± 14.6 ml/m², respectively. Vi.Ki.E. uses a fast-resolution camera placed 45 cm above the open chest, recording cardiac kinematics before and after PVR. An algorithm defines cardiac parameters, such as energy, fatigue, maximum contraction velocity and tissue displacement.

- Results.

There were no perioperative complications, with patients discharged in satisfactory clinical conditions after 7 ± 2 days (range 5–9). Vi.Ki.E. parameters describing right ventricular dysfunction decreased significantly after surgery: energy consumption by 45% [$271\,125 \pm 9422$ (mm/s)² vs $149\,202 \pm 11\,980$ (mm/s)², $P = 0.0001$], cardiac

fatigue by 12% ($292\,671 \pm 29\,369 \text{ mm/s}^2$ vs $258\,755 \pm 42\,750 \text{ mm/s}^2$, $P = 0.01$), contraction velocity by 54% ($3412 \pm 749 \text{ mm/s}$ vs $1579 \pm 400 \text{ mm/s}$, $P = 0.0007$) and displacement by 23% ($27 \pm 4 \text{ mm}$ vs $21 \pm 4 \text{ mm}$, $P = 0.01$). Patients undergoing PVR at lower end-diastolic volumes, had greater functional recovery of Vi.Ki.E. parameters.

- Conclusion.

Intraoperative Vi.Ki.E. shows immediate recovery of right ventricular mechanics after PVR with less cardiac fatigue and energy consumption, providing novel insights that may have a prognostic relevance for functional recovery.

3.2.2. Introduction

Pulmonary regurgitation (PR) is the most common sequela late after repair of tetralogy of Fallot (ToF) [74]. The resulting chronic right ventricle (RV) volume overload leads to varying degrees of ventricular dilatation and dysfunction, which are associated with arrhythmias, cardiac failure and premature death [74]. While pulmonary valve replacement (PVR) has been shown to be effective in resolving PR [75], late results after surgery have not been uniformly associated with clinical improvement [76]. Although to some clinicians, this observation would suggest that the current indications for PVR may be excessively conservative, leading to intervention when irreversible RV dysfunction has ensued [77], others object that a prognosis without PVR may be better in select patient cohorts, due to the additional morbidity associated with PVR surgery [78]. Therefore, the indication and timing for PVR remain a matter of debate.

The current international guidelines for PVR after ToF repair focus on RV functional deterioration, even in asymptomatic patients [79].

However, there is mounting evidence that load-dependent and load-independent indices of RV function assessed by cardiac magnetic resonance (CMR), may be instrumental in guiding indication and timing for PVR [80]. Accordingly, both RV

end-diastolic volume (EDV) and RV end-systolic volume (ESV), including ejection fraction, are currently utilized to assess the correct timing of PVR [81]. However, controversy remains on threshold values due to often unpredictable outcomes after PVR. This has stimulated a quest for alternative clinical and experimental methods to investigate the RV function, in patients with chronic PR after ToF repair [82-84]. Theoretically, a technology able to evaluate RV performance during PVR may track functional changes, and ultimately aid in determining the best timing for PVR, in the future. We recently described an original method to elaborate high temporal and spatial resolution parameters of ventricular function in real time during open-chest surgery, using video kinematic recordings [28]. Briefly, this innovative technique was validated in our previous work [28], in which its algorithm efficiency and quality were evaluated by comparing the data obtained from: the cardiac electro-mechanical coupling model; the pendulum harmonic motion; the spatial and temporal resolution and longitudinal assessment of the kinematic parameters and the contraction force by placing a known mass onto the epicardium of a beating rat heart. This pilot study aims to assess safety and efficacy of intraoperative kinematic evaluation to describe acute RV functional changes in patients undergoing PVR late after ToF repair.

3.2.3. Materials and Methods

The study was approved by the Institutional Review Board (# 847CESC Protocol # 13371), and all patients signed an informed consent. Selection criteria for the study were (i) PR after transannular patch repair of ToF with pulmonary stenosis; (ii) symptomatic patients with severe PR or asymptomatic patients with evidence of progressive severe RV dilatation or dysfunction [79]; (iii) PVR using stented bio prostheses; and (iv) feasibility of PVR normothermic cardiopulmonary bypass on the beating heart. The latter criterion was introduced to eliminate the influence of intraoperative myocardial ischemia on postoperative cardiac kinematics. Furthermore, this criterion was also adopted to closely replicate potential advantages of transcatheter PVR, when no additional myocardial ischemia was involved. Between November 2016 and February 2018, 6 consecutive patients were

enrolled. All patients underwent preoperative CMR and transthoracic echocardiographic evaluation. Demographic and laboratory variables are reported in Table 3.2.1.

	N = 6	Mean	Median	Range
Gender (male/female)	3/3			
BSA (m ²)		1.3 ± 0.2	1.4	0.7–1.7
Age at PVR (years)		13.0 ± 2.3	12.2	6.9–20.1
Age at ToF repair (months)		3.0 ± 0.6	2	1–5
Time to PVR (years)		13.8 ± 2.6	12.5	6.9–19.8
NYHA class II–III	4/6			
SR, complete RBBB (EKG)	4/6			
QRS duration (ms)		156.5 ± 8.7	162	128–174
Severe PR (ECHO)	5/6			
Preoperative CMR				
RVEDVi (ml/m ²)		115.6 ± 16.2	108.5	62.5–183.0
RVESVi (ml/m ²)		61.5 ± 14.6	53.7	12.5–104.0
RVEF (%)		55.1 ± 5.5	53.8	42.0–79.0
PR fraction (%)		49.0 ± 6.9	49.0	22.0–73.0
LVEF (%)		56.0 ± 1.7	54.5	51.0–62.0

Table 3.2.1: Demographic and laboratory variables. BSA: body surface area; CMR: cardiac magnetic resonance; LVEF: left ventricular ejection fraction; NYHA: New York Heart Association; PR: pulmonary regurgitation; PVR: pulmonary valve replacement; RBBB: right bundle branch block; RVEDVi: right ventricular end-diastolic volume index; RVEF: right ventricular ejection fraction; RVESVi: right ventricular end-systolic volume index; SR: sinus rhythm; ToF: tetralogy of Fallot

- Surgical methods.

All PVR procedures were performed by 1 surgeon (G.B.L.). Patients underwent PVR via repeat median sternotomy, using aortic and bicaval cannulation and under normothermic (36°C) cardiopulmonary bypass on the beating heart. Video kinematic recordings were focused on the apical trabecular component of the RV, in line with previous evidence showing this portion as the one bearing most of the chronic volume overload [33]. (Fig. 3.2.1A). All patients underwent postoperative transthoracic echocardiographic evaluation.

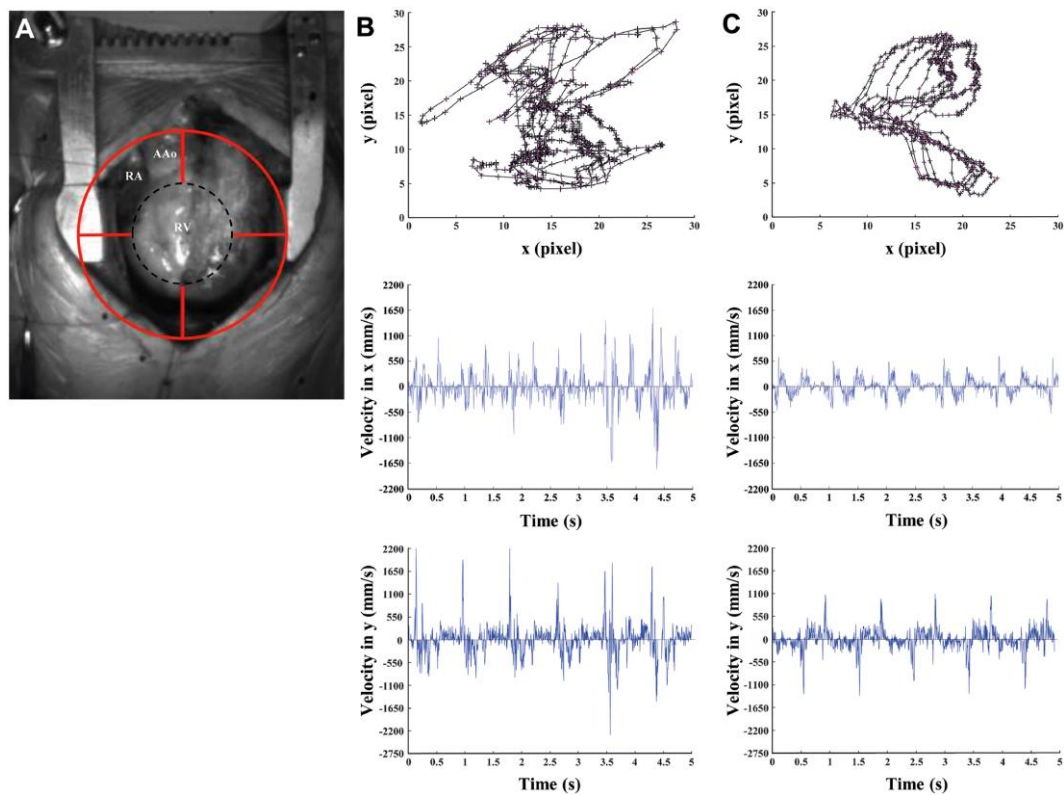


Figure 3.2.1. Video kinematic results obtained pre- and post-pulmonary valve replacement (PVR). (A) Marker position (red circle) on the patient's heart (RV) during open-chest surgery. (B) Upper panel, marker trajectories (black lines with ticks) and acceleration (pink arrows) pre-PVR. Middle panel, video cardiogram in x-axis pre-PVR. Lower panel, video cardiogram in y-axis pre-PVR. (C) Same as (B) but post-PVR. AAo: ascending aorta; Black dashed circle: effective area of analysis; RA: right atrium; RV: right ventricle.

- Experimental Protocol.

For each patient, a high-speed camera (Basler acA1300-200um USB 3.0 with the ON Semiconductor PYTHON 1300 CMOS sensor, Ahrensburg, Germany, equipped with Edmund Optics 6 mm compact fixed focal length lens, Barrington, NJ, USA) was placed approximately 0.4 m above the heart during ToF surgery and 4 videos of 5 s at 200 FPS with a resolution of 1280×1024 and a quality of 10p were recorded at 2 time points. Compared to the previous study [28], this camera and the lenses were specifically chosen for human hearts with the intention of increasing the field of view and assessing the RV kinematics globally. The first recording (pre-PVR) was after chest opening, the second one (post-PVR) around 30 min after weaning from cardiopulmonary bypass exit. In the post-PVR recording, great care was taken to reproduce the same hemodynamic conditions observed in the pre-PVR, including central venous pressure, systolic arterial blood pressure, heart rate and identical ventilator settings. No patient required inotropic support and only one required intravenous antiarrhythmic therapy, as specified below (case #3). The videos were acquired on a high-performance PC (Intel core i7-6700HQ 3.5 GHz, 16GB DDR4 2133 MHz SDRAM, 1TB HDD 7200 RPM With 128GB SSD PCIE $\times 4$) by using an USB 3.0 cable through the camera's own software (Pylon 5 Camera Software Suite 5.0.5 for Microsoft Windows, Ahrensburg, Germany).

- Video Kinematic Evaluation of right ventricle function.

The videos were evaluated by using the Video Spot Tracker software (VST, CISMM, Computer Integrated Systems for Microscopy and Manipulation, UNC Chapel Hill, NC, USA), allowing a virtual marker to be placed on the first frame of the video, which follows the light spots on the epicardial surface, tracking the spatial-temporal coordinates x , y and t of that marker in each frame (Fig. 1A and Video 1). Afterwards, a custom-made algorithm [31] implemented with MATLAB Programming Language (The MathWorks, Inc., Natick, MA, USA) analyses these coordinates, evaluates video cardiograms (ViCGs) and presents the following physical quantities:

Displacement: estimates instantaneous movement of the cardiac tissue;
Contraction velocity: estimates instantaneous velocity of the cardiac tissue;
Force: estimates cardiac fatigue (instantaneous acceleration);
Energy: estimates the kinetic energy during cardiac cycle (it follows the classical and Hamiltonian mechanics for kinetic energy $\frac{1}{2} mv^2$) [28].

The algorithm presents the raw data in pixels and we reported these in SI-accepted unit (m) to provide useful information to surgeons. In the laboratory, we reconstructed a transformation pixel-to-mm curve ($r^2 = 0.9977$) by placing the camera at different heights, from 0.05 to 0.6 m with 0.05 m step, above a millimetre paper (Supplementary Material, Table).

Of note, all scientists involved with experimental data acquisition and interpretation were blinded to preoperative and postoperative clinical and laboratory data.

- Statistical analysis.

Data are presented as mean \pm SEM. The normality of the data was assessed with the Kolmogorov–Smirnov test. The Student’s t-test with Welch’s correction and cumulative distribution with the Kolmogorov–Smirnov test were performed. A value of $P < 0.05$ was considered significant. The programme GraphPad v.6 (GraphPad Software, Inc., La Jolla, CA, USA) was used for analysis and results.

3.2.4. Results

- Clinical outcome

All patients underwent surgical PVR on the beating heart: 4 patients received a 23-mm, 1 patient a 21-mm and 1 patient a 25-mm stented bio prosthesis. There were no perioperative complications, except for 1 patient experiencing reversible subclinical hepatic dysfunction. Patients were discharged after a mean of 7.0 ± 2.0 days (5–9 days) of hospitalization. Transthoracic echocardiogram prior to discharge documented the recovery of normal RV dimensions in 5 out of 6 patients

(83%), preserved (>50%) right ventricular ejection fraction (RVEF) in 3 out of 6 patients and mildly reduced (>40%) RVEF in 3 out of 6 patients. On Doppler examination there was absence of PR in all patients and a mean peak trans-prosthetic pulmonary valve gradient of 16.5 ± 7.1 mmHg. During a mean follow-up of 8.5 ± 4.5 months (2–15 months), all patients were in New York Heart Association (NYHA) I, except 1 patient in NYHA II. No patient experienced adverse cardiovascular events, and all were in regular sinus rhythm, free from oral anticoagulation. The follow-up echocardiogram was similar to that taken before discharge, with a mean peak trans-prosthetic pulmonary valve gradient of 14.5 ± 7.9 mmHg and preserved RVEF in 5 out of 6 patients.

- Intraoperative video kinematic evaluation of right ventricle function in patients with tetralogy of Fallot

The qualitative and quantitative results of the 6 patients were extremely homogeneous, except for 1 patient (#3), who exhibited counterintuitive experimental outcomes. Intraoperatively, this patient showed atrial ectopic tachycardia after PVR, which was initially refractory to antiarrhythmic therapy and eventually subsided 6 h after surgery.

From a qualitative point of view, trajectories and ViCGs differed between pre- and post-PVR condition in all patients (Fig. 3.2.1). In detail, all trajectories showed irregular and chaotic patterns (Fig. 3.2.1B, upper panel) prior to PVR. The same occurred for ViCGs, where systolic and diastolic phases were difficult to differentiate because of background noise in both x and y axes (Fig. 3.2.1B, middle and lower panels). On the contrary, trajectories showed regular, overlapped and well-preserved patterns after PVR (Fig. 3.2.1C, upper panel). The ViCGs displayed both systolic and diastolic phases and we identified less noise in both x and y axes (Fig. 3.2.1C, middle and lower panels). Moreover, marker displacement in trajectories and ViCGs amplitude decreased after PVR when compared to before PVR.

From a quantitative point of view, all kinematic parameters significantly decreased (Fig. 3.2.2A) after PVR when compared to before PVR. On an average, displacement decreased by 23%, maximum contraction velocity by 54%, force by 12% and energy by 45% (Fig. 3.2.2A). Regarding the mechanical performances of individual patients, we noted (Fig. 3.2.2B) that all patients showed a decreasing trend for all parameters, except for patient #3 who exhibited an increasing trend. Prior to PVR, patient #6 showed the highest values for each parameter and the greatest percentage decrease after PVR. In particular, patient #6 values after PVR were greater than the rest of the study population, and, even though these exhibited the greatest decrease, the final parameter values remained 2-fold higher than pre-PVR values from the rest of the study population.

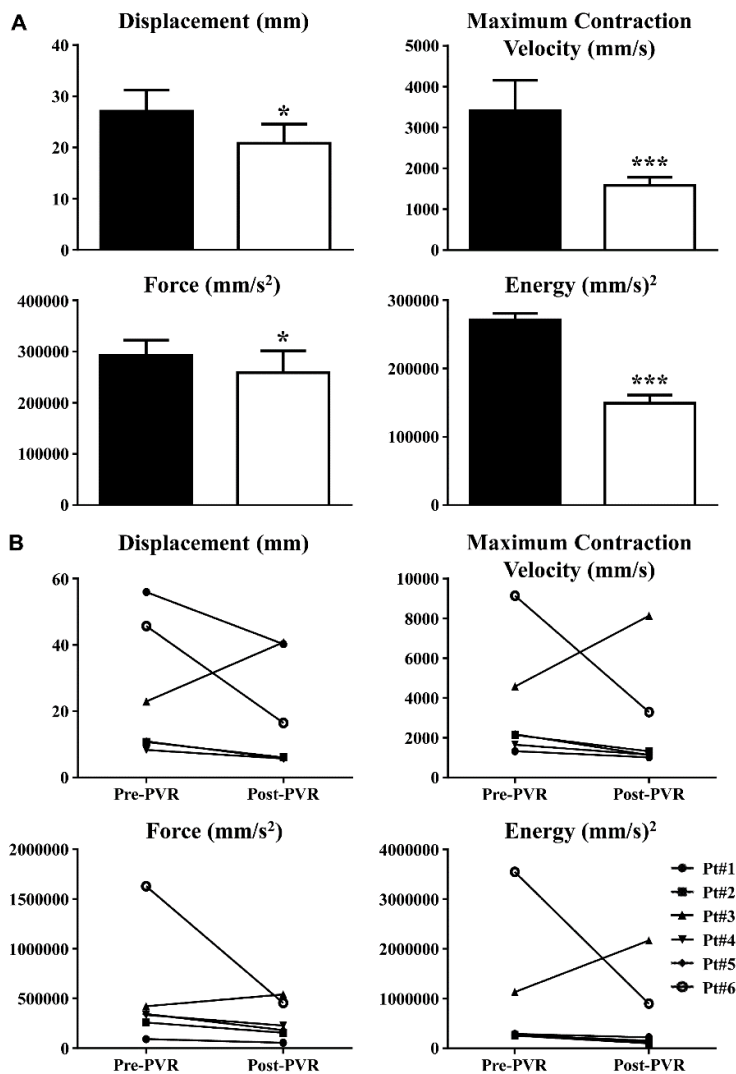


Figure 3.2.2. Kinematic parameters in tetralogy of Fallot patients. (A) Pre-PVR (black columns) was recorded at the chest opening before aortic cannulation. Post-PVR (white columns) was recorded after the surgery and protamine sulphate infusion. Data are shown as mean \pm SEM. * $P < 0.05$ versus pre-PVR, *** $P < 0.001$ versus pre-PVR. (B) Visual representation of video kinematic evaluation parameters, trends for each patient pre- and post-PVR. PVR: pulmonary valve replacement; SEM: standard error of the mean.

To suggest possible clinical correlations, the acquired RV kinematics parameters were compared with CMR, the gold standard RV imaging technique. Thus, we plotted RVEDV index (RVEDVi) versus energy (Fig. 3.2.3, upper panel) and force, a surrogate for cardiac fatigue (Fig. 3.2.3, lower panel), because these kinematic parameters exhibit the strongest clinical implications. In both graphs, patients undergoing surgery with an RVEDV below 129 ml/m² showed a consistent decrease in parameter values after PVR, in line with recovery of minimal contraction energy and cardiac fatigue. Patient #6, who underwent PVR with an RVEDVi of 183 ml/m² (a value currently representing standard indication for surgery) also displayed lower values after PVR with the greatest decrease by far. However, after PVR, energy and force (cardiac fatigue) values in this patient remained higher than the corresponding parameters prior to PVR in the remainder of the study population.

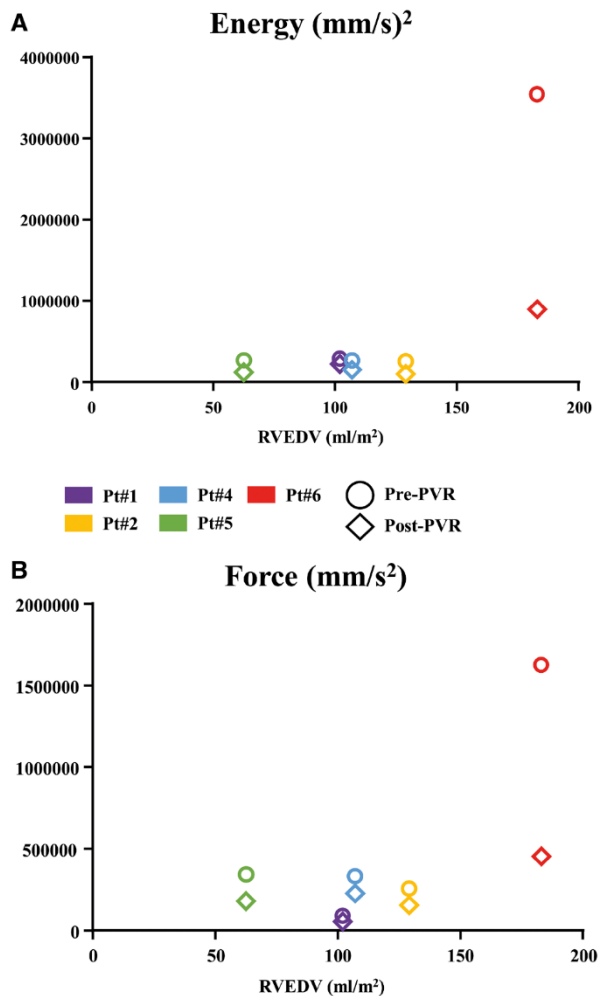


Figure 3.2.3. Correlation between cardiac magnetic resonance and right ventricle kinematic parameters. (A) Graph displaying the relation between RVEDV and energy. Colours represent different patients (see legend), circle is pre-PVR and diamond is post-PVR. (B) Same as (A) but for force. PVR: pulmonary valve replacement; RVEDV: right ventricular end-diastolic volume.

3.2.5. Discussion

Although PVR leads to prompt resolution of PR occurring after ToF repair [75], clinical improvement after PVR is not always predictable [76, 78, 79], leading to controversy over indications and timing for surgery.

Therefore, in addition to clinical observations using meta-analyses [75], propensity matched [78] and prospective [77] studies, efforts have been made to devise experimental models [82-84] able to unravel pathophysiology of the RV following PVR.

In this pilot study, a novel method to describe real time in vivo cardiac kinematics was experimentally applied to offer insight into acute changes of RV properties associated with resolution of volume overload by surgical PVR. This technique was previously applied, in patients undergoing surgical myocardial revascularization [28].

The original experimental approach is a video-based and contactless technique, which can describe precise cardiac kinematic information during open-chest procedures. This technology is versatile, as it may be applied for both basic and clinical research, in conjunction with standard monitoring procedures, without interfering with open-chest cardiac surgery. In patients undergoing surgical myocardial revascularization [28], this technique was able to detect fine contraction of the ischemic/reperfused cardiac tissue areas, which are poorly explored by conventional transesophageal echocardiography. In this study, we focused our attention on RV pathophysiology.

The results of the current experimental study, demonstrate that in patients with previously operated ToF, RV preload reduction by PVR allows: (i) decrease of contraction force (cardiac fatigue) by 12%; (ii) decrease of energy by 45%; and (iii) decrease of maximum contraction velocity and displacement (instantaneous velocity and instantaneous movement of the cardiac tissue, respectively), because

the reduction of force and energy leads to less RV epicardial movement and velocity. One plausible and expected mechanism that could explain this trend is related to the Frank–Starling law: a decrease in RV preload generates a decrease in myocardium stretch (less tension development) and, consequently, a decrease in actin–myosin crossbridge activity leading to less cardiac force and kinetic energy [85].

The pilot study herein provides, for the first time, evidence that PVR may afford immediate recovery of RV functional properties in children and young adults late after ToF repair. Therefore, this work allows one to take the recent findings by Heng et al. [77] on very early (on average 10 days) RV volume recovery at CMR in adults undergoing PVR for chronic PI after ToF on step further. It is noteworthy that when applying standard CMR criteria for PVR, early and late mortality are not negligible and the rate of adverse cardiovascular events (death, VT) does not correlate with either EDV or ESV indices [77, 78]. This suggests that current RV threshold volumes at preoperative CMR will not reliably predict clinical outcome, whereas decline in systolic function (RVEF) may [77, 78, 81]. Surprisingly, the same observations have been made even when using more proactive criteria to refer for PVR [78]. The latter finding may lead one to consider conservative management preferable rather than PVR in patients with PR after repaired ToF. Alternatively, it can be hypothesized that even the use of proactive CMR criteria to refer ToF patients for PVR may be too restrictive to favorably influence late prognosis.

Indeed, evidence by Frigiola et al. [86] suggests that PVR, when performed in children and adolescents (younger than 18 years old) and with more aggressive CMR indications ($RVEDVi < 150 \text{ ml/m}^2$), may be associated with negligible early and late mortality. Furthermore, their surgical referral policy may allow normalization of RV volumes, improvement in biventricular function and normalization of VE/VCO_2 , a parameter of exercise capacity, which best reflects everyday requirements [86].

Our patient population differs in many ways from most large clinical series on PVR late after ToF repair [75-78, 80, 81]. First and foremost, the average age at primary ToF repair was in the first 3 months of life, representing current standard timing for infant repair, and the average age at PVR was in the early teenage years. On the other hand, most published series report on patients in the third and fourth decade of life undergoing PVR 20–30 years after originally having had ToF repair at a preschool or school age. Therefore, exposure to the consequences of chronic RV overload had significantly shorter duration in our series. Furthermore, the underlying diagnosis in this study was restricted to ToF with pulmonary stenosis, whereas prior series encompassed a variety of cardiac defects, associated with ToF, including pulmonary atresia. The latter often imply more complex surgery, repair using a period of myocardial ischemia and the use of extra-cardiac conduits, all factors that may adversely affect RV function. In addition, average RV volumes at preoperative CMR in our series were well below even proactive criteria for PVR in older ToF patients, although closer to the ones reported by Frigiola et al. [86] on PVR in adolescent ToF patients. Finally, and most importantly, unlike most other series, we selected only patients who could undergo beating heart PVR on normothermic cardiopulmonary bypass. Therefore, the additional influence of RV dysfunction due to myocardial ischemia was eliminated in our study. It is noteworthy, that the series with clinical and CMR variables similar to ours also resorted to routine beating heart PVR [86]. The feasibility of beating heart PVR is important, as prior studies have surmised that failure of PVR to affect mid-term clinical outcome might also be due to the additional surgical trauma incurred during the procedure [75, 76, 78], thus advocating wider use of transcatheter PVR. Based on this hypothesis, we are witnessing a trend towards recommending the lowering of CMR thresholds for PVR when transcatheter intervention is possible [87].

This study suggests a correlation between RV volumes at CMR and contraction force, index of cardiac fatigue, and energy even in patients with preoperative RVEDVi lower than current ‘proactive’ recommendations for surgery (115 vs 152 ml/m²). This observation is in line with prior experimental findings using

cardiac catheterization and CMR, where a rapid decline in RV power and efficiency are seen at critical values of 139 ml/m^2 RVEDV and 75 ml/m^2 RVESV index [88].

3.2.6. Limitations

As a pilot study, the current work is limited by the small cohort size. We focused our attention on young patients with ToF undergoing PVR in a single centre. Moreover, our observations were restricted to the intraoperative acute phase of RV changes following PVR. Both circumstances hamper the ability of this study to generate experimental indices, which may reflect its prognostic clinical value. A 6-month postoperative CMR is currently underway to ascertain whether video kinematic parameters may predict late RV remodelling.

A technical limitation of video kinematic evaluation is related to the use of a 2-dimensional camera (for which depth is obviously missing) in acquiring the 3-dimensional cardiac phenomenon. Nevertheless, the algorithm is already implemented for the 3-dimensional motion. Employing a second camera in the operating room will be the next upgrade.

Finally, although video kinematic evaluation may display limited acute prognostic ability in ToF patients undergoing elective PVR, as the perioperative course of these patients is generally uncomplicated, this novel technology is currently being tested in other operative settings, far more commonly exposed to acute perioperative RV failure, such as staged palliation of single RVs (i.e. aortic or mitral atresia) and LVAD implantation in cardiomyopathies.

3.2.7. Conclusions

Video kinematic analysis is a safe, contactless and valid intraoperative technique, which demonstrates prompt improvement of RV functional properties through the reduction of cardiac fatigue and kinetic energy in select ToF patients after PVR.

3.2.8. Supplementary data

Supplementary Table: Echocardiographic Findings:

N=6	Preoperative	Intraoperative	Postoperative
	TTE	TEE	TTE
No PR	-	6	6
Mild PR	-	-	-
Moderate PR	1	-	-
Severe PR	5	-	-
Peak transpulmonary pressure (mmHg)	22±18.9	-	16.5±7.1
No RV dilation	-	4	5
Mild RV dilation	-	1	1
Moderate RV dilation	2	1	-
Severe RV dilation	4	-	-
No RV dysfunction	2	4	5
Mild RV dysfunction	1	2	1
Moderate RV dysfunction	3	-	-
Severe RV dysfunction	-	-	-

TEE, transesophageal echocardiogram; TTE, transthoracic echocardiogram; PR, pulmonary regurgitation; RV, right ventricular.

The study on patients with Tetralogy of Fallot, reported above, primarily takes into consideration the average kinematic behavior of the RV in all the patients. However, focusing on the single patient's behavior, it can be noted that patient #3 suffered from an increase in all the mechanical parameters that can be considered as a “suffering” or “struggling” heart. The patients, however, was dismissed without any complications and in the average dismiss time.

This unexpected behavior was clarified examining what happened in the acute phase of the surgery.

It was noted that the patient in the Post-PVR time-point showed a qualitative improvement compared to Pre-PVR (Figure 29). It was also noted that the patient suffered from an atrial ectopic tachycardia in the Post-PVR time-point, as visible in the number of beats in the ViCGs (Figure 29). The hypothesis was that the heart rate could modify the heart mechanical behavior leading to an increase in the Vi.Ki.E. parameters.

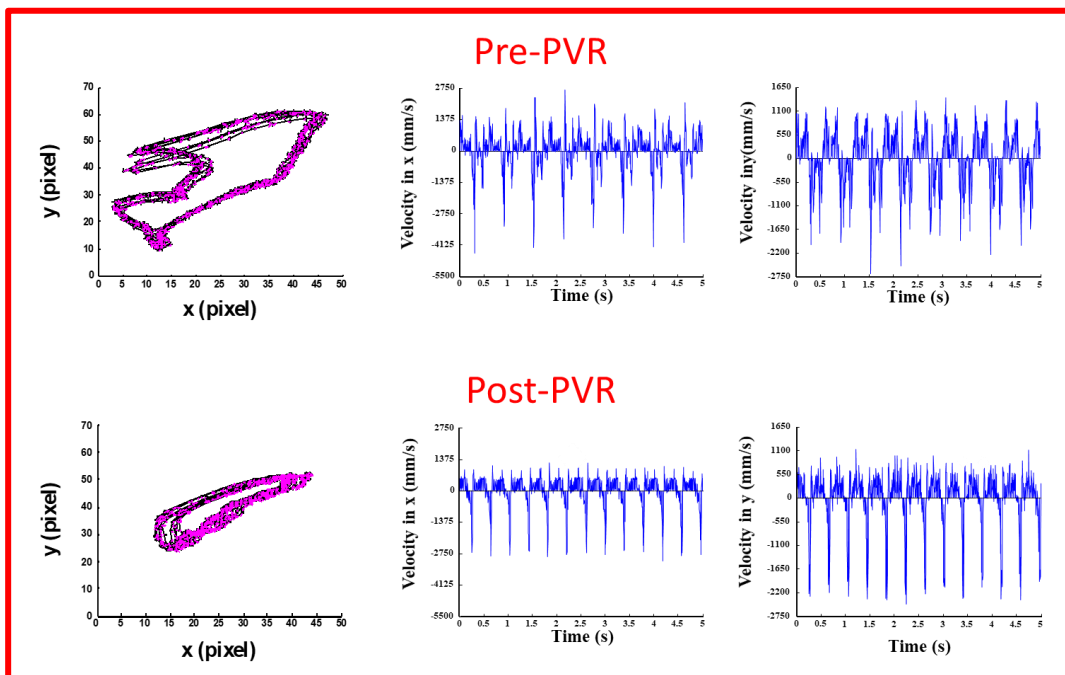


Figure 29. Mechanical parameters of patient #3. Top panel: trajectories and ViCGs before the pulmonary valve Replacement (PVR). Bottom panel: same as Top but after the PVR. To note that after PVR the number of beats is highly increased. Even if the trajectories and ViCGs Post-PVR are qualitative better compared to Pre-PVR the quantitative data was opposite of what we expected.

Therefore, an experimental protocol to pace a rat heart at different rates and evaluate its mechanical behavior (see chapter 3.3) was set up.

3.3. In-situ optical assessment of rat epicardial kinematic parameters reveals frequency-dependent mechanic heterogeneity related to gender [30].



Contents lists available at ScienceDirect

Progress in Biophysics and Molecular Biology

journal homepage: www.elsevier.com/locate/pbiomolbio



Original Research

In-situ optical assessment of rat epicardial kinematic parameters reveals frequency-dependent mechanic heterogeneity related to gender

Francesco Paolo Lo Muzio^{a, b, 1}, Giacomo Rozzi^{a, b, 1}, Stefano Rossi^b, Amparo Guerrero Gerbolés^b, Lorenzo Fassina^c, Giovanna Pelà^b, Giovanni Battista Luciani^a, Michele Miragoli^{b, d, *}

^a Department of Surgery, Dentistry, Paediatrics and Gynaecology, University of Verona Via S. Francesco 22, 37129, Verona, Italy

^b Department of Medicine and Surgery, University di Parma, via Gramsci 14, 43126, Parma, Italy

^c Department of Industrial Engineering and Informatics, University of Pavia, Via Ferrata 1, 27100, Pavia, Italy

^d Humanitas Clinical and Research Center, Via Manzoni 56, 20089, Rozzano, Italy

3.3.1. Abstract

- Background

Gender-related cardiac mechanics following the electrical activity has been investigated from basic to clinical research, but results are still controversial. The aim of this work is to study the gender related cardiac mechanics and to focus on its heart rate dependency.

- Methods

We employed 12 Sprague Dawley rats (5 males and 7 females) of the same age and, through a novel high resolution artificial vision contactless approach, we evaluated in-situ cardiac kinematic. The hearts were paced on the right atria appendage via cathodal stimuli at rising frequency.

- Results

Kinematic data obtained at rising pacing rates are different between male and female rat hearts: male tended to maintain the same level of cardiac force, energy and contractility, while female responded with an increment of such parameters at increasing heart rate. Female hearts preserved their pattern of contraction and epicardial torsion (vorticity) at rising pacing rates compared to male. Furthermore, we observed a difference in the mechanical restitution: systolic time vs. diastolic time, as an index of cardiac performance, reached higher value in male compared to female hearts.

- Conclusion

Our innovative technology was capable to evaluate in-situ rat epicardial kinematic at high stimulation frequency, revealing that male preserved kinematic parameters but varying the pattern of contraction/relaxation. On the contrary, female preserved the pattern of contraction/relaxation increasing kinematic parameters.

3.3.2. Introduction

The relationship between protection from cardiovascular diseases (CVDs) and gender has fascinated researchers and cardiologists for decades. The reason is strictly related to the presence of female and male hormones, targeting their effects almost in all part of the cardiomyocyte: ion channel repertoire [89, 90], receptors [91], calcium handling machinery [92], mitochondria [93], intracellular pathways, genome [94] and epigenome [95]. It emerges that cardiac electrophysiology is, undeniably, affected by estrogen and testosterone [96], having effects on all phases of the action potential. This would suggest a possible “protection” against the progression towards CVDs for female in premenopausal age compared to male hearts. Nonetheless, all that glitters is not gold. Bazett in 1920 suggested how both sex difference and heart rate (HR) have an impact on the ECG (and he further developed the famous correction QTc formula that report his name). Women have a long QT in respect to men and this exposes the female at risk of some life-

threatening arrhythmias, such as torsade de pointes especially when is drug-induced [97]. Park et al. [98] elegantly summarized the physiological divergences between male and female heart. Moreover, at the single cell level, numerous studies did not observe gender difference in the peak of Ca^{2+} current except Farrell et al. [99] that demonstrated significant modifications via voltage clamp. Cellular contraction has also been taken into account by numerous investigations. Rosenkranz-Weiss et al. reported that female rat ventricular myocytes display high-level of myosin heavy chain (MHC) as well as upregulation of actin mRNA compared to males [100]. Notably, they found no difference in the α -to β -ratio of MHC proteins, suggesting that those sex differences are abolished after post-translational modifications. Petre et al. [101] and Schwertz et al. did not find any gender-related difference in terms of force of contraction in ventricular trabeculae. In detail, Schwertz et al. [102] found that ATPase activity was higher in female rats at any given extracellular Ca^{2+} concentration compared to male, suggesting that the female contractile machinery had a greater Ca^{2+} sensitivity. Experimentally, the single cell contraction is smaller in female ventricular myocytes compared to male especially when those cells are paced at rapid rates [103]. This would indicate that high stimulation frequency may highlight the gender difference in cardiac performance. Some authors showed an increment in isolated ventricular myocyte contraction [104], while others reported a reduction [105]. A robust evidence regarding the role of female hormone on cardiac activity has been observed in female rats undergoing ovariectomy. To note such differences were completely reversed when 17- β -estradiol was replaced. Androgen receptors are usually present in cardiac tissue and study efforts were mostly focused on their action on intracellular Ca^{2+} handling machinery [106] rather than contractile performance. Few studies have been performed at multicellular cardiac level after gonadectomy and reported a decrement in the maximum contraction and the peak of Ca^{2+} . Studies on papillary muscle [102] recapitulated the evidence observed at single cell level, i.e. the greater affinity of female myofibrils to Ca^{2+} , demanding less extracellular Ca^{2+} for evoking the same force of contraction in comparison to male. On the contrary, the same authors reported that in the Langerdorff perfused heart, male generated a greater ventricular pressure

compared to female. Such disparate findings indicate that methodological preparations influenced gender dissimilarity.

Based on the observations above, it is evident that rodents are an appropriate animal model for studying the relationship between cardiac performance and gender [107]. In particular, rodent models may be well suited for dissecting the biophysical mechanisms underlying the propensity to develop CVDs. In spite of the great efforts and the results obtained at single cell and tissue levels, in-vivo investigations on gender-related ventricular kinematic are lacking. We are aware that canonical in-vivo gender-related data are merely analyzed from echocardiography [108], cardiac MRI and SPECT [109] exquisitely describing the heart global mechanical function. Unfortunately, these imaging techniques provide only minimal information on kinematic.

In this paper, we adopted the optical-image based technology called Video Kinematic Evaluation (Vi.Ki.E.) [28, 31, 59], completely developed in our laboratory, to evaluate in-situ high resolution ventricular tissue kinematic in male and female beating hearts, paced at different frequencies.

We observed a frequency-dependent increment of epicardial ventricular contractility, force and kinetic energy in female rat hearts compared to male. Female rats tended to preserve their pattern of contraction and the total perimeter of trajectories at different basic cycle lengths (BCL) resulting in less heart torsion compared to male. Sex difference does not influence the systolic area/diastolic area (S/D area) but it denotes a consistent variation in systolic time/diastolic time (S/D time) between the two groups. Data from our innovative optical-based and contactless technique indicate a profound gender difference in the heart mechanics, opening avenues for further evaluation in the clinical setting.

3.3.3. Materials and methods

- Experimental animals

The study population consisted of 12 Sprague Dawley rats (5 males and 7 females) bred in our animal facility (approved protocols: 281/2017, 989/2017). The study was conformed to Italian (D.L.4/3/2014) and European guidelines (2010/63/UE). Rats, 6 months old weighting 250–275 g, were anesthetized with 0.20 mg/kg ip of a mixture of tiletamine hydrochloride and zolazepam hydrochloride (Zoletil; Virbac S.r.l., Carros, France) + 0.15 mg/kg ip medetomidine hydrochloride (Domitor; Orion Corporation, Espoo, Finland). The heart was exposed through a median thoracotomy and suspended in a pericardial cradle under artificial ventilation (RoVent® Small Animal Ventilator, Kent Scientific, CT, USA). Body temperature was maintained constantly at 37 °C with heath lamp radiation and further doses of anesthetic was administered as needed during the experiment. This type of anesthesia invariably suppressed the sympathetic tone in rodents and so our results are not biased by the autonomous nervous system [110]. Animals where sacrificed with a lethal injection of sodium pentothal as indicated in the protocols.

- In-vivo atrial stimulation

The heart was stimulated with a cathodal suprathreshold train of stimuli (10 Vpp) at different basic cycle length (BCL: 390 ms, 330 ms, 290 ms, 260 ms, 230 ms, 210 ms, 190 ms, 170 ms, 160 ms) by driving the right atrium with a silver electrode (0.05 mm) with one end connected to a stimulus generator (SIU-102, Warner Instruments CT, USA) and the other hooked to the atrial auricle appendage (Fig. 1A). The current return silver electrode has been placed in the right forearm. The stimulus generator was triggered by a function generator (Aim-TTi TG310, RS Components, Milano, IT).

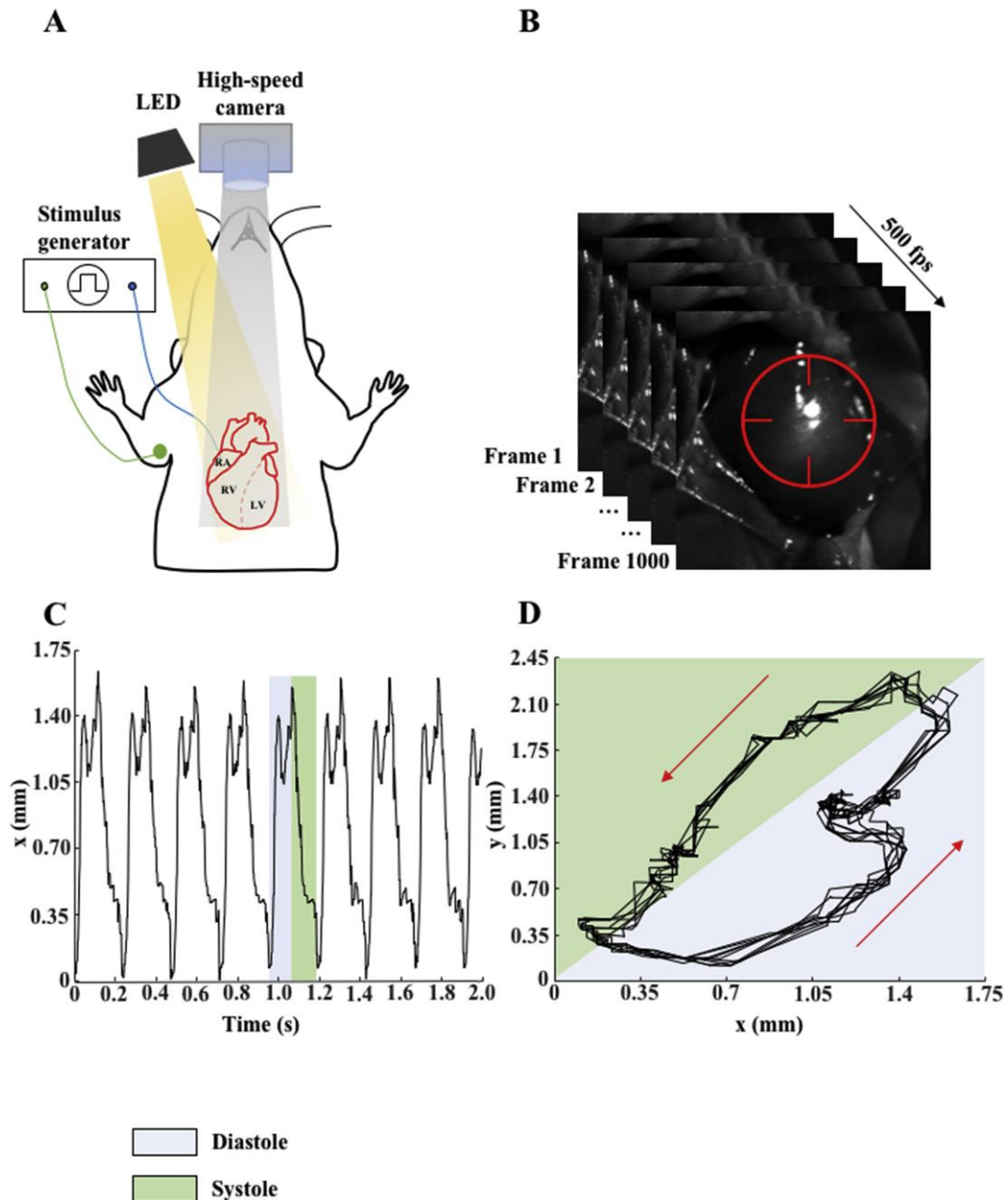


Fig. 3.3.1. Schematic representation of the experimental setup. **A.** The heart (red cartoon) is exposed after median thoracotomy. One end of the stimulating electrode (blue line) is hooked on the Right Atrial (RA) auricle appendage to perform atrial stimulation, while the other end is connected to a stimulus generator (black rectangular box). The current return electrode (green line) is placed on the right forearm. The high-speed camera is placed perpendicular to the heart to record anterior epicardial kinematic. The grey shaded region represents the video camera field of view. The LED is placed beside the camera. The yellow shaded region represents the light beam. RV, Right Ventricle; LV, Left Ventricle; dashed red line, interventricular septum. **B.** Stack of images of rat hearts recorded at 1280×1024 pixel at 500 fps. Red target represents the virtual marker positioned in that frame. **C.** Example of the marker movement in x coordinate during 2 s recording. The light blue rectangular indicates the diastolic phase, while the light green rectangle indicates the systolic phase. **D.** Example of trajectories in x-y plane drawn by the marker in 2 s recording. Each loop represents a single cardiac cycle. The light blue and the light green triangles represent the diastolic and systolic phases, respectively. Red arrows indicate the direction of the cardiac cycle.

- In-situ optical assessment of kinematic parameters

To evaluate cardiac kinematic parameters, 2 s videos with the temporal resolution of 500 fps (Fig. 3.3.1B) were acquired for each BCL, with a spatial resolution of 1280×1024 pixel. The camera (Baumer HXC13, Baumer Italia S.r.l., Milano, Italy) was connected with full CameraLink® interface to a frame grabber acquisition board PCIe 1433 (National Instruments, Assago, Italy) and placed at 20 cm above the heart. The camera was equipped with a macro-objective Kowa Industrial Lenses LM35XC, $F = 1:2.0$, $f = 35$ mm, picture size 13.8–18.4 mm (RMA Electronics, Hingham, MA, USA). The acquisition board was integrated into a Workstation HP Z220 (Crisel Instruments, Roma, Italy) with 24 GB RAM and the acquisition software was custom made in LabVIEW 2013 Visual Programming Language (National Instruments, Assago, Italy). Only videos with observed 1:1 capture were included in the final analysis.

The videos were elaborated by Video Spot Tracker, an open source software (VST, CISMM, Computer Integrated Systems for Microscopy and Manipulation, UNC Chapel Hill, NC, USA), that enables to place a virtual marker (Fig. 1B, red target) with a chosen kernel on the first video frame. The marker follows the light spots onto the epicardial surface and tracks its coordinates in x and y for each frame. The movement of the light spot is a function of the surface curvature and because it moves back and forth from apex to base during cardiac cycle, it can be assumed as the direct deformation of the epicardial tissue (Supp. Video 1). Afterwards, a custom-made algorithm [28] implemented with Matlab Programming Language (The MathWorks, Inc., Natick, MA, USA) analyzes these coordinates (Fig. 3.3.1C), draws the trajectories (Fig. 3.3.1D) and returns the following kinematic parameters [28]: i) Contractility, expressed in [mm/s], as the average of the maximum module of epicardial velocity for each systolic phase; ii) Force, expressed as [mm/s²], as the average of cardiac force expended over the entire cardiac cycle during the acquisition period; iii) Energy, expressed as [mm/s]², as the average of the cardiac kinetic energy expended over the entire cardiac cycle during the acquisition period. Here we included the novel parameter of trajectory (perimeter, corrected for the number of beats) that measures the marker path length during cardiac cycles. We

took advantage of a MathWorks tool named Particle Image Velocimetry (PIV; <https://it.mathworks.com/matlabcentral/fileexchange/27659-pivlab-particle-image-velocimetry-piv-tool>) as previously used from us [28] and others [111] for the evaluation of the epicardial torsion. Kinematic data are expressed in the standard SI unit following a conversion: we reconstruct a transformation pixel-to-mm curve by placing the camera at different heights above a graph paper (data not shown).

- Systolic and diastolic area and time

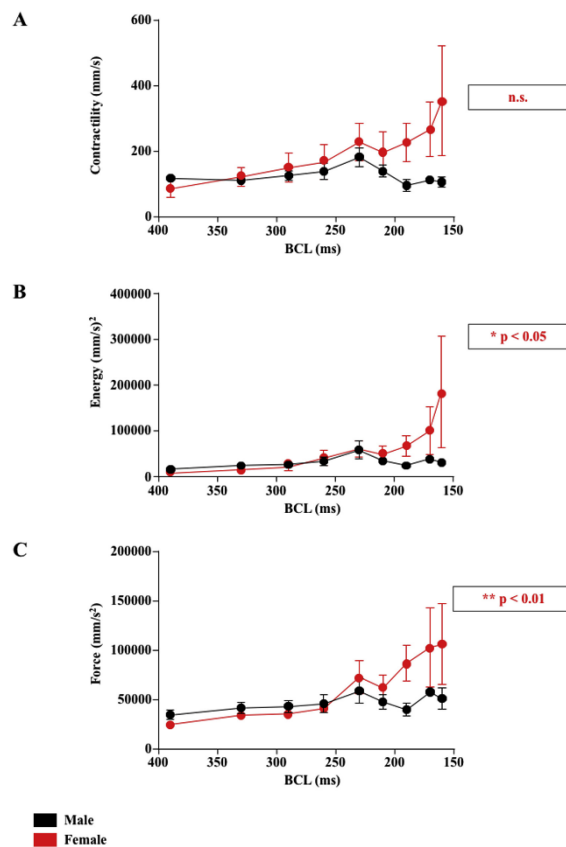
We have extracted from the last complete cardiac cycle of the recorded video the maximal relaxation area (during the diastole) and the minimal contraction area (during systole) for each BCL. Areas were evaluated using a dedicate plug-in from Fiji (ImageJ 9.0, National Institutes of Health, USA) by selecting the frames displaying the maximum relaxation and maximum contraction. Moreover, the systolic and diastolic times were evaluated from the videos as the time interval between the maximum relaxation and maximum contraction and vice-versa, respectively.

- Statistical analysis

All data are presented as mean \pm standard error of the mean (S.E.M.). The normality of the data was assessed with the Kolmogorov-Smirnov test. Kruskal Wallis test and 2-way ANOVA were performed. A value of $p < 0.05$ was considered significant. The program GraphPad v.6.0 (GraphPad Software, Inc., La Jolla, CA, USA) was used for the statistical analysis and results display.

3.3.4. Results

We evaluate via Vi.Ki.E. technology the global epicardial kinematics at different BCL ranging from 390 ms to 160 ms. We observed that male hearts tend to maintain the same contractility, force and energy (Fig. 3.3.2A), while female rat hearts tend to increase the same parameters at the rising stimulation frequency (Fig. 3.3.2B). In detail female epicardial force and energy displayed a significant increasing trend ($p=0.0019$ and $p=0.017$ respectively). During our experimental protocol, we noticed that, from BCL = 230 ms onward, an increase of the kinematics parameters occurred in all animals. After this time-point we noticed different trends between male and female. Therefore, we studied in deep the gender-related mechanical behaviour in the following timepoints (BCL: 230 ms, 210 ms, 190 ms, 170 ms) that resemble the range of rat physiological HR. We highlighted this difference in Fig. 3.3.3 with representative experiments that display trajectories and coordinates for both male (black) and female (red). As it can be noticed male trajectories (Fig. 3.3.3 A-A3 top panels) varied at each BCL indicating different patterns of contraction.



On the contrary, female trajectories (Fig. 3.3.3 B–B3 top panels) are preserved at each BCL for every cycle. The bottom panels in Fig. 3.3.3 A-B display the keeping of 1:1 capture for each cardiac cycle at increasing HR.

Fig. 3.3.2. Effect of the rising frequency of stimulation on epicardial kinematic parameters. Graphs displaying relationship between epicardial kinematic parameters and basic cycle length (BCL) for male (black) and female (red). Trend comparison between male and female for: Contractility (A), Energy (B) and Force (C). Data are shown as Mean \pm S.E.M. * $p < 0.05$, ** $p < 0.01$.

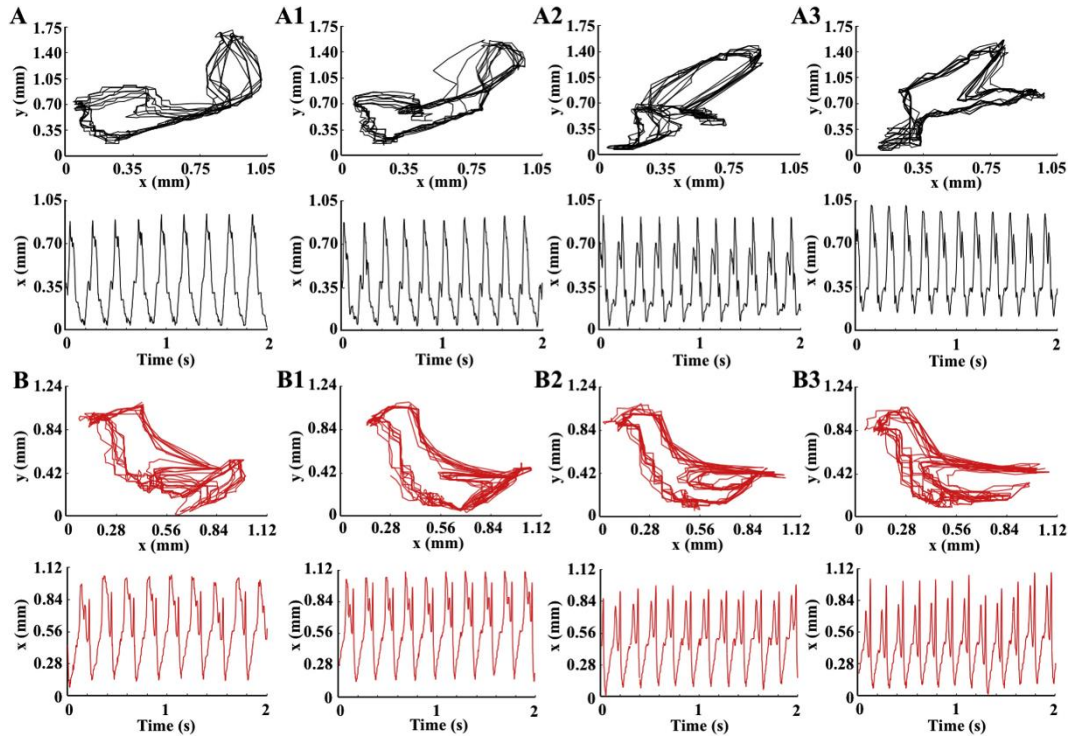


Fig. 3.3.3. Contraction patterns at different stimulation frequencies. Examples of male rat heart (black) and female rat heart (red) trajectories and coordinates at four different basic cycle length (BCL). **A, A1, A2, A3:** male trajectories (top panels) and respective coordinates vs. time (bottom panels) at 230 ms, 210 ms, 190 ms and 170 ms respectively. **B, B1, B2, B3:** same as A, but for female rat heart.

- Frequency of epicardial torsion obtained via Particle Image Velocimetry

In order to provide a global information of epicardial torsion following the gender-related pattern of contraction observed in Fig. 3.3.3, we sought to evaluate, for each BCL, the cardiac vorticity by analyzing the videos with PIV (Fig. 3.3.4A). Fig. 3.3.4B shows that cardiac vorticity parameters display an increasing trend statistically significant for both gender during the stimulation protocol ($p = 0.0006$). Moreover, the male trend was statistically significant compared to female trend ($p < 0.0001$).

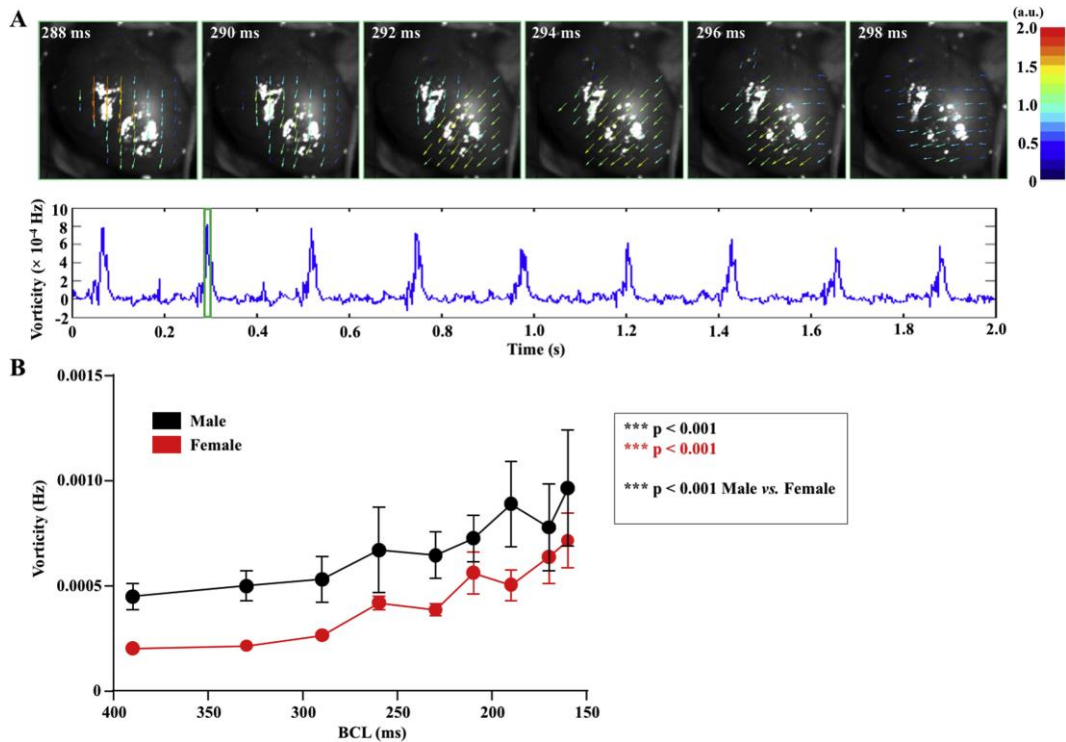


Fig. 3.3.4. Epicardial torsion observed by Particle Image Velocimetry. A: Upper panel. Six consecutive frames (step: 2 ms) of Particle Image Velocimetry (PIV) evaluation. The colored arrows represent the velocity vectors; the vector module and colors represent the different epicardial velocities. Bottom panel. Epicardial vorticity parameter (Hz) in 2 s recording. The green rectangle highlights the six frames displayed in top panel. B: Relationship between the mean Vorticity parameters and basic cycle length (BCL) in male (black) and female (red) rat hearts. Data are shown as Mean \pm S.E.M. *** $p < 0.001$.

- Geometrical spatiotemporal variation at different BCL

The dissimilarity of contraction patterns in male rats at rising frequency suggested that the frequency-dependent epicardial deformation can be related to gender. We sought to investigate the mechanical behaviour at different BCL for both trajectory's perimeter and the maximal contraction (systolic) and maximal relaxation (diastolic) areas. As expected, the data displayed a not-preserved perimeters (Fig. 3.3.5A) (ranging from 5.890 ± 0.5597 mm to 3.747 ± 0.3422 mm) over different BCL in male rat hearts (black) compared to female (red) (ranging from 4.220 ± 0.1566 mm to 4.566 ± 0.8934 mm). The male epicardial areas (Fig. 3.3.5B) during maximal systolic and diastolic phases were higher compared to female rat hearts (by ca. 11%); however male areas were more statistically spread at higher frequency in contrast to female, suggesting once more a preservation of the mechanical phenotype of cardiac beating over different BCL in female rats.

A

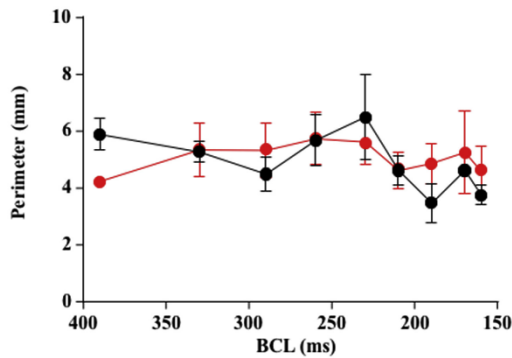
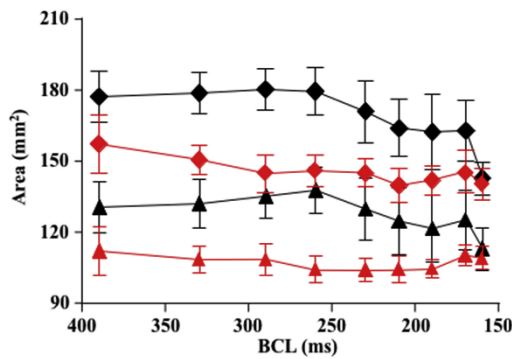


Fig. 3.3.5. Relationship between perimeter and area vs basic cycle length. **A:** Male (black) and female (red) perimeter corrected for the number of acquired cardiac cycles for each basic cycle length (BCL). **B:** Average systolic and diastolic area for each BCL in both male (black) and female (red). Diamond: diastole; Triangle: systole. Data are shown as Mean \pm S.E.M.

B



Male Diastole
 Female Systole

- Rising stimulation frequency unmasks gender difference at the single cardiac cycle

We thus recognized that sex differences can be also investigated during the single cardiac cycle extracted from different BCL. Therefore, we plotted the S/D time for both male and female rats beating hearts at rising frequencies of stimulation (Fig. 3.3.6). We demonstrated that while S/D area was preserved for both male and female hearts (average male 0.737 ± 0.026 , average female 0.753 ± 0.029), paradoxically the S/D time differed (Fig. 3.3.6). In the male rats we observed a significant increasing trend (from 0.359 ± 0.029 at 390 ms to 0.913 ± 0.049 at 160 ms, $p < 0.0001$). A significant increasing trend has also been observed for the female rat S/D time (from 0.357 ± 0.031 at 390 ms to 0.815 ± 0.067 at 160 ms, $p < 0.0003$). The S/D time data suggest a different gender-related mechanical restitution at high pacing rates.

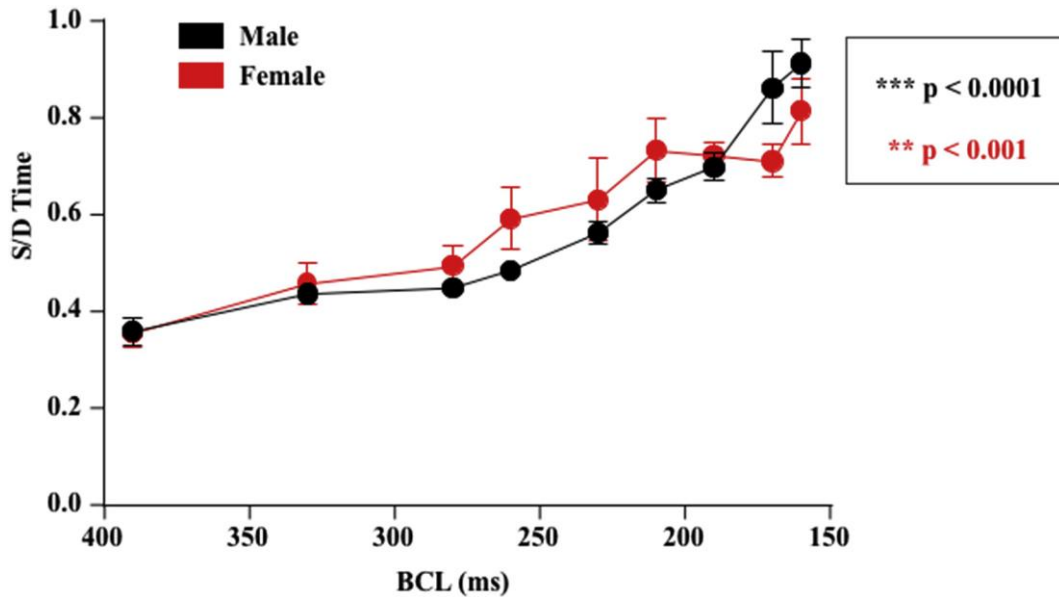


Fig. 3.3.6. Mechanical restitution of systolic/diastolic time. Simultaneous plot of systolic/diastolic time (S/D time) in both male (black) and female (red) rat hearts. Data are shown as Mean \pm S.E.M. ** $p < 0.001$, *** $p < 0.0001$.

3.3.5. Discussion

In this study, we applied our high spatial and temporal resolution video kinematic technology to understand the gender-related response of epicardial mechanics during atrial pacing. An additional goal was to examine whether female propensity to cardiac protection against CVDs can be unraveled thanks to our optical-based experimental protocol. From a physiological standpoint it is well known that female has low BMI, low LVED pressure [112] but higher velocity of contraction suggesting that women are in constant hyperdynamic state [113]. In clinical research, sex difference in cardiac performance is unmasked during physiological exercise [114] and with RA pacing during cardiac catheterization [115]. At the pathological level, gender has an influence on the manifestation of myocardial infarction [116], with the incidence of ischemic heart disease being much lower in premenopausal women than age-matched men [117]. However, the incidence of CVDs after menopause exceed that of men [118]. Only recently, sex differences have been considered in clinical and preclinical studies for CVDs (Consideration of Sex as a Biological Variable in NIH-funded Research, 2015). It is also known that sex differences in ventricular mechanics occur during acute physiological challenges, exacerbated by adrenergic stimulation [119]. In this work, we showed

that in-situ female beating hearts tended to show a “kinetic reservoir” due to a possible female hyperdynamic state [113] in terms of contractility, energy and force that can be expended at lower BCL in accordance with the positive role exerted by estrogens on the excitation-contraction machinery [89]. However, we cannot exclude the gender-related difference in the excitation-contraction (EC) coupling machinery including the SERCA activity [99, 120]. In agreement to Williams et al. we would expect, for female hearts, an acute ventricular mechanical adaptation to the rising pacing rate. We also notice that female rats data dispersion occurred at high frequency of stimulation according to what has been measured in human females during exercise by Bombardini et al [114]. Moreover, our video kinematic technology captured a change in the mechanical pattern of epicardial mechanics (trajectories) for male hearts starting from BCL = 230 ms, whereas female hearts trajectories seem to be unaltered at rising frequency of stimulation. This is further confirmed by PIV and trajectory perimeter analysis where the epicardial vorticity and perimeter variation were higher in male compared to female. Because our technique can be applied during open chest surgery [28] we investigated whether such changes may impact on the area of contraction of maximal ejection (systolic phase) and on the area of relaxation of maximal ventricular filling (diastolic phase). Epicardial area changes during heart stimulation and it is an index of ventricular ejection and filling [121], reflecting the Frank-Starling mechanism which leads to inotropic effect. Accordingly, the systolic and diastolic areas (bigger for male in respect to female, as expected) tended to decrease in male at increasing frequency of stimulation, whereas they seem to be preserved in female. This would suggest that the acute cardiac mechanical adaptation observed in male is necessary to compensate the nonappearance of the “kinetic reservoir” hypothesized in female rat hearts.

One of the echocardiographic index used in clinics is the ratio between systolic and diastolic time intervals [122]. This parameter, together with the rising frequency of stimulation, can provide the mechanical restitution of the heart [123]. Vi.Ki.E. can be adopted to measure S/D time at high temporal resolution extracted from our coordinates in x and in y. We observed a rising S/D time ratio in both male and

female hearts displaying the difference in mechanical restitution. Moreover, the tendency to reach important quasi-pathological values for S/D time ratio, i.e. > 1.0 has been observed only in male rats, which is in accordance to the major masculine CVDs-susceptibility observed in humans.

3.3.6. Conclusions and limitations

Our video technology unmasked gender-related kinematic cardiac differences in-situ, displaying two different mechanisms of adaptation for male and female heart at increasing frequency. Male hearts tended to change their intrinsic spatiotemporal pattern of contraction/relaxation at the rising frequency of stimulation and to preserve their kinematics for all BCL. Female hearts denoted an opposite trend tending to preserve the spatiotemporal pattern and modify their kinematic response at different BCL. Our results are limited by the absence of the z-dimension and we recapitulate a 3D phenomenon in a 2D analysis. However, this precise and repeatable approach is useful to simplify the analysis without losing the main goal of the study and allow us to make comparison between several experimental sets. Future technological implementation will aim to introduce a second high-speed camera together with a PV-loop, a pressure catheter for peripheral resistance measurement and echocardiographic investigation for simultaneous acquisition of 3D epicardial kinematics and cardiac function.

3.4. Unpublished Results

In this chapter, all the data not yet published, deriving from the evaluation of different pathologies will be reported and discussed.

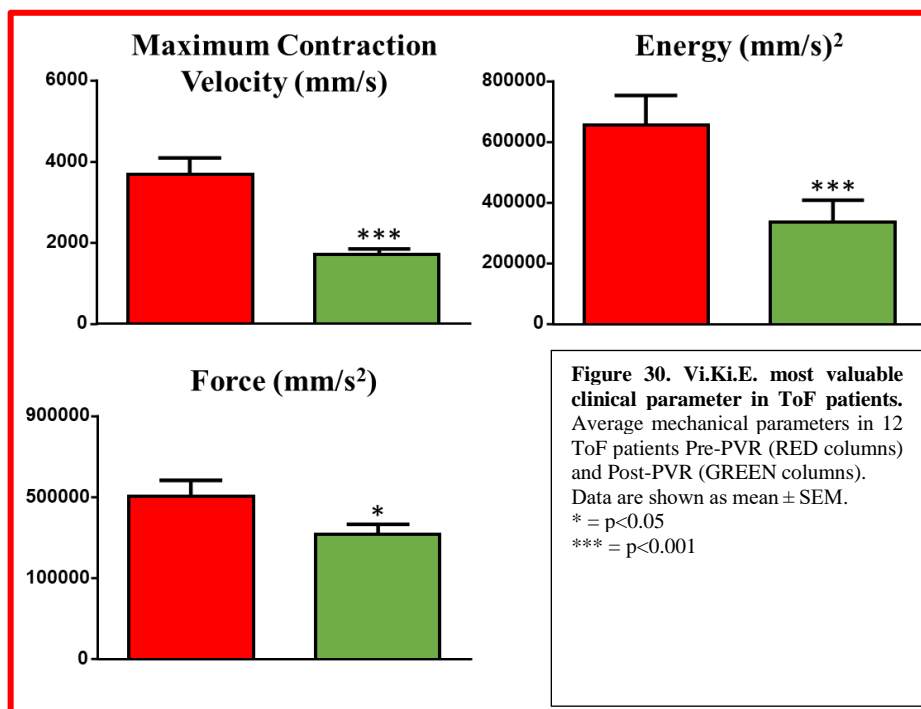
3.4.1. Tetralogy of Fallot

To confirm the positive results from the pilot study, and to take part in the debate on RVEDV thresholds for surgery, the Vi.Ki.E technology was then applied to adult patients.

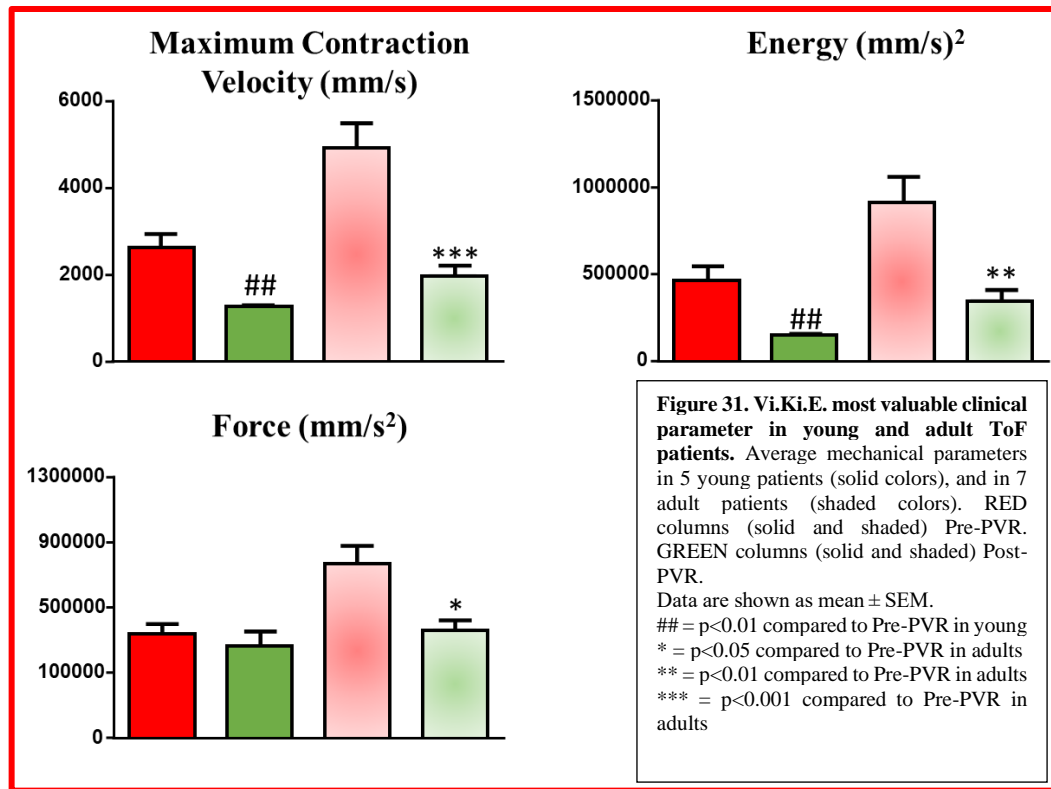
Results

Six adult patients, undergoing PVR, were enrolled from March 2018 to November 2018 with an average age of 41.7 ± 21.7 years. Three of these patients suffered from atrial fibrillation and also underwent the surgical maze protocol. The same statistical analysis approach of the previous work was adopted to assess the acute effect of the surgery on Vi.Ki.E. evaluation.

Figure 30 shows the mean parameters of the entire 12 patients' population before and after PVR; all parameters significantly decrease after PVR



However, the study population consisted of two main groups, the young and adult patients. Therefore, the data was evaluated individually for each group to investigate possible differences of the surgical impact. Figure 31 shows what has been found.



The data subdivision in the two groups highlighted that, although for the young patients (Figure 31 solid colors) the recovery was significant (except for the Force), it was lower than the adult group (Figure 31 shaded colors) in which it was significant for all set of parameters. However, in the adult group the overall recovery was lower compared to the young group, with the Post-PVR values often twofold higher than young Post-PVR values.

As it concerns the single patient evaluation, Figure 32 shows that the young group (Figure 32, Purple), undergoing surgery below the clinical suggested threshold of $RVEDV > 150\text{ml/m}^2$, had a very small recovery in terms of Energy and Force between Post-PVR (Figure 32, Circle) and Pre-PVR (Figure 32, Rhombus). However, the data distribution is less spread for young patients than for the adult ones who, on the contrary, underwent surgery at the suggested threshold of $RVEDV > 150\text{ml/m}^2$ (Figure 32, Yellow). An exception could be made for Patient #3 (highlighted in the graph) whose intraoperative tachycardia influenced the mechanical parameters

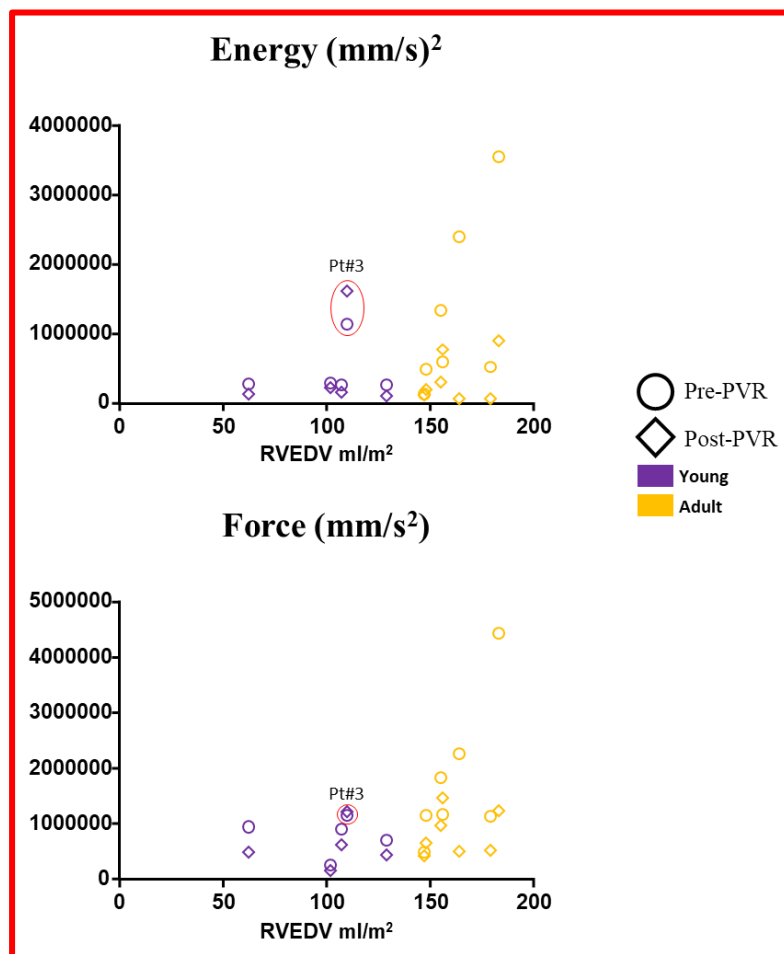


Figure 32. Correlation between MRI parameter RVEDV and Vi.Ki.E. clinical marker parameters in ToF patients. Average mechanical parameters in young patients (Purple) Pre-PVR (Circle) and Post-PVR (Rhombus), and in adult patients (Yellow) Pre-PVR (Circle) and Post-PVR (Rhombus). Red circle Highlight the Patient #3 that suffers of an intraoperative tachycardia influencing the mechanical parameters. It is added in the graph only for visual purpose.

Discussions

The most interesting and pivotal part of the study concerns the debate about the timing for PVR. There are two way of thinking, some clinical equips are more “conservative” awaiting until the pathology reaches an advanced stage, and others, with a more “aggressive” approach, assert the importance to perform surgery as soon as possible to avoid cardiac remodeling and impairment through years.

One of the used parameters in the ESC guidelines to time the PVR is the MRI RVEDV threshold at $165\text{ml}/\text{m}^2$. However, there are some studies showing that this value could be too high and the patient could be in a late stage of the pathology [86], but even this is a matter of debate. In this study, patients above and under this threshold were enrolled. What it has been noticed, comparing the most valuable Vi.Ki.E. clinical parameters (Energy and Force) with the RVEDV distribution, it was that patients under the $150\text{ml}/\text{m}^2$ had a very small recovery and parameters distribution. On the contrary, patients above $150\text{ml}/\text{m}^2$ showed a high intra-surgery recovery. However the overall recovery was far from the basal recovery, with values often twofold higher compared to those who underwent PVR under the threshold. To note, the data distribution was very high.

Moreover, the conventional intervention (i.e. above $150\text{ml}/\text{m}^2$) denoted advantages in terms of patient’s recovery compared to those operated early. However, the overall recovery is far from the baseline reached by the patients operated earlier. This could lead to the development of future cardiac pathologies or re-hospitalization. On the contrary, the unconventional intervention (i.e. below $150\text{ml}/\text{m}^2$) has a little impact on the cardiac functionality but could be performed, as a prevention, to avoid possible future cardiac pathologies. In particular the baseline parameters are drastically lower in those patients rather than in patients operated with the conventional surgery. The follow-up monitoring of those patients, in the next 5 to 10 years, as well as this study (and the further ones), could lead to a reduction of the actual threshold for the surgery and the amelioration of the patients’ outcomes.

3.4.2. Hypoplastic Heart Syndrome

The increasing Vi.Ki.E. trust and attractiveness in the clinical approach led to the testing the of the technology in more complex pathologies, such as the patients suffering from ventricular hypoplasia (Hypoplastic Heart Syndromes HHS or univentricular patients).

Results

A total of 6 patients were enrolled for this preliminary study. Four suffered from Hypoplastic Left Heart Syndrome (HLHS), while the other 2 suffered from Hypoplastic Right Heart Syndrome (HRHS). Since the patients were in different surgical repair stages, the data are presented, at first, as total mean to highlight the global mechanical behavior, and later data were divided and analyzed separately following the 2 surgical stages: GLENN and FONTAN.

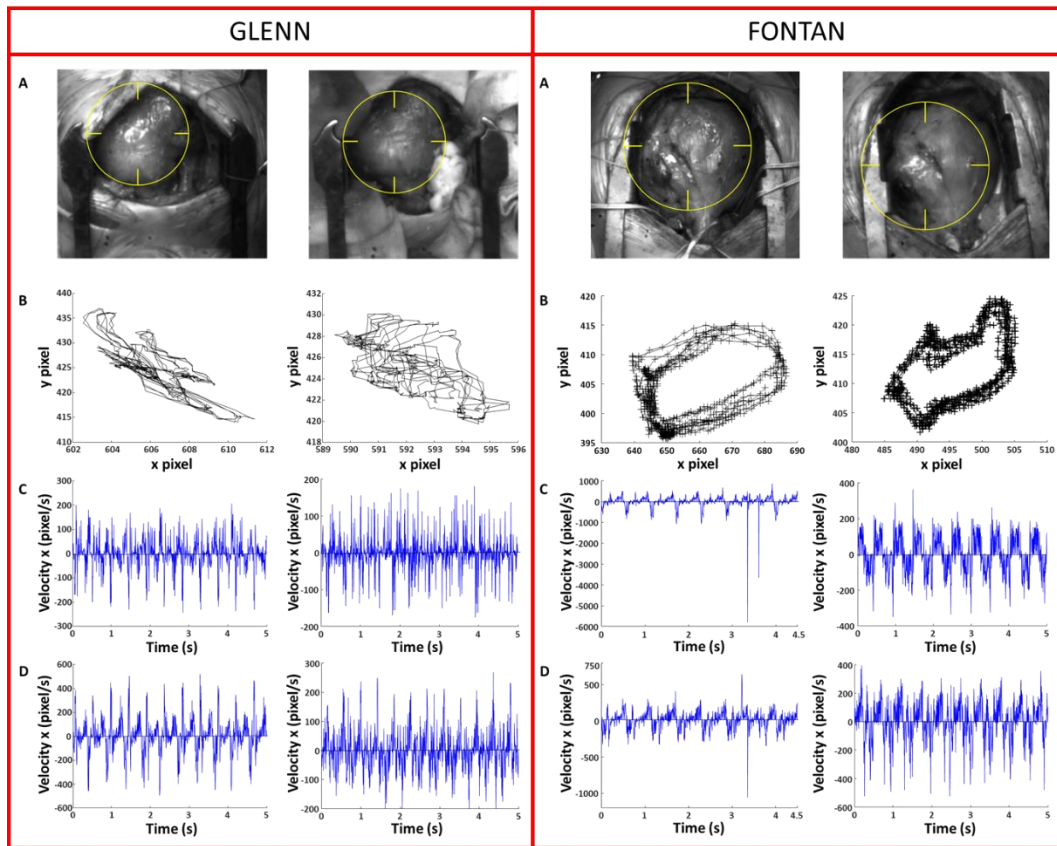
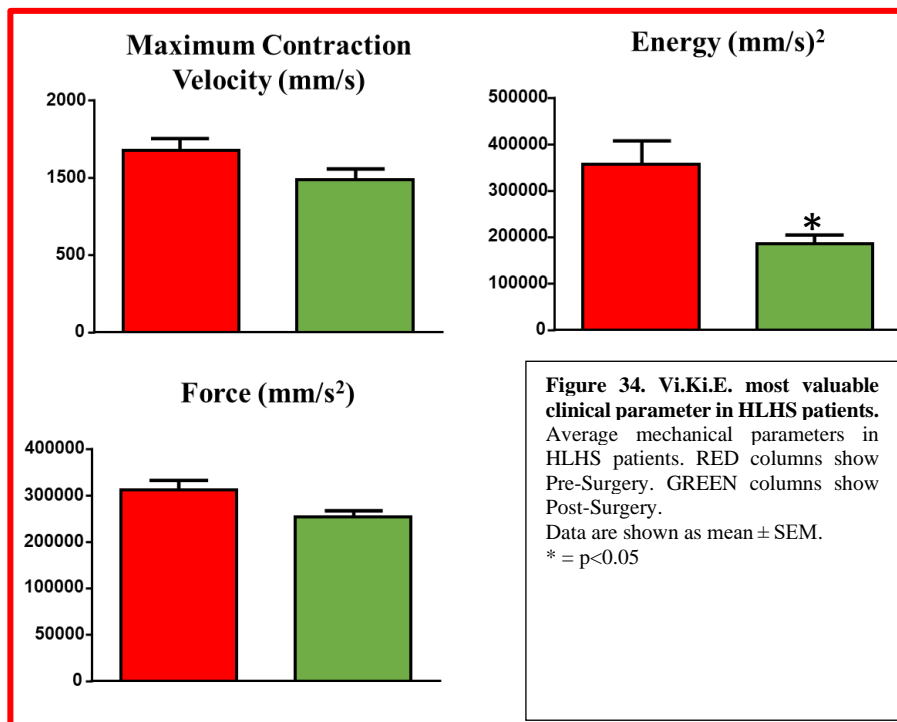


Figure 33. Vi.Ki.E. qualitative data in patients with Hypoplastic Left Heart Syndrome, divided by surgical stages. Most explanatory patients at GLENN and FONTAN surgical stages. **GLENN**, left column is before the surgery. Right column is after the surgery. **A.** Hearts with marker (yellow circle) showing the tracked area. **B.** Trajectories of the yellow marker. **C.** ViCGs in x axis **D.** ViCGs in y axis. **FONTAN**, same as GLENN.

Figure 33 shows the qualitative parameters in HLHS hearts at different surgical stages. In the GLENN stage, the trajectories after the surgery (right column) appear less compressed and, even if shifted, they appear conserved compared to those before the surgery. However, it is not possible to state the same for the ViCGs that, after the surgery, appear less conserved in both x and y axes resulting very challenging to evaluate compared to those before the surgery. In the FONTAN stage, as it concerns the trajectories, at first sight, they could be considered both good. However, they differ because the “+” distribution (indicating the marker position in each frame) after the surgery is more homogeneously distributed along the trajectory compared to the one before the surgery. To stress the difference, it can be noted that before the surgery the “+” are mostly concentrated in the bottom left corner, meaning the presence of the marker in that region for a long period of time during the cardiac beats. As it concerns the ViCGs, it can be noted that after the surgery they are very readable and, even if somehow noisy, easy to evaluate.

- HLHS Patients

Figure 34 shows the mean parameters of all HLHS patients. While there is a significant reduction for the Energy, the other parameters remain unchanged.



As it concerns the different surgical stages of patients, 2 of them underwent GLENN repair, while the other 2 underwent FONTAN repair. In Figure 35, it is highlighted the different surgical impact of the procedure on patients. In fact, while the GLENN repair does not show any mechanical difference, the FONTAN repair shows significant reduction in Maximum Contraction velocity and Energy consumption.

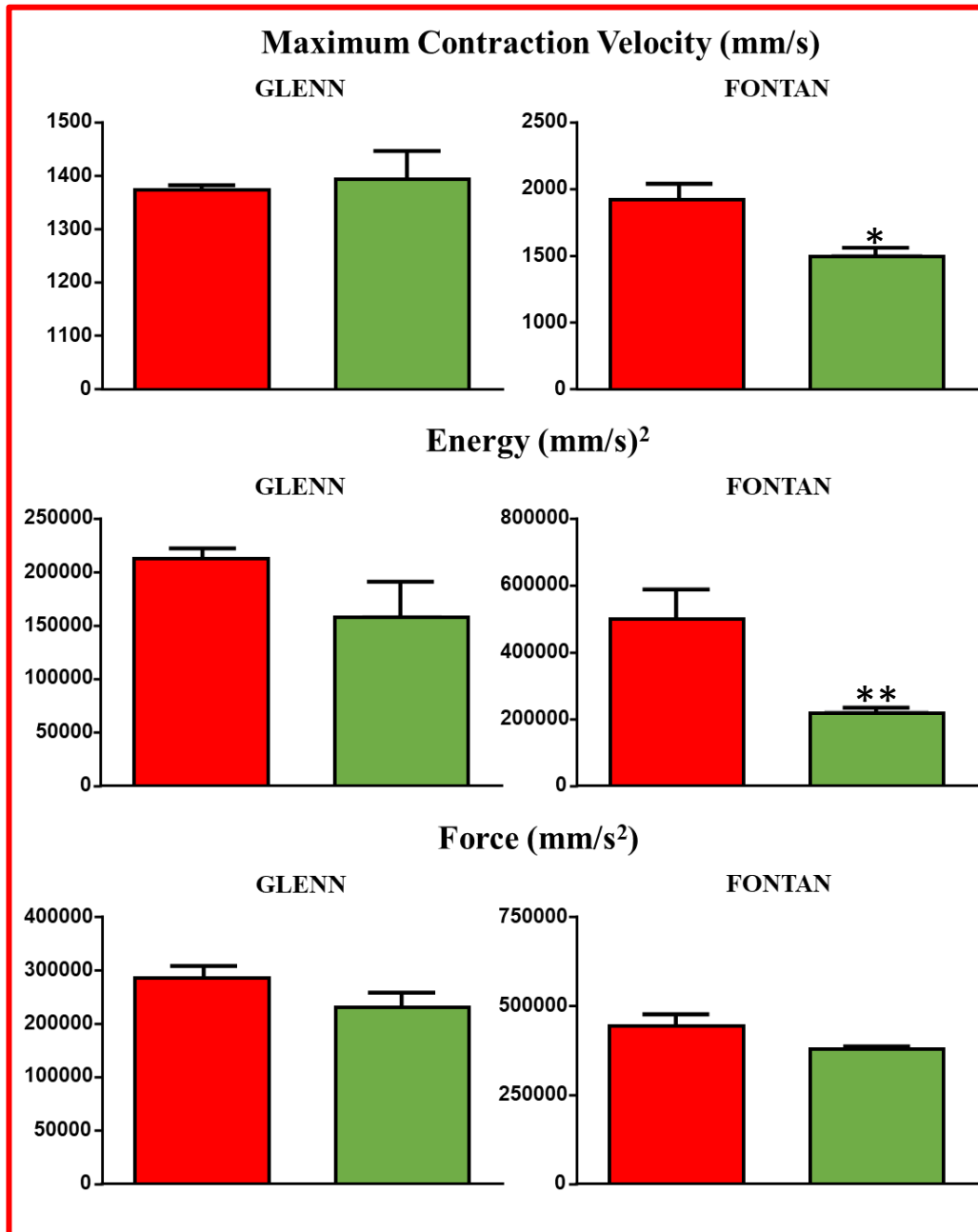
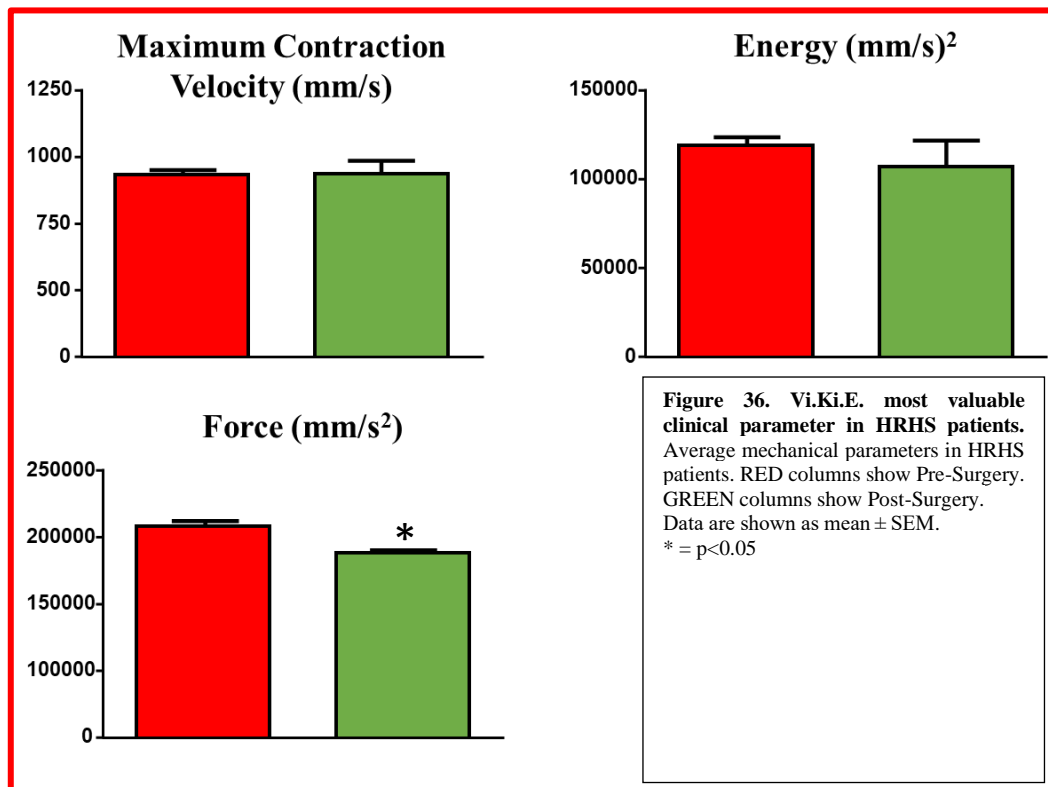


Figure 35. Vi.Ki.E. most valuable clinical parameter in HLHS patients sorted by different clinical stages. Average mechanical parameters in HLHS patients sorted by GLENN repair (left column) and FONTAN repair (right column). RED columns show Pre-Surgery. GREEN columns show Post-Surgery. Data are shown as mean \pm SEM.
 * = $p < 0.05$
 ** = $p < 0.01$

- HRHS Patients

The pathophysiology of HRHS is rarer than HLHS. Furthermore, only 2 patients were enrolled in the study, 1 of them was in GLENN surgical stage and the other one was in FONTAN surgical stage. As for HLHS, Figure 36 shows the average mechanical behavior of the heart in both patients, while Figure 37 highlights the single patient mechanical impact of the surgery (qualitative data are similar to HLHS furthermore they are not shown).



As it can be noted, there are no differences in the average mechanical parameters before and after the surgery, except for the Force that is significantly reduced. Regarding the different surgical stages (Figure 37), it can be noted that, while Force and Energy consumption significantly decrease in the GLENN patient after the surgery, the FONTAN stage does not show any relevant changes in the parameters.

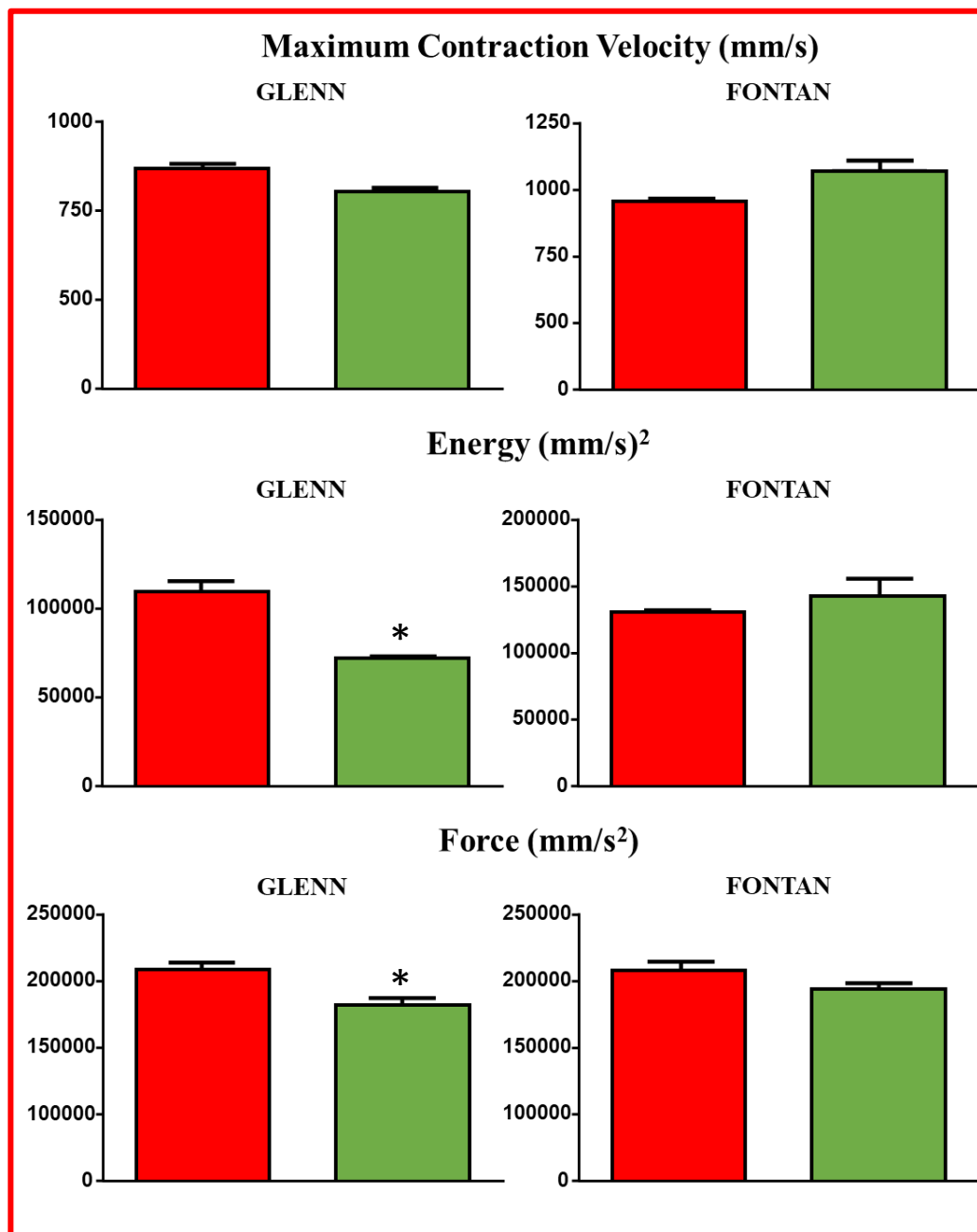


Figure 37. Vi.Ki.E. most valuable clinical parameter in HRHS patients sorted by different clinical stages. Average mechanical parameters in HRHS patients sorted by GLENN repair (left column) and FONTAN repair (right column). RED columns show Pre-Surgery. GREEN columns show Post-Surgery. Data are shown as mean \pm SEM. * = $p < 0.05$

Discussions

The hypoplastic heart syndrome is a rare congenital disease with a very dangerous pathophysiology incompatible with life until two decades ago. Nowadays the surgical approach is the only way to survive, and it requires three or more surgeries in the first three years of life. In this thesis, 4 patients with hypoplastic left ventricle and 2 patients with hypoplastic right ventricle were evaluated. Patients were taken in different surgical stages (GLENN and FONTAN) and no one was followed since the Norwood stage, thus it is difficult to assess the heart behavior. However, some interesting speculation can be made. In the HLHS, the GLENN surgery seems to have a low impact on the cardiac mechanics, probably due to the deviation of the Superior Vena Cava (SVC) flux into the pulmonary artery during the surgery. The SVC is responsible for about 20% of the venous flux returning to the right atrium. Nevertheless, the importance of this step is well known for its crucial effect on the pulmonary vasculature development able to manage the entire venous blood flow after the FONTAN step. As a matter of fact, in the FONTAN surgical step, the Inferior Vena Cava (IVC) is deviated into the Pulmonary Artery, finally separating the venous and the arterial fluxes. In this step the ventricle is unloaded because the IVC brings about 80% of the venous system to the Right Atrium. The Vi.Ki.E. parameters are in line with this physiological state showing a reduction in all the parameters.

As it concerns the two patients with right hypoplastic ventricle, the data are similar to those with left hypoplasia. The main difference is that the GLENN surgery seems to have a stronger impact on the ventricle mechanic, while the FONTAN does not show any changes. With only one patient for each repair stage, it is very hard and inaccurate to assess some hypothesis, however, the difference could be related to the different ventricle roles. In the HLHS the RV becomes the systemic ventricle, but it does not have the histological properties to perform this task. The RV is, indeed, sensible to the load. In the HRHS, the LV is the systemic ventricle perfectly fitting its task. The LV is sensible to the pressure and less sensible to load compared to RV. The different histological and mechanical properties of LV and RV could lead to the different behaviors observed during surgical steps. However, these theories need more studies to be confirmed or retracted.

3.4.3. Treatments for the Heart Failure

The high Vi.Ki.E. capability to finely evaluate the RV and to provide interesting intraoperative data on the heart mechanics in an innovative contactless fashion, led to apply this technology on the “holy grail” of the heart pathologies: the heart failure. Patients with heart failure have a high percentage of death [124] and the only ways to survive are the Ventricular Assist Devices (VAD) implantation and/or the Heart Transplantation (HT). Vi.Ki.E. was tested on both pathologies and surgeries. In the LVAD implantation, the importance of the RV evaluation is related to the statistics, showing that one out of four patients suffers from a RV overload after LVAD implantation and a consequent RV failure. For the HT, the importance of stating a healthy mechanical behavior after hours of stunning/hibernated myocardium, was the main goal of the Vi.Ki.E. evaluation. In the following two chapters data regarding patients who underwent LVAD implantation and HT will be shown.

3.4.3.1 Left Ventricular Assist Device (LVAD) implantation

Results

In this preliminary study on LVAD implantation (Heart mate III™), 5 patients were enrolled with an average age of 52.6 ± 17 years. As for the previous surgeries, the same epicardial area was tracked before and after the surgery as shown in Figure 38 A. The Vi.Ki.E. trajectories and ViCGs, which represents the qualitative data of the technique, are displayed in Figure 38 B and C-D, respectively. As it can be noted, the ViCGs after the Heart Mate III™ implant (Figure 38, right panels) display more noise than those before the surgery (Figure 38, left panels). The same occurs for the trajectories where, after the implant, the marker movement is random, shrunk and not overlapped (Figure 38, right panel) compared to the one before the surgery (Figure 38, left panel). The quantitative data, shown in Figure 39, highlights a significant reduction of all the mechanical parameters following LVAD implantation.

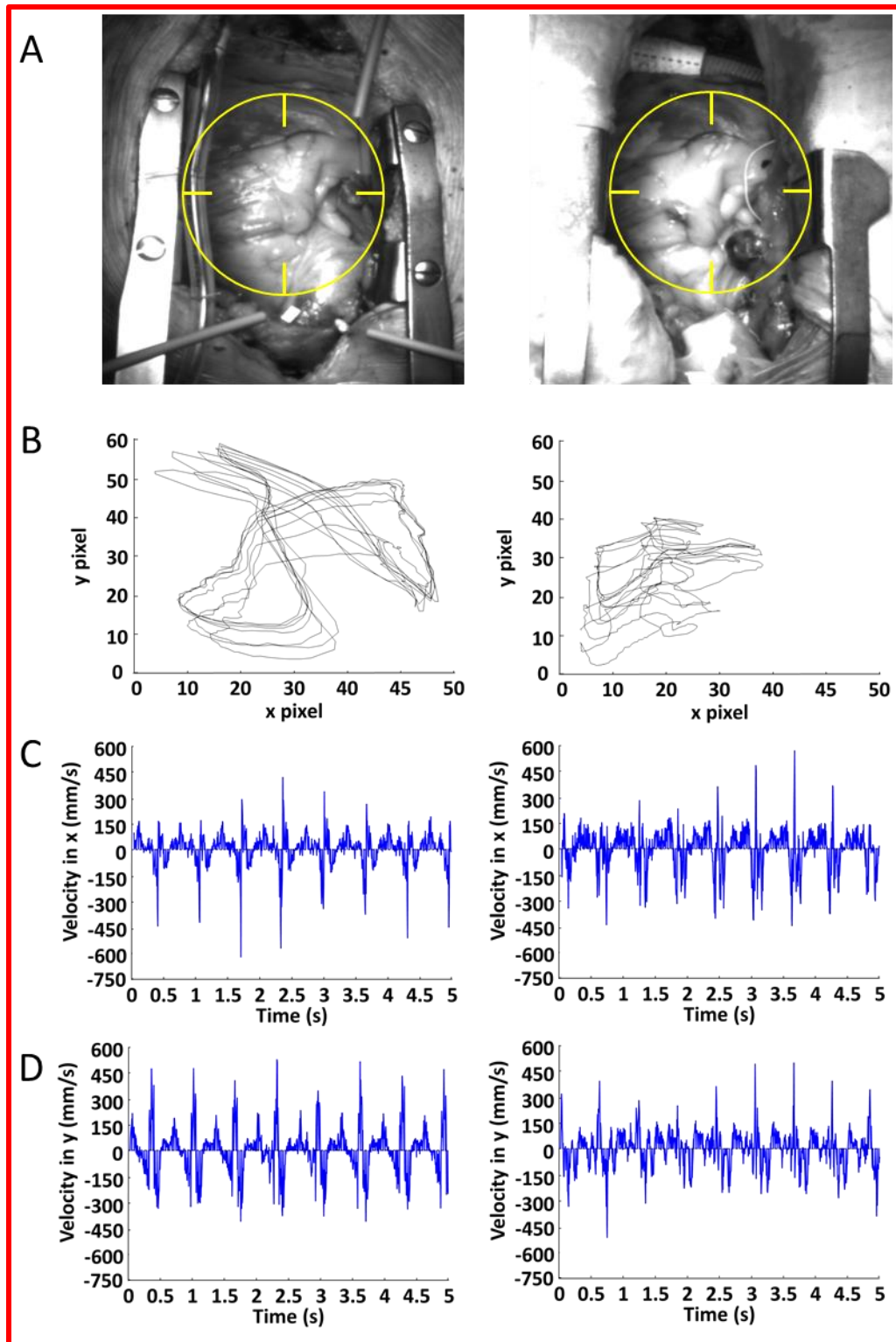
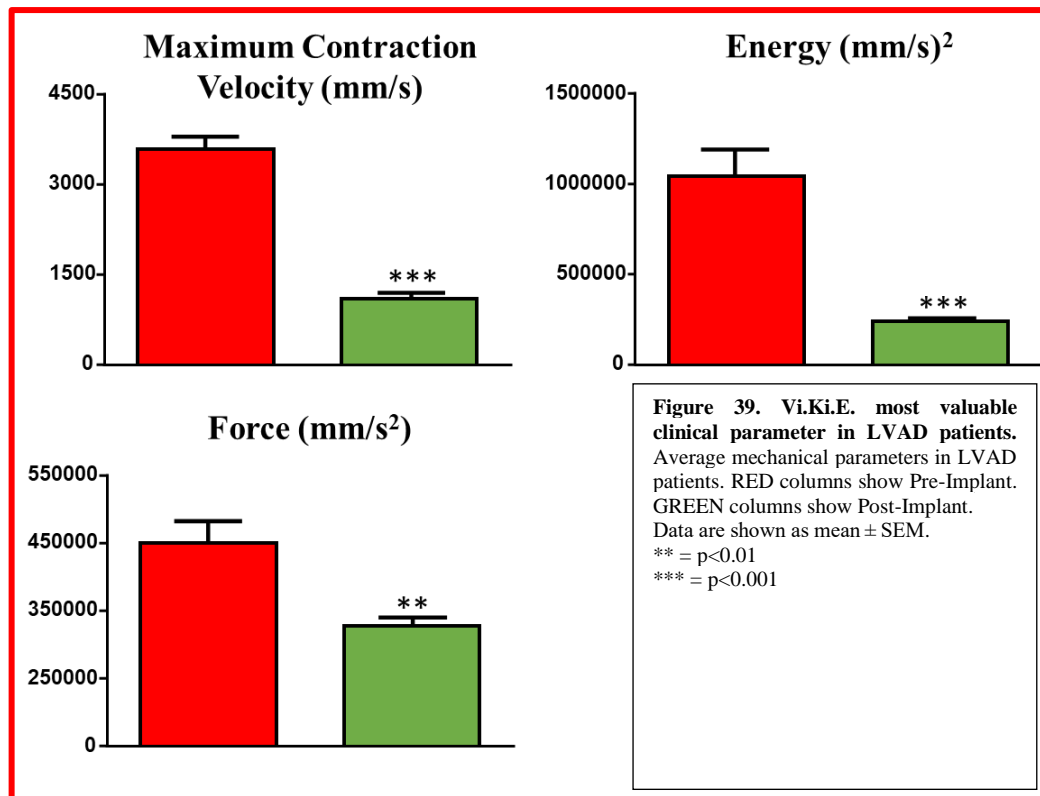


Figure 38. Vi.Ki.E. qualitative data in patients with left ventricular assist device implant. Most explanatory patient with LVAD implant. Left column is before the implant. Right column is after the implant. **A.** Hearts with marker (yellow circle) showing the tracked area. **B.** Trajectories of the yellow marker. **C.** ViCGs in x axis **D.** ViCGs in y axis.



Discussions

The assist devices are small turbines sucking the blood from the LV apex and carrying it directly in the Aorta, therefore bypassing the LV. The VAD implantation could be a destination therapy or a palliative before the heart transplantation. One of the main issues during the surgery, apart from bleeding and often the risky patient's conditions, is that, once the VAD is turned on, about 30 to 40% of patients develop an acute RV overload with a consequent failure that can lead to death [7]. The restoring of the arterial flux velocity to a more physiological condition, due to the VAD implant, in most cases unload the RV ventricle since the LV request of blood supply form the pulmonary circulation is restored, thus restarting the venous circulation. However, in some cases, although the patient does not show any pulmonary hypertension before surgery (that is an ESC guideline pre-request for surgery), the starting of the VAD can lead to an acute engulf in the pulmonary circulation with a consequent pulmonary hypertension and RV overload.

During the video kinematic evaluation of the LVAD patients in this work both the situation mentioned above were encountered.

Five out of Six patients enrolled in this study showed a mechanical RV unload and a consequent decrease in all the Vi.Ki.E. parameters after the Heart Mate III™ implant with a good clinical outcome. The sixth patient will be presented later on as Case Study Patient #2.

3.4.3.2. Heart Transplantation evaluation

Heart transplantation is probably one of the most challenging and delicate heart surgeries. It requires a very skilled equipe, time and a deep functional parameter monitoring. The possibility to have an intraoperative contactless technology able to help surgeons in the assessment of the heart mechanics, could be important for the patient's health/recovery as well as the comprehension of phenomena like the stunning/hibernated myocardium. The importance to evaluate a healthy heart could set the basis for physiological/pathological thresholds usable in the operating rooms as a comparison for the good recovery of the patients' heart after the surgery.

Results

Figure 40 shows the marker positioning (A, yellow circle) on the two different epicardial surfaces before (Left Column), and after (Right column) the transplant. As it concerns the Vi.Ki.E. trajectories (Figure 40 B, left and right panels) it can be noted that the implanted heart shows a more organized and stable pattern of contraction, even if shifted compared to those of the failing heart. As it concerns the ViCGs (Figure 40 C-D left and right panels), it can be noted that after the implant of the healthy heart (right panels), show less noise than the failing one (left panels) in both x and y axes. Furthermore, they are easy to evaluate.

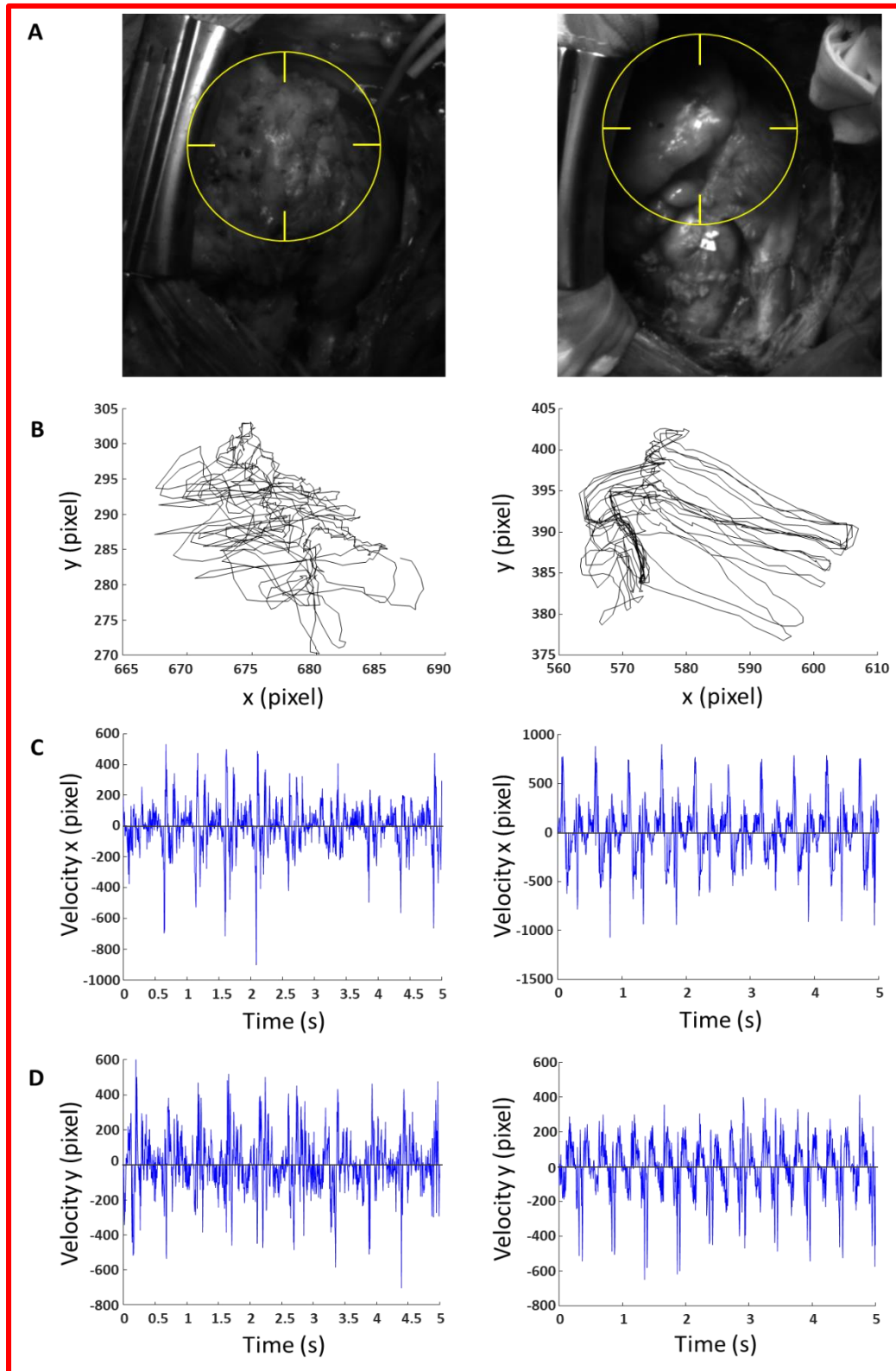
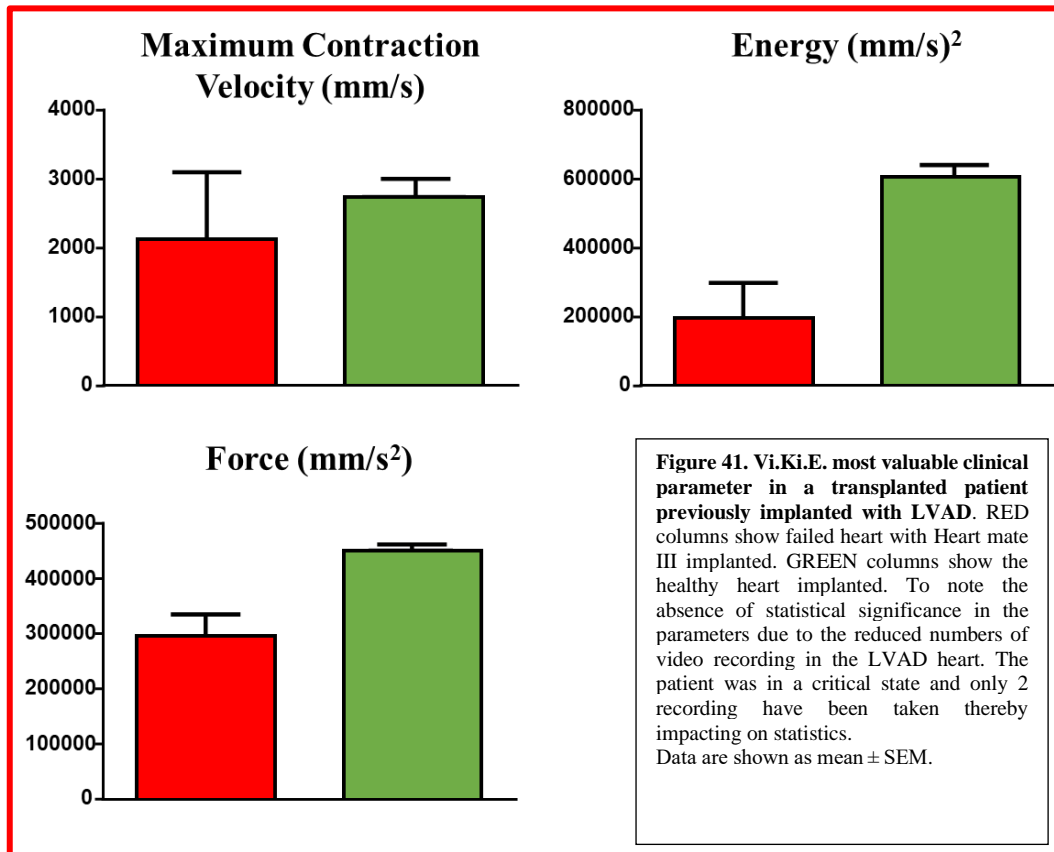


Figure 40. ViKi.E. qualitative data in patients with transplanted heart. Most explanatory patient with transplanted heart. Left column is the failed heart before the explanation. Right column is healthy heart after the implant. **A.** Hearts with marker (yellow circle) showing the tracked area. **B.** Trajectories of the yellow marker. **C.** ViCGs in x axis **D.** ViCGs in y axis.

The quantitative data of the 2 patients presented in this chapter will be individually shown in a HT performed on a patient with a LVAD and in a HT due to a failing heart.

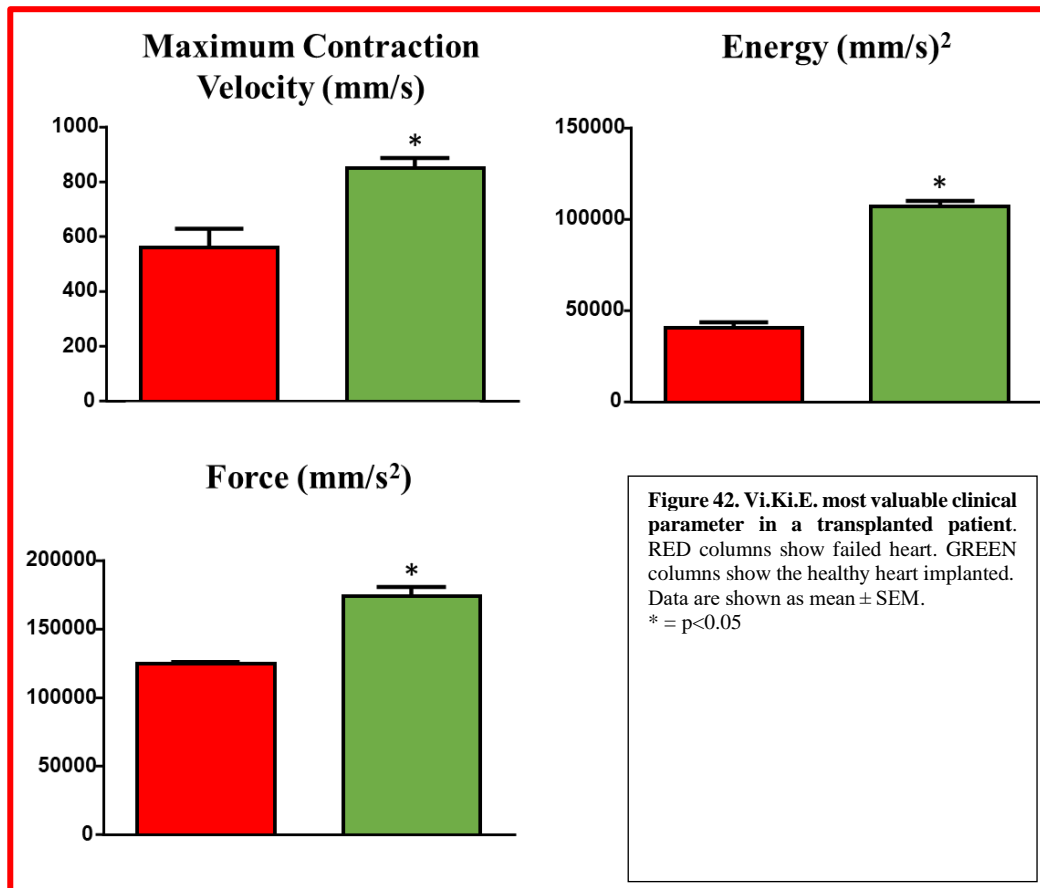
- Patient#1 (58 years), VAD Bridge to Transplant

Figure 41 shows the parameters of the failing heart with a LVAD implanted (RED columns), and the parameters of the healthy heart (GREEN columns). As it can be noted, the mechanical parameters of the implanted heart are all higher than those of the failing heart even if helped by the Herat Mate III™. There is no statistical significance in the data since the patient was in a dangerous state, thus the video-recording was limited to let the surgery proceed, thereby invalidating the statistics.



- Patient#2 (56 years)

Figure 42 shows the parameters of the failing heart (RED columns), and the parameters of the healthy heart (GREEN columns). As it can be noted, the mechanical parameters of the implanted heart are all significantly higher than those of the failing heart.



Discussions

The importance of the evaluation of a non-pathological heart will provide important physiological/pathological thresholds that could be extremely useful for clinicians in the operating room, as an outcome comparison to the basal parameters of a healthy heart.

In this preliminary study, only 2 patients were enrolled in two different stages. One of them was a patient with VAD implanted that obtained the HT. The other one was a patient with a failing heart due to post-ischemic dilatative cardiomyopathy. As expected, all the mechanical parameters increased in the implanted hearts compared

with failing ones. However, the implanted hearts, in both cases, suffered from a 4-hour ischemia and hibernation. A deep myocardium hibernation requires a lot of time to recover, moreover, this procedure is fastened by the administration of inotropic drugs. All these conditions can impair the mechanical evaluation with misleading interpretations. Furthermore, the obtained data needs to be handled with care.

3.4.4. Case studies

In this paragraph, it will be presented data from 2 patients with inauspicious prognosis unfortunately leading them to death for post-surgical complications.

Results

The first case presented is a patient with congenital valvulopathy of both the tricuspid and the pulmonary valves (Case Study Patient #1). The patient underwent surgical valvotomy at the age of 4. During years, the patient developed moderate tricuspid insufficiency, pulmonary, and arterial hypertension leading to an RV heart failure. The physiopathology of this patient is somehow similar to the Tetralogy of Fallot, so the results obtained by Vi.Ki.E. were compared to those from the ToF study.

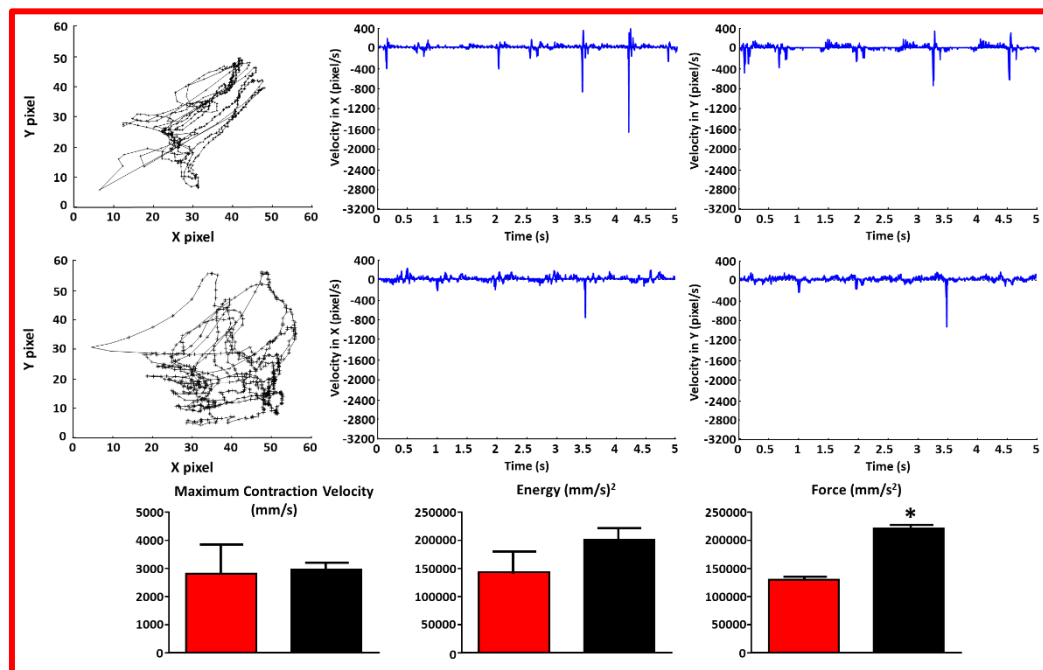


Figure 43. Vi.Ki.E. qualitative and quantitative data in case study patient#1. Upper panels: Trajectories (left) and ViCGs in x axis (middle) and y axis (right) before the replacement of both tricuspid and pulmonary valves. **Middle panels;** same as upper panels but after the replacement of the valves. **Bottom panels;** quantitative parameters before (Red columns) and after (Black) the valve replacements.

Data are shown as mean \pm SEM.

* = $p < 0.05$

Figure 43 shows both the qualitative and quantitative parameters of the Case Study Patient #1. As it concerns the qualitative parameters, it is detectable that there are no differences both in trajectories and ViCGs before and after the valves'

replacement. In fact, in the trajectories before the surgery, the “+” density is in the right top corner showing that the marker was “stuck” in that area, sometimes moving in a random way. The same occurs in the trajectories after the surgery, where the “+” density is in the bottom right corner of the graph. The ViCGs show a very noisy signal with very high spikes that shrink the scale of the graph, making it very hard to evaluate. The same behavior occurs in the quantitative data, where the parameters after the surgery are higher than those before the surgery but only the cardiac fatigue increased significantly.

Discussions

In the Case Study Patient #1, with a physiopathology comparable with the Tetralogy of Fallot, all the parameters increased after the PVR suggesting a worsening in the patient’s condition due to an augmented cardiac fatigue and energy consumption. The patient was in a critical state even before the surgery due to an elevated degree of valvulopathy. Unfortunately, this patient died some days after surgery in the intensive care unit.

The second case study patient (Case Study Patient #2) is a patient with a post-ischemic dilatative cardiomyopathy due to an unhealthy diet and smoke abusing. Therefore, the patient was scheduled for LVAD implantation.

Results

Figure 44 shows both the qualitative and quantitative parameters of the Case Study Patient #2. The trajectories before the Heart Mate III™ implant (Top panel, left) are well conserved and overlapped. After the implant, the trajectories are totally randomized (Middle panel, left). As it concerns ViCGs, it can be noted that before the LVAD implant, both x and y axes are easily readable and evaluable (Top panel, middle and right). Instead, ViCGs after the VAD implant present spikes and, in some cases, are difficult to interpret. As it concerns the quantitative parameters it can be noted that the mechanical functioning of the heart is impaired with a higher ATP consumption and cardiac fatigue. Once again, the lack of statistical significance is due to a limited number of recordings caused by the patient's conditions.

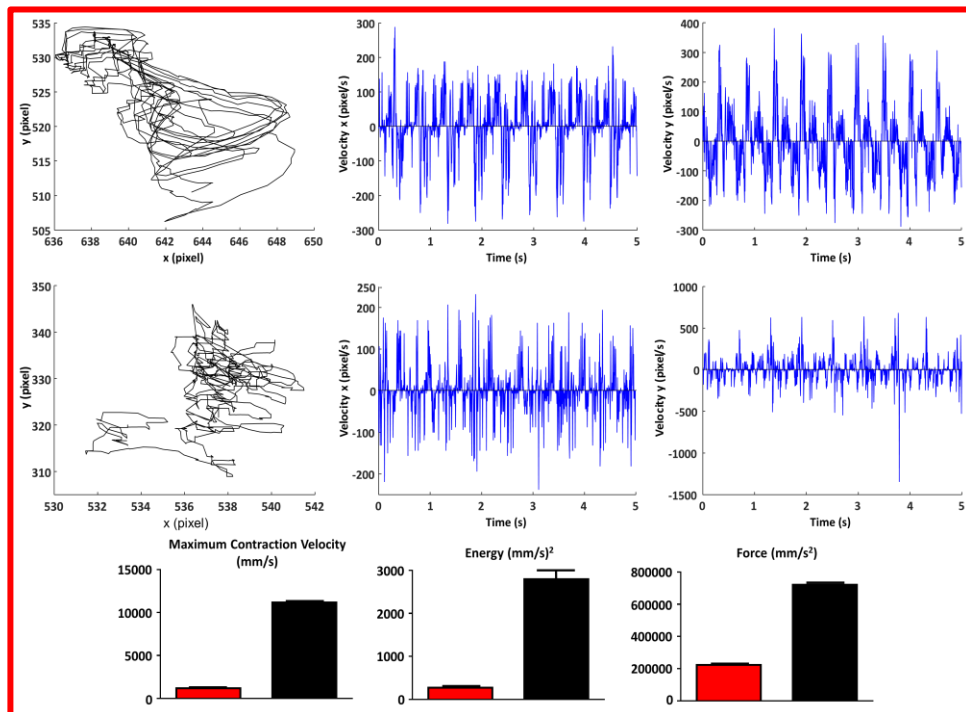


Figure 44. Vi.Ki.E. qualitative and quantitative data in Case Study Patient#2. Upper panels; Trajectories (left) and ViCGs in x axis (middle) and y axis (right) before the LVAD implant. **Middle panels;** same as upper panels but after the LVAD implant. **Bottom panels;** quantitative parameters before (Red columns) and after (Black) the LVAD implant. Data are shown as mean \pm SFM.

Discussions

As stated before a good outcome for LVAD patients is the reduction of all the Vi.Ki.E. parameters, since the restored blood flow in the pulmonary circulation and the consequent RV unloading. The Case Study Patient #2, however, showed a consistent increase of all the mechanical parameters, with a consequent bad outcome that worsened during the following days, until the patient, unfortunately, passed away.

4. DISCUSSIONS

During this Ph.D. period, the Vi.Ki.E. technology has proven a widespread use in the clinical field showing a high capabilities to obtain real-time and post-processing data from different cardiac pathologies. However, it is essential to discuss “how” and “why” a parameter trend could be, in some cases, an improvement, and in others could lead to death. Furthermore, the pathophysiological background of the patients is crucial and must be taken into account for data interpretation. In this chapter the discussion of all the followed surgeries will be merged and summarized.

4.1. CABGs

The pathophysiology of patients in need of coronary bypass lies in the lumen reduction of the coronaries usually due to atherosclerotic plaque formation. This leads to a decrease in the downstream blood flow, with a consequent ischemia in that region. An ischemic region is less contractile due to the decrease of oxygen supply, which implies a decrease in the cardiomyocytes ATP production, leading to a smaller ejection fraction, and, consequently, to the patients’ fatigue and the well know retrosternal pain. The more the arteries are occluded the higher the probability that patients will suffer from stroke or cardiac infraction.

In the Vi.Ki.E. first work [28], it was performed an evaluation in normal rat hearts after the sternotomy and pericardial suspension. The anterior descending aorta was ligated for 12 minutes, and then it was performed a second kinematic evaluation. Finally, the ligation was removed, and a Vi.Ki.E. evaluation was performed after 12 minutes of reperfusion. Data showed a drastic reduction of all mechanical parameters after ischemia and a recovery after the reperfusion. However, the heart mechanic after reperfusion was still impaired and did not totally recover compared to the data before the ischemia.

Moving to the patients the same behavior was noticed. The first recording was performed at the chest opening in a pathophysiological stage comparable to the rat ischemic time-point. After the surgery, a re-evaluation of the heart showed an

increase in all the parameters compared to the pathological stage before the surgery. It was hypothesized that, with a restored blood flow and optimal oxygen supply, the ischemic area recovered due to the augmented ATP formation/consumption and consequently the myocardium mechanics ameliorated. Moreover, also the Echo EF showed data which ranges around normal values after the surgery.

4.2. ToF

As it concerns the Tetralogy of Fallot physiopathology, the focus and the hypothesis-driven approach was completely different compared to CABGs. ToF is a congenital heart disease consisting of four simultaneous pathological states (whence tetralogy). ToF patients undergo surgery multiple times, depending on the development degree of the pulmonary circulation. Once the pulmonary circulation is full developed, the child is ready to correct the pathology through the surgery with the pulmonary valve replacement (PVR).

In this work all the patients were in the PVR stage, at different ages as stated before. The defects corrected at this stage are the Pulmonary valve stenosis/hypoplasia and the consequent RV hypertrophy. Removing the stenosis, thanks to the new synthetic pulmonary valve, the RV pressure will decrease with a better blood outflow leading to a proper RV unload.

What Vi.Ki.E. stated, as soon as the valve was replaced, was that all the RV parameters drastically decreased. In detail, the cardiac fatigue (an index of Starling effect) decreased due to the reduced pressure in the RV after PVR and the removal of the related hypertrophy. Energy consumption was reduced as well since the myocardium restored a healthy beat reducing its fatigue and thus ATP expenditure. Finally, the maximum contraction velocity was reduced due to the ventricular unload and fatigue reduction (reduced Starling effect).

The data obtained with Vi.Ki.E. did not unravel anything new; it is noteworthy that the unloading of the ventricle leads to a reduction in the parameters. However, the most interesting and pivotal part of that study concerned the debate about the timing for PVR. There are two factions, some clinical equips are more “conservative” awaiting until the pathology reaches an advanced stage, and others, with a more

“aggressive” approach, assert the importance to perform surgery as soon as possible to avoid cardiac remodeling and impairment through years.

One of the used parameters in the ESC guidelines to time the PVR is the MRI RVEDV threshold at 165ml/m^2 . However, there are some studies showing that this value could be too high and the patient could be in a late stage of the pathology [86], but even this is a matter of debate. In this thesis, patients above and under this threshold were enrolled. What it has been noticed, comparing the most valuable Vi.Ki.E. clinical parameters (Energy and Force) with the RVEDV distribution, it was that patients under the 150ml/m^2 had a very small recovery and parameters distribution. On the contrary, patients above 150ml/m^2 showed a high intra-surgery recovery. However the overall recovery was far from the basal recovery, with values often twofold higher compared to those who underwent PVR under the threshold. To note, the data distribution was very high.

Moreover, the conventional intervention (i.e. above 150ml/m^2) denoted advantages in terms of patient’s recovery compared to those operated early. However, the overall recovery is far from the baseline reached by the patients operated earlier. This could lead to the development of future cardiac pathologies or re-hospitalization. On the contrary, the unconventional intervention (i.e. below 150ml/m^2) has a little impact on the cardiac functionality but could be performed, as a prevention, to avoid possible future cardiac pathologies. In particular the baseline parameters are drastically lower in those patients rather than in patients operated with the conventional surgery. The follow-up monitoring of those patients, in the next 5 to 10 years, as well as this study (and the further ones), could lead to a reduction of the actual threshold for the surgery and the amelioration of the patients’ outcomes.

As it concerns the case study patient#1, with a physiopathology comparable with the Tetralogy of Fallot, all the parameters increased after the PVR suggesting a worsening in the patient’s conditions due to an augmented cardiac fatigue and energy consumption. The patient was in a critical state even before the surgery due to an elevated degree of valvulopathy. Unfortunately, this patient died some days after surgery in the intensive care unit.

4.3. Gender differences

During the ToF study one patient, Patient #3, suffered from an intraoperative tachycardia at the ECC exit and all the Vi.Ki.E. parameters resulted higher after the PVR compared to those before the PVR. Starting from what happened in the Case Study Patient#1, the entire equip was worried about the Patient #3's condition and she was monitored carefully. The patient was dismissed in the average time of the other patients with a good outcome. This fact raised a question about Vi.Ki.E. technology reproducibility. The only difference in Patient #3 compared to the others was the high sinus rhythm reaching a stable 155 beats per minute. It was hypothesized that the high frequency could impair or change the heart kinematic. Furthermore, it was performed a pacing protocol on rats (both males and females), driving the atrium at different basic cycle lengths (BCL), and finally the data were evaluated separately in both genders [30]. The results obtained showed that the female kinematic increased exponentially with the pacing increase, while the male one showed an increase until reaching a plateau followed by a decrease, with a changed pattern of contraction. The data confirmed the trend observed in Patient #3 (a female), confirming the high accuracy of the Vi.Ki.E. technology. Moreover, the results confirmed what is already known in literature, asserting that female heart is stronger than male heart, probably due to estrogen production, which exerts protective properties on the cardiovascular system.

This work, started as a collateral work, placed the basis for the normalization of the Vi.Ki.E parameters according to the cardiac frequency in those cases where the reproducibility of the same physiological conditions before and after the surgery is challenging.

4.4. Hypoplastic Heart Syndromes

The hypoplastic heart syndrome is a rare congenital disease with a very dangerous pathophysiology incompatible with life until two decades ago. Nowadays the surgical approach is the only way to survive, and it requires three or more surgeries in the first three years of life. In this thesis, 4 patients with hypoplastic left ventricle

and 2 patients with hypoplastic right ventricle were evaluated. Patients were taken in different surgical stages (GLENN and FONTAN) and no one was followed since the Norwood stage, thus it is difficult to assess the heart behavior. However, some interesting speculation can be made. In the HLHS, the GLENN surgery seems to have a low impact on the cardiac mechanics, probably due to the deviation of the Superior Vena Cava (SVC) flux into the pulmonary artery during the surgery. The SVC is responsible for about 20% of the venous flux returning to the right atrium. Nevertheless, the importance of this step is well known for its crucial effect on the pulmonary vasculature development able to manage the entire venous blood flow after the FONTAN step. As a matter of fact, in the FONTAN surgical step, the Inferior Vena Cava (IVC) is deviated into the Pulmonary Artery, finally separating the venous and the arterial fluxes. In this step the ventricle is unloaded because the IVC brings about 80% of the venous system to the Right Atrium. The Vi.Ki.E. parameters are in line with this physiological state showing a reduction in all the parameters.

As it concerns the two patients with right hypoplastic ventricle, the data are similar to those with left hypoplasia. The main difference is that the GLENN surgery seems to have a stronger impact on the ventricle mechanic, while the FONTAN does not show any changes. With only one patient for each repair stage, it is very hard and inaccurate to assess some hypothesis, however, the difference could be related to the different ventricle roles. In the HLHS the RV becomes the systemic ventricle, but it does not have the histological properties to perform this task. The RV is, indeed, sensible to the load. In the HRHS, the LV is the systemic ventricle perfectly fitting its task. The LV is sensible to the pressure and less sensible to load compared to RV. The different histological and mechanical properties of LV and RV could lead to the different behaviors observed during surgical steps. However, these theories need more studies to be confirmed or retracted.

4.5. LVAD

The pathophysiology of patients in need of a ventricular assist device is simple: the heart failure. The heart failure is the most worldwide spread disease and its

incidence will keep increasing in the next decades, especially in the developing countries.

The assist devices are small turbines sucking the blood from the LV apex and carrying it directly in the Aorta, therefore bypassing the LV. The VAD implantation could be a destination therapy or a palliative before the heart transplantation. One of the main issues during the surgery, apart from bleeding and often the risky patient's conditions, is that, once the VAD is turned on, about 30 to 40% of patients develop an acute RV overload with a consequent failure that can lead to death [7]. The restoring of the arterial flux velocity to a more physiological condition, due to the VAD implant, in most cases unload the RV ventricle because the LV request of blood supply from the pulmonary circulation is restored, thus restarting the venous circulation. However, in some cases, although the patient does not show any pulmonary hypertension before surgery (that is a ESC guideline pre-request for surgery), the starting of the VAD can lead to an acute engulf in the pulmonary circulation with a consequent pulmonary hypertension and RV overload.

During the video kinematic evaluation of the LVAD patients in this work both the situation mentioned above were encountered.

Five out of Six patients enrolled in this study showed a mechanical RV unload and a consequent decrease in all the Vi.Ki.E. parameters after the Heart Mate implant with a good clinical outcome. The sixth patient was presented as Case Study Patient#2 in the Results section. The patient showed a consistent increase of all the mechanical parameters, with a consequent bad outcome that worsened during the following days, until the patient, unfortunately, passed away. The LVAD study is currently on, thanks to a recently founded European Project (LVAD-STRAT) aimed to understand how LVAD implant may impact on LV recovery.

4.6. Heart Transplantation

The final series of surgeries followed was the heart transplantations. The importance of the evaluation of a non-pathological heart will provide important physiological/pathological thresholds that could be extremely useful for clinicians in the operating room, as an outcome comparison to the basal parameters of a

healthy heart. Furthermore, the increasing request of hearts for transplantation, due to the aforementioned heart failure incidence increase, has led the researcher all over the world to work on recreating laboratory functional organs thanks to the 3D printing technique. The Vi.Ki.E. technology will play a pivotal role in this field of research since the 3D printed hearts will need to pass extremely restrictive requirements to be implanted in humans. Vi.Ki.E. could be the Gold Standard technique for the evaluation of the mechanical functioning and pressure/load managing of those hearts.

In this preliminary study, only 2 patients were enrolled in two different stages. One of them was a patient with VAD implanted that obtained the HT. The other one was a patient with a failing heart due to post-ischemic dilatative cardiomyopathy. As well as Hypoplastic patients, the obtained data needs to be handled with care because there is no statistical potency. As expected, all the mechanical parameters increased in the implanted hearts compared with failing ones. However, the implanted hearts, in both cases, suffered from a 4-hour ischemia and hibernation. A deep myocardium hibernation requires a lot of time to recover, moreover, this procedure is fastened by the administration of inotropic drugs. All these conditions can impair the mechanical evaluation with misleading interpretations. Furthermore, although data seems in line with the expected physiology, it was set up a new protocol with the AOUI of Verona with the possibility to record the healthy heart just before the explant and finally after the implant in the new patient to compare both the condition and correct the errors that could have been introduced in the two patients evaluated. The new protocol is still under the evaluation of the ethic committee. Moreover, The Verona Hospital performs very few cases of “in house” transplant every year. Most of the hearts for HT derive from other Hospitals all around Italy where it is actually not possible to have access to. Therefore, a multicentric collaboration is crucial to continue this study.

5. LIMITATIONS

The limitations of this study are both technical and theoretical.

The main technical limitation is the recording of a 3D movement with a two-dimensional approach. This limitation will be overcome with the novel set-up of a single 3D camera or multiples 2D cameras synchronized together to create a 3D photogrammetry stereovision.

As it concerns the theoretical limitations, the main limitation consist in the small number of patients for each cohort, limiting the statistic potency. Furthermore, except in some isolated studies, the deep correlation between Vi.Ki.E. and Imaging Gold Standard techniques like Echocardiography and MRI is lacking.

Ongoing studies are focusing on the correlation between the kinematics data and the PV loop obtained through cardiac catheterization in small (rats) and big (pigs) animals as well as the Working Heart/Langendorff approaches.

Future studies will focus on the correlations with the Gold Standard techniques despite the presence of important technical gaps between technologies.

6. CONCLUSIONS

During my Ph.D. fellowship, I had the unique opportunity to join the Professor Giovanni Battista Luciani's surgical equipe and learn the pathophysiological aspects behind each pathology. I also discovered how an operating room works, discussing with perfusionists and anesthetists, sharing the knowledge underneath our Video Kinematic technology. I also had the opportunity to grow up as an "expert" constantly discussing with Elite Scientists, always trying to push me towards improvement.

The experimental environment forced me to be extremely precise and to create flawless models and protocols. It was essential in the "review phase" of our published articles.

The Clinical and the Experimental fields led me to understand the translational aspects of the research activities, where the data of an ischemia/reperfusion rat protocol were compared to the data deriving from revascularized hearts through

aortocoronaric bypass, or when an uncommon heart mechanical behavior was noted in a female patient leading us to study the heart mechanical aspects in both genders. Finally, the development of the Vi.Ki.E. technology and the data obtained from the clinical field in a multitude of different procedures led us to consider our technology safe and not invasive, with promising possible clinical applications.

The ease in the evaluation and the algorithm-based approach makes Video Kinematic Evaluation a widespread technique from the cellular level to Human cases, covering the entire experimental field with *in-vivo* evaluation and possibly Langendorff/Working Heart approaches.

7. REFERENCES

1. Mahia-Casado, P., et al., *Update on Cardiac Imaging Techniques 2014*. Revista Espanola De Cardiologia, 2015. **68**(2): p. 129-135.
2. Mohamed, A.A., A.A. Arifi, and A. Omran, *The basics of echocardiography*. J Saudi Heart Assoc, 2010. **22**(2): p. 71-6.
3. Mason, W.P., *Piezoelectric crystals and their application to ultrasonics*. The Bell Telephone Laboratories series. 1950, New York,: Van Nostrand. xi, 508 p.
4. Ashley EA, N.J., *Cardiology Explained*. . Vol. London: Remedica;Chapter 4, Understanding the echocardiogram. 2004.
5. Luc L. Mertens, M.L.R., Estela S. Horowitz,Robert H. Anderson, *Paediatric Cardiology*. Vol. CHAPTER 18A Cross Sectional Echocardiographic and Doppler Imaging. 2010.
6. Edler, I. and K. Lindstrom, *The history of echocardiography*. Ultrasound Med Biol, 2004. **30**(12): p. 1565-644.
7. Silverton, N.A., et al., *Intraoperative Transesophageal Echocardiography and Right Ventricular Failure After Left Ventricular Assist Device Implantation*. Journal of Cardiothoracic and Vascular Anesthesia, 2018. **32**(5): p. 2096-2103.
8. Goland, S., et al., *Fatal ventricular arrhythmia as a complication of transesophageal echocardiography*. Eur J Echocardiogr, 2005. **6**(2): p. 151-3.
9. Shiota, T., *3D echocardiography: the present and the future*. J Cardiol, 2008. **52**(3): p. 169-85.
10. Wu, V.C. and M. Takeuchi, *Three-Dimensional Echocardiography: Current Status and Real-Life Applications*. Acta Cardiol Sin, 2017. **33**(2): p. 107-118.
11. Lee, W.W., *Recent Advances in Nuclear Cardiology*. Nucl Med Mol Imaging, 2016. **50**(3): p. 196-206.
12. NK., S., *State of the art in nuclear cardiology*. Heart 2017, 2017. **103**: p. 790–799.

13. Henzlova, M.J., et al., *ASNC imaging guidelines for SPECT nuclear cardiology procedures: Stress, protocols, and tracers*. J Nucl Cardiol, 2016. **23**(3): p. 606-39.
14. Peterson, L.R. and R.J. Gropler, *Radionuclide imaging of myocardial metabolism*. Circ Cardiovasc Imaging, 2010. **3**(2): p. 211-22.
15. Schroeder, S., et al., *Cardiac computed tomography: indications, applications, limitations, and training requirements: report of a Writing Group deployed by the Working Group Nuclear Cardiology and Cardiac CT of the European Society of Cardiology and the European Council of Nuclear Cardiology*. Eur Heart J, 2008. **29**(4): p. 531-56.
16. McKavanagh, P., et al., *The Essentials of Cardiac Computerized Tomography*. Cardiol Ther, 2015. **4**(2): p. 117-29.
17. Stary HC, C.A., Dinsmore RE, *A definition of advanced types of atherosclerotic lesions and a histological classification of atherosclerosis. A report from the Committee on Vascular Lesions of the Council on Arteriosclerosis, American Heart Association*. Circulation 1995. **92**: p. 1355–74.
18. Detrano, R., et al., *Coronary calcium as a predictor of coronary events in four racial or ethnic groups*. New England Journal of Medicine, 2008. **358**(13): p. 1336-1345.
19. Einstein, A.J., M.J. Henzlova, and S. Rajagopalan, *Estimating risk of cancer associated with radiation exposure from 64-slice computed tomography coronary angiography*. Jama-Journal of the American Medical Association, 2007. **298**(3): p. 317-323.
20. Faletra, F.F., et al., *Estimate of lifetime attributable risk of cancer associated with single radiation exposure from 64-slice prospective and retrospective ECG-gating computed tomography coronary angiography*. European Heart Journal, 2009. **30**: p. 748-749.
21. Tseng, W.Y., M.Y. Su, and Y.H. Tseng, *Introduction to Cardiovascular Magnetic Resonance: Technical Principles and Clinical Applications*. Acta Cardiol Sin, 2016. **32**(2): p. 129-44.

22. Sutton, M.G. and N. Sharpe, *Left ventricular remodeling after myocardial infarction: pathophysiology and therapy*. *Circulation*, 2000. **101**(25): p. 2981-8.
23. Kathiria, N.N., C.B. Higgins, and K.G. Ordovas, *Advances in MR imaging assessment of adults with congenital heart disease*. *Magn Reson Imaging Clin N Am*, 2015. **23**(1): p. 35-40.
24. Kohi, M.P., et al., *CMR assessment of right ventricular function in patients with combined pulmonary stenosis and insufficiency after correction of tetralogy of Fallot*. *Acta Radiol*, 2013. **54**(10): p. 1132-7.
25. Preston, D.C., *Magnetic Resonance Imaging (MRI) of the Brain and Spine: Basics*. 2006.
26. Saeed, M., et al., *Cardiac MR imaging: current status and future direction*. *Cardiovasc Diagn Ther*, 2015. **5**(4): p. 290-310.
27. Saeed, M., et al., *T1-relaxation kinetics of extracellular, intracellular and intravascular MR contrast agents in normal and acutely reperfused infarcted myocardium using echo-planar MR imaging*. *European Radiology*, 2000. **10**(2): p. 310-318.
28. Fassina, L., et al., *Cardiac kinematic parameters computed from video of in situ beating heart*. *Sci Rep*, 2017. **7**: p. 46143.
29. Rozzi, G., et al., *Real-time video kinematic evaluation of the in situ beating right ventricle after pulmonary valve replacement in patients with tetralogy of Fallot: a pilot study*. *Interact Cardiovasc Thorac Surg*, 2019.
30. Lo Muzio, F.P., et al., *In-situ optical assessment of rat epicardial kinematic parameters reveals frequency-dependent mechanic heterogeneity related to gender*. *Prog Biophys Mol Biol*, 2019.
31. Fassina, L., et al., *Video evaluation of the kinematics and dynamics of the beating cardiac syncytium: an alternative to the Langendorff method*. *Int J Artif Organs*, 2011. **34**(7): p. 546-58.

32. Prinz, C., et al., *Echocardiographic particle image velocimetry for the evaluation of diastolic function in hypertrophic nonobstructive cardiomyopathy*. *Echocardiography*, 2014. **31**(7): p. 886-94.
33. Bodhey, N.K., et al., *Functional analysis of the components of the right ventricle in the setting of tetralogy of Fallot*. *Circ Cardiovasc Imaging*, 2008. **1**(2): p. 141-7.
34. Yao, J., et al., *Viscoelastic material properties of the myocardium and cardiac jelly in the looping chick heart*. *J Biomech Eng*, 2012. **134**(2): p. 024502.
35. Colli-Franzone, P., Pavarino, L. F. & Scacchi, S., *Bioelectrical effects of mechanical feedbacks in a strongly coupled cardiac electro-mechanical model*. *Math Mod Meth Appl*, 2016.
36. ten Tusscher, K.H., et al., *A model for human ventricular tissue*. *Am J Physiol Heart Circ Physiol*, 2004. **286**(4): p. H1573-89.
37. Niederer, S.A. and N.P. Smith, *A mathematical model of the slow force response to stretch in rat ventricular myocytes*. *Biophys J*, 2007. **92**(11): p. 4030-44.
38. Land, S., et al., *An analysis of deformation-dependent electromechanical coupling in the mouse heart*. *J Physiol*, 2012. **590**(18): p. 4553-69.
39. Eriksson, T.S.E., et al., *Influence of myocardial fiber/sheet orientations on left ventricular mechanical contraction*. *Mathematics and Mechanics of Solids*, 2013. **18**(6): p. 592-606.
40. Ten Tusscher, K.H., R. Hren, and A.V. Panfilov, *Organization of ventricular fibrillation in the human heart*. *Circ Res*, 2007. **100**(12): p. e87-101.
41. Rodriguez, B., et al., *Effect of acute global ischemia on the upper limit of vulnerability: a simulation study*. *Am J Physiol Heart Circ Physiol*, 2004. **286**(6): p. H2078-88.
42. Luciani, G.B., et al., *Severe ischemic left ventricular failure: coronary operation or heart transplantation?* *Ann Thorac Surg*, 1993. **55**(3): p. 719-23.

43. Wong, S.C. and M.B. Leon, *Intracoronary stents*. *Curr Opin Cardiol*, 1995. **10**(4): p. 404-11.
44. Weintraub, W.S., et al., *Comparative Effectiveness of Revascularization Strategies*. *New England Journal of Medicine*, 2012. **366**(16): p. 1467-1476.
45. Sipahi, I., et al., *Coronary artery bypass grafting vs percutaneous coronary intervention and long-term mortality and morbidity in multivessel disease: meta-analysis of randomized clinical trials of the arterial grafting and stenting era*. *JAMA Intern Med*, 2014. **174**(2): p. 223-30.
46. Danad, I., et al., *New Applications of Cardiac Computed Tomography Dual-Energy, Spectral, and Molecular CT Imaging*. *Jacc-Cardiovascular Imaging*, 2015. **8**(6): p. 710-723.
47. Plass, A., et al., *The Potential Impact of Functional Imaging on Decision Making and Outcome in Patients Undergoing Surgical Revascularization*. *Thorac Cardiovasc Surg*, 2015. **63**(4): p. 270-6.
48. Lehtinen, M., et al., *Combining FDG-PET and 99mTc-SPECT to predict functional outcome after coronary artery bypass surgery*. *Eur Heart J Cardiovasc Imaging*, 2015. **16**(9): p. 1023-30.
49. Hudaverdi, M., et al., *Echocardiography for the clinician: a practical update*. *Intern Med J*, 2010. **40**(7): p. 476-85.
50. Clegg, S.D., et al., *Integrated 3D echo-x ray to optimize image guidance for structural heart intervention*. *JACC Cardiovasc Imaging*, 2015. **8**(3): p. 371-4.
51. Mahmood, F. and S.K. Shernan, *Perioperative transoesophageal echocardiography: current status and future directions*. *Heart*, 2016. **102**(15): p. 1159-67.
52. Erbel, R., et al., *Coronary-artery stenting compared with balloon angioplasty for restenosis after initial balloon angioplasty*. *Restenosis Stent Study Group*. *N Engl J Med*, 1998. **339**(23): p. 1672-8.
53. Landesberg, G., et al., *Perioperative myocardial infarction*. *Circulation*, 2009. **119**(22): p. 2936-44.

54. Eagle, K.A., et al., *ACC/AHA guidelines for coronary artery bypass graft surgery: executive summary and recommendations : A report of the American College of Cardiology/American Heart Association Task Force on Practice Guidelines (Committee to revise the 1991 guidelines for coronary artery bypass graft surgery)*. Circulation, 1999. **100**(13): p. 1464-80.
55. Ashikaga, H., et al., *Transmural dispersion of myofiber mechanics: implications for electrical heterogeneity in vivo*. J Am Coll Cardiol, 2007. **49**(8): p. 909-16.
56. Waldman, L.K., Y.C. Fung, and J.W. Covell, *Transmural myocardial deformation in the canine left ventricle. Normal in vivo three-dimensional finite strains*. Circ Res, 1985. **57**(1): p. 152-63.
57. Ortmaier, T., et al., *Motion estimation in beating heart surgery*. IEEE Trans Biomed Eng, 2005. **52**(10): p. 1729-40.
58. Ganguly, S., et al., *Cytoplasmic streaming in Drosophila oocytes varies with kinesin activity and correlates with the microtubule cytoskeleton architecture*. Proc Natl Acad Sci U S A, 2012. **109**(38): p. 15109-14.
59. Meraviglia, V., et al., *Higher cardiogenic potential of iPSCs derived from cardiac versus skin stromal cells*. Front Biosci (Landmark Ed), 2016. **21**: p. 719-43.
60. Savi, M., et al., *Titanium dioxide nanoparticles promote arrhythmias via a direct interaction with rat cardiac tissue*. Part Fibre Toxicol, 2014. **11**: p. 63.
61. Onorati, F., et al., *"Polarizing" microplegia improves cardiac cycle efficiency after CABG for unstable angina*. Int J Cardiol, 2013. **167**(6): p. 2739-46.
62. Oei, G.T.M.L., et al., *Prolonged Helium Postconditioning Protocols during Early Reperfusion Do Not Induce Cardioprotection in the Rat Heart In Vivo: Role of Inflammatory Cytokines*. Journal of Immunology Research, 2015.
63. Wang, N.C., *Third-degree atrioventricular block following commotio cordis*. Ann Noninvasive Electrocardiol, 2013. **18**(5): p. 491.
64. Hillis, L.D., et al., *2011 ACCF/AHA Guideline for Coronary Artery Bypass Graft Surgery: executive summary: a report of the American College of Cardiology*

- Foundation/American Heart Association Task Force on Practice Guidelines. Circulation*, 2011. **124**(23): p. 2610-42.
65. Sedlis, S.P., *Mechanisms of ventricular arrhythmias in acute ischemia and reperfusion*. *Cardiovasc Clin*, 1992. **22**(1): p. 3-18.
66. Kloner, R.A., K. Przyklenk, and G.L. Kay, *Clinical evidence for stunned myocardium after coronary artery bypass surgery*. *J Card Surg*, 1994. **9**(3 Suppl): p. 397-402.
67. Greenfield, R.A. and J.L. Swain, *Disruption of myofibrillar energy use: dual mechanisms that may contribute to postischemic dysfunction in stunned myocardium*. *Circ Res*, 1987. **60**(2): p. 283-9.
68. Janse, M.J. and A.L. Wit, *Electrophysiological mechanisms of ventricular arrhythmias resulting from myocardial ischemia and infarction*. *Physiol Rev*, 1989. **69**(4): p. 1049-169.
69. Swain, J.L., et al., *Prolonged myocardial nucleotide depletion after brief ischemia in the open-chest dog*. *Am J Physiol*, 1982. **242**(5): p. H818-26.
70. Vial, C., et al., *Regional myocardial energetics during brief periods of coronary occlusion and reperfusion: Comparison with S-T segment changes*. *Cardiovasc Res*, 1978. **12**(8): p. 470-6.
71. Miragoli, M., et al., *Microtubule-Dependent Mitochondria Alignment Regulates Calcium Release in Response to Nanomechanical Stimulus in Heart Myocytes*. *Cell Rep*, 2016. **14**(1): p. 140-151.
72. Pavarino, L.F., S. Scacchi, and S. Zampini, *Newton-Krylov-BDDC solvers for nonlinear cardiac mechanics*. *Computer Methods in Applied Mechanics and Engineering*, 2015. **295**: p. 562-580.
73. Franzone, P.C., L.F. Pavarino, and S. Scacchi, *Parallel multilevel solvers for the cardiac electro-mechanical coupling*. *Applied Numerical Mathematics*, 2015. **95**: p. 140-153.

74. Gatzoulis, M.A., et al., *Risk factors for arrhythmia and sudden cardiac death late after repair of tetralogy of Fallot: a multicentre study*. Lancet, 2000. **356**(9234): p. 975-81.
75. Ferraz Cavalcanti, P.E., et al., *Pulmonary valve replacement after operative repair of tetralogy of Fallot: meta-analysis and meta-regression of 3,118 patients from 48 studies*. J Am Coll Cardiol, 2013. **62**(23): p. 2227-43.
76. Harrild, D.M., et al., *Pulmonary valve replacement in tetralogy of Fallot: impact on survival and ventricular tachycardia*. Circulation, 2009. **119**(3): p. 445-51.
77. Heng, E.L., et al., *Immediate and Midterm Cardiac Remodeling After Surgical Pulmonary Valve Replacement in Adults With Repaired Tetralogy of Fallot: A Prospective Cardiovascular Magnetic Resonance and Clinical Study*. Circulation, 2017. **136**(18): p. 1703-1713.
78. Bokma, J.P., et al., *A propensity score-adjusted analysis of clinical outcomes after pulmonary valve replacement in tetralogy of Fallot*. Heart, 2018. **104**(9): p. 738-744.
79. Warnes, C.A., et al., *ACC/AHA 2008 Guidelines for the Management of Adults with Congenital Heart Disease: a report of the American College of Cardiology/American Heart Association Task Force on Practice Guidelines (writing committee to develop guidelines on the management of adults with congenital heart disease)*. Circulation, 2008. **118**(23): p. e714-833.
80. Bokma, J.P., et al., *Preoperative thresholds for mid-to-late haemodynamic and clinical outcomes after pulmonary valve replacement in tetralogy of Fallot*. Eur Heart J, 2016. **37**(10): p. 829-35.
81. Geva, T., et al., *Preoperative Predictors of Death and Sustained Ventricular Tachycardia After Pulmonary Valve Replacement in Patients With Repaired Tetralogy of Fallot Enrolled in the INDICATOR Cohort*. Circulation, 2018. **138**(19): p. 2106-2115.
82. Tang, D.L., et al., *Patient-Specific MRI-Based Right Ventricle Models Using Different Zero-Load Diastole and Systole Geometries for Better Cardiac Stress*

and Strain Calculations and Pulmonary Valve Replacement Surgical Outcome Predictions. Plos One, 2016. **11**(9).

83. Shibata, M., et al., *Flow Energy Loss as a Predictive Parameter for Right Ventricular Deterioration Caused by Pulmonary Regurgitation After Tetralogy of Fallot Repair.* Pediatric Cardiology, 2018. **39**(4): p. 731-742.
84. Kopic, S., et al., *Isolated pulmonary regurgitation causes decreased right ventricular longitudinal function and compensatory increased septal pumping in a porcine model.* Acta Physiol (Oxf), 2017. **221**(3): p. 163-173.
85. Pavlov, D.A. and A. Landesberg, *The cross-bridge dynamics is determined by two length-independent kinetics: Implications on muscle economy and Frank-Starling Law.* Journal of Molecular and Cellular Cardiology, 2016. **90**: p. 94-101.
86. Frigiola, A., et al., *Biventricular response after pulmonary valve replacement for right ventricular outflow tract dysfunction: is age a predictor of outcome?* Circulation, 2008. **118**(14 Suppl): p. S182-90.
87. Tretter, J.T., et al., *Defining and refining indications for transcatheter pulmonary valve replacement in patients with repaired tetralogy of Fallot: Contributions from anatomical and functional imaging.* Int J Cardiol, 2016. **221**: p. 916-25.
88. Fogel, M.A., et al., *Power loss and right ventricular efficiency in patients after tetralogy of Fallot repair with pulmonary insufficiency: clinical implications.* J Thorac Cardiovasc Surg, 2012. **143**(6): p. 1279-85.
89. Ravens, U., *Sex differences in cardiac electrophysiology.* Can J Physiol Pharmacol, 2018. **96**(10): p. 985-990.
90. Tadros, R., et al., *Sex differences in cardiac electrophysiology and clinical arrhythmias: epidemiology, therapeutics, and mechanisms.* Can J Cardiol, 2014. **30**(7): p. 783-92.
91. Dworatzek, E., et al., *Sex-specific regulation of collagen I and III expression by 17beta-Estradiol in cardiac fibroblasts: role of estrogen receptors.* Cardiovasc Res, 2019. **115**(2): p. 315-327.

92. Ayaz, O., et al., *Long-term testosterone deficiency modifies myofilament and calcium-handling proteins and promotes diastolic dysfunction in the aging mouse heart*. *Am J Physiol Heart Circ Physiol*, 2019. **316**(4): p. H768-H780.
93. Milerova, M., et al., *Sex difference in the sensitivity of cardiac mitochondrial permeability transition pore to calcium load*. *Mol Cell Biochem*, 2016. **412**(1-2): p. 147-54.
94. Kerr, K.F., et al., *Genome-wide association study of heart rate and its variability in Hispanic/Latino cohorts*. *Heart Rhythm*, 2017. **14**(11): p. 1675-1684.
95. Cong, B., et al., *Estrogens protect myocardium against ischemia/reperfusion insult by up-regulation of CRH receptor type 2 in female rats*. *Int J Cardiol*, 2013. **168**(5): p. 4755-60.
96. Weerateerangkul, P., et al., *Early testosterone replacement attenuates intracellular calcium dyshomeostasis in the heart of testosterone-deprived male rats*. *Cell Calcium*, 2017. **67**: p. 22-30.
97. Makkar, R.R., et al., *Female Gender as a Risk Factor for Torsades-De-Pointes Associated with Cardiovascular Drugs*. *Jama-Journal of the American Medical Association*, 1993. **270**(21): p. 2590-2597.
98. Parks, R.J. and S.E. Howlett, *Sex differences in mechanisms of cardiac excitation-contraction coupling*. *Pflugers Arch*, 2013. **465**(5): p. 747-63.
99. Farrell, S.R., J.L. Ross, and S.E. Howlett, *Sex differences in mechanisms of cardiac excitation-contraction coupling in rat ventricular myocytes*. *Am J Physiol Heart Circ Physiol*, 2010. **299**(1): p. H36-45.
100. Rosenkranz-Weiss, P., et al., *Gender-specific differences in expression of mRNAs for functional and structural proteins in rat ventricular myocardium*. *J Mol Cell Cardiol*, 1994. **26**(2): p. 261-70.
101. Petre, R.E., et al., *Sex-based differences in myocardial contractile reserve*. *American Journal of Physiology-Regulatory Integrative and Comparative Physiology*, 2007. **292**(2): p. R810-R818.

102. Schwertz, D.W., et al., *Sex differences in the response of rat heart ventricle to calcium*. Biol Res Nurs, 2004. **5**(4): p. 286-98.
103. Grandy, S.A. and S.E. Howlett, *Cardiac excitation-contraction coupling is altered in ventricular myocytes from aged male but not female mice*. Journal of Molecular and Cellular Cardiology, 2006. **40**(6): p. 876-877.
104. Curl, C.L., et al., *Effects of ovariectomy and 17 beta-oestradiol replacement on $[Ca^{2+}]_i$ in female rat cardiac myocytes*. Clin Exp Pharmacol Physiol, 2003. **30**(7): p. 489-94.
105. Ren, J., et al., *Impact of estrogen replacement on ventricular myocyte contractile function and protein kinase B/Akt activation*. Am J Physiol Heart Circ Physiol, 2003. **284**(5): p. H1800-7.
106. Er, F., et al., *Impact of testosterone on cardiac L-type calcium channels and Ca^{2+} sparks: acute actions antagonize chronic effects*. Cell Calcium, 2007. **41**(5): p. 467-77.
107. Raddino, R., et al., *Action of steroid sex hormones on the isolated rabbit heart*. Pharmacology, 1989. **38**(3): p. 185-90.
108. Gori, M., et al., *Sex-specific cardiovascular structure and function in heart failure with preserved ejection fraction*. Eur J Heart Fail, 2014. **16**(5): p. 535-42.
109. Shaw, L.J., *Sex Differences in Cardiovascular Imaging*. JACC Cardiovasc Imaging, 2016. **9**(4): p. 494-7.
110. Tan, T.P., et al., *Assessment of cardiac function by echocardiography in conscious and anesthetized mice: importance of the autonomic nervous system and disease state*. J Cardiovasc Pharmacol, 2003. **42**(2): p. 182-90.
111. Goliash, G., et al., *CRT improves LV filling dynamics: insights from echocardiographic particle imaging velocimetry*. JACC Cardiovasc Imaging, 2013. **6**(6): p. 704-13.
112. Wingate, S., *Cardiovascular anatomy and physiology in the female*. Crit Care Nurs Clin North Am, 1997. **9**(4): p. 447-52.

113. Buonanno, C., et al., *Left ventricular function in men and women. Another difference between sexes*. Eur Heart J, 1982. **3**(6): p. 525-8.
114. Bombardini, T., et al., *Diastolic time - frequency relation in the stress echo lab: filling timing and flow at different heart rates*. Cardiovasc Ultrasound, 2008. **6**: p. 15.
115. Wainstein, R.V., Z. Sasson, and S. Mak, *Frequency-dependent left ventricular performance in women and men*. Am J Physiol Heart Circ Physiol, 2012. **302**(11): p. H2363-71.
116. Mehta, L.S., et al., *Acute Myocardial Infarction in Women: A Scientific Statement From the American Heart Association*. Circulation, 2016. **133**(9): p. 916-47.
117. Mehta, P.K., J. Wei, and N.K. Wenger, *Ischemic heart disease in women: a focus on risk factors*. Trends Cardiovasc Med, 2015. **25**(2): p. 140-51.
118. Blenck, C.L., et al., *The Importance of Biological Sex and Estrogen in Rodent Models of Cardiovascular Health and Disease*. Circ Res, 2016. **118**(8): p. 1294-312.
119. Williams, A.M., et al., *The influence of adrenergic stimulation on sex differences in left ventricular twist mechanics*. J Physiol, 2017. **595**(12): p. 3973-3985.
120. Bupha-Intr, T., J. Laosiripisan, and J. Wattanapermpool, *Moderate intensity of regular exercise improves cardiac SR Ca²⁺ uptake activity in ovariectomized rats*. J Appl Physiol (1985), 2009. **107**(4): p. 1105-12.
121. McCulloch, A.D., B.H. Smaill, and P.J. Hunter, *Regional left ventricular epicardial deformation in the passive dog heart*. Circ Res, 1989. **64**(4): p. 721-33.
122. Sarnari, R., et al., *Doppler assessment of the ratio of the systolic to diastolic duration in normal children: relation to heart rate, age and body surface area*. J Am Soc Echocardiogr, 2009. **22**(8): p. 928-32.
123. Franz, M.R., et al., *Electrical and mechanical restitution of the human heart at different rates of stimulation*. Circ Res, 1983. **53**(6): p. 815-22.

124. Bytyci, I. and G. Bajraktari, *Mortality in heart failure patients*. *Anatol J Cardiol*, 2015. **15**(1): p. 63-8.

ACKNOWLEDGEMENTS

Preface

It all started in 2014 when I was looking for a master thesis project to complete the study course in Biology and Biomedical Applications at the University of Parma.

Thanks to my bachelor's degree tutors, Prof. Emilio Macchi and Ph.D. Stefano Rossi, I was introduced to Ph.D. Michele Miragoli, a promising researcher with a remarkable curriculum in terms of publications and research experiences, in order to start a master's degree thesis project.

Dr. Miragoli, at that time, was working on a very interesting topic that was a trend for that period. He was working on nanoparticles and nanowires on cardiac cell cultures to understand the electromechanical coupling behavior in collaboration with one of the best Italian private research institute: the Humanitas research center in Milan.

I was very happy to collaborate with this high rated research environment, but Dr. Miragoli made me a different propose for my thesis.

He said to me that I was not made for cell seeding because I liked to work a lot in “creating something” instead of “doing something” extremely precise and repetitive.

He introduced me the work of Lorenzo Fassina a Ph.D. in Engineering at the University of Pavia.

Dr. Fassina created an algorithm able to capture cardiac cell movements providing important kinematic information.

Dr. Miragoli asked me if I was interested in creating and developing a study on *in-vivo* rat hearts using this algorithm. He proposed this thesis to other students before me, but no one was interested in something not so “trendy” as cell cultures.

At a first moment I was sad Dr. Miragoli gave me something that could sounds like a B-plan, however I decided to accept the challenge and be the trigger for something new.

Thanks to my decision and Dr. Miragoli foresight I was able to finish my studies the 24th of April 2015 and start my research career.

The first step was the presentation of a Poster during the XX Congress of the Italian Society of Cardiovascular Research” (Imola, 26-28 November 2015), where for the first time I had to strongly defend my work with deep argumentations against experts on cardiac field.

That experience made me fall in love with this world made of reasoning and discussions with the only purpose to improve the knowledge.

The second and the most relevant step for my career, and for me as “expert”, was the introduction of this project in the clinical field thanks to the foresight of Prof. Giuseppe Faggian, the director of the Cardiovascular Surgery at the AOUI of Verona. He gave me the permission and the unique opportunity to watch some surgery and use the technology I developed in my master thesis directly on patients. Since my Master thesis defense, I worked over one year unemployed just to test the technology on animals and humans and finally the 22nd July 2016 I presented the Vi.Ki.E. project to the Cardiovascular Sciences Ph.D. commission at the University of Verona and I obtained the Ph.D. scholarship.

At the beginning of my PhD scholarship Prof. Giovanni Battista Luciani became my Tutor and proposed me to study pediatric patients with cardiac congenital pathologies.

In the meanwhile, the collaboration between Dr. Miragoli (actually Associate Professor) and Dr.Fassina, proceeded and Prof. Miragoli became my Tutor for the “basic science” part of the study at the University of Parma.

All the information about the project are in the presented Thesis.

Acknowledgements

The first thank is indeed to both my mentors Prof. Michele Miragoli and Prof. Giovanni Battista Luciani. In these 3 years of intensive work you have always let me “try”, and “move freely” in order to improve myself, even through failure. Thanks to this you shaped and forged me as the young expert I am now, with a good knowledge of the national and international scientific environments, as well as a deep knowledge of the Research mentality and all its implications. Moreover the collaboration between basic research and clinic has taught me the translational aspects of the Research and the importance, as well as the capability, to create constructive collaborations between the biological and the clinical fields that constantly struggle to communicate.

Thank to Prof. Giuseppe Faggian that firstly saw new perspective in the Vi.Ki.E. technology inviting me to test it in the surgical environment. THAT started my research career.

Thanks to Maddalena Tessari. I have always considered you as “the students’ mom” since you’re so cute with all of us, always putting all your effort to help us, listening to our moaning and comforting us.

Thanks to Camilla Sandrin, a Ph.D colleague and collaborator, always willing to help me in different personal situations, as well as her efficiency during our collaboration period.

Thanks to ALL the surgeons and technicians of the Verona equipes. I cannot mention you name by name, since I don’t remember all your names. However the memories of the hours spent together to discuss about the surgeries, talk of our life experiences, sleeping on uncomfortable chairs waiting for a transplant, and laughing hard (yes... you are ALL extremely funny) will remain vivid and pleasant moments in my heart. Thanks to you, the surgeries were indeed the BEST moments of my Ph.D. period!

As it concerns the research environment in Parma I would like to thank Ph.D. Stefano Rossi, that helped me to grow up since 2011, first as bachelor/master degree thesis tutor, and after as a colleague and friend during my Ph.D. period. We've experienced together a lot of funny moment in the last decade that always bring me a smile.

Thanks to Maricla, Cristina, Amparo, Ruben, Giuseppe and Chiara. Your presence in lab have created a familiar environment (bringing all the pros and cons of a real family) in which I'm very happy and proud to participate on a daily basis. There are no words for all the moments spent together and the deep relationships we have. Thanks to all the students that participated in our Lab Family. Every one of you helped me to start that "teaching process" I always hated (since I don't think I can properly teach) as well as bringing that "freshness" in the Lab.

A special thanks to Francesco, my friend and brother, as well as my right arm in the Vi.Ki.E. project. Our relationship is led by destiny since we're at the same time so similar and so different that we perfectly fit in a sort of "yin-yang" balance!! You came in the Lab as my first student and, same as in tails, the student overcomes the Master. I am proud of all your achievements obtained and I hope that together we will build a great research environment wherever it will be!

Last but not Least...

Thanks to my parents Edo and Luisa. The month I've spent unemployed, waiting for an eventual Ph.D. scholarships were hard for you. I can only imagine how a parent struggles seeing and uncertain future for his son. However, your faith in me has led to my personal and professional fulfillment and I'll be always grateful to you for this.

Thanks to my brother Marco, and all the new family components, Laura, Elena and Filippo. Seeing you with a perfect life is the best pleasure I could wish for you. As big brother you were always one step ahead me and your professional experience, as well as the long "work" talks, taught me how to behave in the professional environment.

Thanks to Elisa, my sweetheart. They say that behind a great man there is always a great woman. I'm not sure to be a great man (and probably I'll never be), but I'm sure that you are the greatest woman I could wish. If I'll become someone in the professional environment it will be only thanks to you.

Thanks to Enrico, Mac, Fonta and Matti. You know why I thank you. Never forget where and how we started.

An honorable mention in this acknowledgments section goes to the band Beast in Black. I casually discover your album and your music permeated my soul so deeply that my thesis writing (with your music hard and loud in my headphones) became one of the best moments of my journey!

Thank you all guys!!! I wish you all the best for your life!!!

Giacomo Rozzi della tribù dei Rozzi